The Pennsylvania State University

The Graduate School

Eberly College of Science

EXPLORING CATALYTIC ACTIVE SITES: INVESTIGATIONS OF ACTIVATED OXYGEN SPECIES AND SUPERATOMIC MIMICS IN THE GAS-PHASE

A Dissertation in

Chemistry

by

Eric C. Tyo

Submitted in Partial Fulfillment
of the Requirements
for the Degree of

Doctor of Philosophy

May 2012

The dissertation of Eric C. Tyo was reviewed and approved* by the following:

A. Welford Castleman, Jr.
Evan Pugh Professor of Chemistry and Physics
Eberly Distinguished Chair in Science
Dissertation Advisor
Chair of Committee

Ayusman Sen
Distinguished Professor of Chemistry

Raymond E. Schaak
Professor of Chemistry

Robert J. Santoro
George L. Guillet Professor of Mechanical Engineering

Barbara J. Garrison
Shapiro Professor of Chemistry
Head of the Department of Chemistry

*Signatures are on file in the Graduate School

ABSTRACT

The following dissertation presents mass spectrometric and theoretical investigations of metal oxide cationic clusters reacting with various molecules of interest. Gas-phase clusters model catalytic active sites, the following studies determine the molecular level interactions occurring in catalytic mechanisms. There is a focus on investigating various forms of activated oxygen species as well as identifying similarities in reactivity between ions of isovalent character.

Investigations of titanium oxide cationic clusters utilize a guided ion beam mass spectrometer to determine if pronounced reactivity occurs upon the introduction of CO, C_2H_2, C_2H_4, and C_3H_6. $Ti_2O_4^+$ and to a lesser extent TiO_2^+, are identified to preferentially transfer oxygen to the molecules of interest. Density functional calculations determine an oxygen centered radical located within the $Ti_2O_4^+$ cluster to be responsible for the observed oxygen transfer.

With the goal of identifying other forms of activated oxygen in mind, additional mass spectrometric and theoretical studies of $Zr_xO_{2x+1}^+$ (x = 1-3) clusters are performed. Calculations determine the cluster structures containing two oxygen atoms sharing a spin unpaired electron known as a superoxide (O_2^-). Experiment and theory provide evidence that the size of the cluster has marked influence over the reactivity properties towards C_3H_6, C_4H_6, and C_2H_2. In particular, $Zr_2O_5^+$ is highly reactive for the oxidation of the three hydrocarbons while ZrO_3^+ only presents substantial reactivity towards butadiene. In addition, $Zr_3O_7^+$ primarily associates the reactants, revealing only minor oxidation channels.

Replacements are sought for expensive group 10 metals in catalytic applications. A study is presented comparing the reactivity between Pd^+ and the isovalent ion ZrO^+ utilizing both experimental and theoretical means. The findings reveal common reactivity for the ions upon introduction of ethane and propane. The primary reaction mechanism observed is C—C cracking

while hydrogen abstraction is observed in appreciable quantities for both ions. It is proposed that the similar reactivity is due to ZrO^+ having molecular orbitals with 4d components that participate in the reaction in a similar way as the 4d orbitals of Pd^+.

Further investigations of isovalent ions are performed to extend the concept of superatomic mimics to systems of varied composition and larger size. This study investigates the reactivity of C_2H_4 and CO with the pairs NiO^+/TiO_2^+ and PdO^+/ZrO_2^+. A primary oxidation channel is observed for interaction of C_2H_4 with both pairs creating acetaldehyde as the most energetically favorable product while all species exhibit limited oxygen transfer to CO. These investigations provide several examples in which the reactivity of early transition metal species have been modified through the addition of a nonmetallic component and present similar characteristics to group 10 species.

TABLE OF CONTENTS

LIST OF FIGURES

LIST OF TABLES

ACKNOWLEDGEMENTS

Many thanks are owed to the people whom have aided in my research, provided guidance throughout my academic career, and given support during difficult times. As I would not have begun my career as a graduate student without the support of my family I will start by offering my enduring gratitude to my sister Ashley, brother Dustin, mother Dorothea, and father Keith. Your continued guidance has been a key to my success.

I have great appreciation for the work of my collaborators. Professor Shiv N. Khanna and Dr. Arthur C. Reber of Virginia Commonwealth University provided significant insight into our research through their theoretical contributions as well as many thought provoking interactions. I thank the members of the Bonačić-Koutecký group at the Humboldt-University Berlin for their hospitality during my many visits. Specifically, Professor Vlasta Bonačić-Koutecký, Dr. Roland Mitrić, Dr. Melanie Nößler, and Sabine Rabe who performed many of the calculations in this dissertation and took part in drafting our manuscripts.

My coworkers in the Castleman Group have been enormously valuable by aiding in developing chemical theories and providing guidance during instrumental difficulties. A special thanks to Dr. Grant Johnson for mentoring me during my early years of graduate school. I am grateful for the wonderful friends I've had and the outstanding times we've shared, they have made my time as a graduate student much more enjoyable.

Finally, I would like to express my deepest gratitude to Prof. A. W. Castleman Jr. He has presented me with innumerable opportunities to grow as a researcher, continually challenged my abilities, and provided me the freedom to perform many self guided studies. I owe my drive for scientific discovery and abilities as a researcher to the years spent in his group.

Chapter 1

Introduction

1.1 Clusters as a Model for Catalytic Sites

Catalyst selection has been largely based on the empirical observation of large batches of samples that determine the influence of preparation methods and reaction conditions, however little account is taken of the active site specific reactivity relationships. The ideal method of catalyst development is to tailor atomically the structure of an active catalyst so as to convert reactants directly to products without the creation of co-products, that typically go on to become waste.[1] Advances in surface characterization techniques have made possible the investigation of model catalytic systems for the identification of reactive sites.[2] Detailed reaction mechanisms can be elucidated through the investigation of gas-phase clusters that model catalytic active sites. Through tandem mass spectrometry, gas-phase clusters of specified size, stoichiometry, composition, and charge state may be selected and reacted under controlled conditions with a molecule of interest to determine their reactivity.[3] This method of investigation has become popular and a wealth of detailed studies have been performed probing ion-molecule reactions.[3-4] Gas-phase studies provide direct insight into reactivity patterns, elementary steps, and structure-reactivity relationships that are necessary for the directed design of improved catalysts.[4,5]

On the molecular level, a heterogeneous catalytic process is plainly the interaction of adsorbed species at a surface site that promotes a chemical reaction. A cluster of several atoms provides a simple model of a surface site in catalytic processes.[6] Clusters are large enough to allow for charge donation or withdrawal by neighboring atoms, as well as rearrangement of reactants, that are phenomena important to heterogeneous catalytic processes. Furthermore,

catalytic reaction in bulk systems is enabled by cluster-like surface chemical bonds involving a surface metal and its next nearest neighbors.[2,6] In fact, the vibrational spectrum of chemisorbed ethylidyne on a bulk rhodium surface is nearly identical to that of an organometallic cluster containing ethylidyne attached to three rhodium atoms.[7] Thus, the interaction of reactant molecules with a cluster is an effective approximation for the process of chemisorption on a surface.

Numerous sub-nanometer sized clusters have been found to be catalytically active species when deposited on a surface.[8] Thus, in addition to modeling interactions at surface active sites, gas-phase investigations show potential for identifying species with enhanced catalytic activity for deposition on a surface as the active catalytic material. In the context of deposited clusters, charging effects from substrate to supported active catalytic clusters have been observed;[9,10] while, the gas-phase investigation of size selected clusters has identified the influence of charge transfer on the activation of molecules such as O_2.[11] Additionally, cluster studies have revealed the effect of charge state on the course of numerous oxidation mechanisms.[12,13] Gas-phase reactivity studies have been fruitful in identifying many cluster species with potential as active sites responsible for a variety of catalytic reactions and have contributed to the further development of the knowledge of fundamental molecular level interactions through guided-ion-beam mass spectrometry (GIB-MS) investigations.

Experimental methods in the field of gas-phase cluster research have broadened the capabilities to model catalytic active sites and enhanced the fundamental knowledge of catalytic processes. Studies are capable of determining reaction kinetics,[14,15] temporal dynamics,[16] intermediate complexes,[17] competing mechanisms,[18] and adsorption energies[19] thus providing a better understanding of molecular-scale interactions. Gas-phase experiments are also capable of investigating neutral clusters providing complementary mechanistic insight to ionic cluster reactivity.[20] Furthermore, the reduced size and finite electron count of gas-phase clusters are

easily modeled through theoretical methods, that provide complementary reaction profiles for a detailed understanding of the reactions.[4,21-23] Ion-molecule investigations in concert with computational studies can provide fundamental details of structure-reactivity relationships in catalytic mechanisms necessary for the directed design of improved catalysts.

Following will be an introduction of current catalytic processes and an outlook on future research directions. Sections will cover catalysis in industrial manufacturing, fuel production, and combustion processes; environmentally driven catalysis; unique catalytic properties of nanoparticles; and the replacement of expensive precious metals in catalysis. Lastly, a synopsis of each chapter is presented.

1.2 Catalysis in Industrial Manufacturing, Fuel Production, and Combustion Processes

Catalysis is an ever growing field of study aimed at exerting control over a chemical reaction through application of a non-consumed reagent. According to the council for chemical research,[24] 60 percent of today's chemical products and 90 percent of current chemical processes are catalyst based. Heterogeneous catalysts are employed to aid in a variety of reactions including oxidation, C-C bond cracking, C-H bond cleavage, cyclization, and isomerization among others.[25] Due to the prevalence of catalyst-based chemical processes in industry, fundamental research probing catalytic mechanisms will be greatly beneficial for increasing efficiency and overall yield of chemical processes.

Aspects of daily life are deeply influenced by catalytic processes, including energy sources, food supply, and the production of various plastic and synthetic materials. Of note, the fixation of nitrogen through the Haber-Bosch process is utilized in the production of agricultural fertilizers that has been linked to a large increase in global population.[26] This process employs an iron surface to initiate dissociation of both N_2 and H_2 in the formation of ammonia.[27,28] Gas-phase

investigations have studied the dissociation of H_2[29,30] on $Fe_n^{+/-}$ clusters and other transition metal clusters[31,32] in an effort to develop a fundamental understanding of the Haber-Bosch process. Such achievements will be needed to improve catalytic technology and keep production rates of fertilizers on pace with the growing global population.

Furthermore, as the global population continues to increase, larger quantities of refined hydrocarbons will become essential as both a transportation fuel and chemical feedstock. The process of reforming petrochemicals for the production of various aromatic feedstocks and transportation fuels is conducted over a multifunctional catalyst consisting of group 10 metals, zeolite supports, and other active components.[33,34] The formation of aromatics from alkanes is the core reaction in the reforming process that has driven substantial catalytic research since the early 1960s. Factors including structure sensitivity and acidic sites have been examined and their influence in catalytic reforming determined. However, further research may increase the selectivity of the process, reduce the degradation of catalyst by coke formation, and lower the operating temperatures of the reaction. Fine chemicals manufacturing also requires the use of catalysts to increase reaction rates and product selectivity to a profitable level.[33] For example, studies have shown vanadium oxide surfaces to be active for the oxidation[35] and oxidative dehydrogenation[36] of hydrocarbons. Through gas-phase investigations, radical oxygen species have been identified as the active site for both reaction mechanisms.[37,38] Identification of active sites involved in various oxidation, dehydrogenation, and cracking reactions can be determined through GIB-MS investigations. Such knowledge is necessary for the design of tailored catalysts.

Novel applications of catalytic materials are being identified in combustion processes. Catalysis presents a method of increasing the ignition rate and combustion kinetics of high energy density fuels.[39] Additionally, many combustion processes benefit from thermal cracking mechanisms.[40] Nanocatalysts are proposed to act as initiators of endothermic catalytic cracking

reactions. Mass spectrometric investigations of metal and metal oxide ions are able to investigate and model such cracking processes while comparing rate constants between systems of interest.

These examples highlight the importance of catalytic technology to industrialized society. Continued research will provide fundamental molecular level insights of catalytic mechanisms for the development of catalytic materials possessing increased activity and selectivity beyond their predecessors.

1.3 Environmentally Driven Catalysis

Early catalysts were developed through empirical means for the sole purpose of increasing the reaction rate of a chemical process. These catalysts were proficient at increasing the rate of reaction, yet lacked selectivity towards a desired product and an abundance of co-products were created. As environmental concerns have grown due to issues including acid rain, depletion of ozone, and pollution of drinking water, catalytic processes have been improved to display a higher selectivity and thus create fewer co-products. To improve selectivity, research has moved from empirical observations to the study of molecular-scale interactions between active site and reactant.

In addition to improving the activity and selectivity of industrial chemical processes, catalytic technology has also been employed for the remediation of pollutants from sources including combustion engines and industrial waste. For example, membranes containing titanium oxide nanoparticles show promise as catalysts for the degradation of pollutants in wastewater effluent.[41,42] Studies performed in our laboratory have investigated the oxidative properties of titanium oxide clusters and found those containing an oxygen centered radical to be highly active.[43] Researchers have also determined that supported transition metal catalysts are effective for the total oxidation of pollutant organic compounds.[44,45] In an effort to understand the

interactions occurring in this process, gas-phase investigations have determined the influence of charge state and cluster size on the activation and reactivity of O_2 in catalytic processes.[46,47]

In response to the detrimental effect of automobile exhaust on ambient air quality, the three way catalytic converter was developed for the oxidation of CO, hydrocarbons, and sulfurous compounds as well as the reduction of NO_x compounds.[48] The three way catalytic converter utilizes deposited nanoparticles of palladium, platinum, cerium and others as the active phases.[48] To determine the active site specific interactions occurring at various nanoparticles within the catalytic converter, gas-phase experiments investigated the reduction of NO_x compounds by CO to revealed the role of transition metal ions in the catalytic mechanism.[4] Such investigations provide for kinetic comparisons between the reactive nature of species of varying chemical composition, size, and charge state. Recent developments in catalytic technology have been directed toward green applications as concerns for the environment have grown in the late 20th century.

1.4 Unique Catalytic Properties of Nanoparticles

Impregnated and supported nanoparticles have long been used in industrial catalysts due to the high concentration of surface active sites present for the promotion of catalytic reactions; yet direct investigation of their properties has been impeded due to the complexity of these systems. Deposited nanoparticles on well defined surfaces are being employed as models of industrial catalysts to study various aspects of catalytic processes. Such investigations have led to the remarkable finding that supported gold nanoparticles are active in the catalytic oxidation of CO.[49,50] Bulk gold is commonly accepted as being unreactive; the reported catalytic activity of gold nanoparticles highlighted the unique properties of nanocatalysts. Furthermore, studies have found that the size of a gold nanoparticle has significant influence over the activity and selectivity

observed in a catalytic process.[33] Gas-phase investigations of ionic gold clusters have shed further light on the dependence size and charge state have on reactive properties while elucidating detailed reaction mechanisms.[47] Ionic silver clusters have also been investigated to determine the influence varying the species of interest has towards reactivity.[51] As interest in the catalytic properties of nanoparticles continues to grow, all means of study including GIB-MS should be utilized to develop a detailed understanding of the catalytic systems.

As properties of monometallic nanoparticles are becoming understood, interesting character has been observed from bimetallic nanoparticles due to the alloying of metals. For example, Au_xPd_{1-x} nanoparticles exhibit core-shell structures with Au-rich cores and Pd-rich shells that display higher turnover rates than the parent monometallic nanoparticles.[52] Investigations of well defined, mixed metal, ionic clusters are being performed in the gas-phase[47] to investigate unique catalytic properties obtained through the mixing of electronic states, thus creating new materials that hybridize the properties of the elemental components. Current research is proving that nano-structures have unique catalytic behavior apart from their bulk due to quantum confinement, a lower coordination number for surface atoms, as well as charging effects due to deposition on various supports.

1.5 Replacement of Expensive Precious Metal Catalysts

Precious metals are employed as the active phase in many catalytic processes due to their ability to promote reactivity. As mentioned earlier, platinum and palladium are both utilized in the three way catalytic converter. Additionally, platinum is active for the oxidative dehydrogenation of propane to propene[53] while supported size-selected palladium clusters promote the cyclotimerization of acetylene.[54] Due to limited supplies of precious metals, catalytic materials are often very expensive, limiting their widespread utility. The identification of

alternative active phases will have a great economic impact in both industrial chemical processes and environmental pollution remediation.

Investigations probing the catalytic behavior of various surfaces have identified similarities in their reactive nature. Of note, tungsten monocarbide surfaces exhibit platinum-like behavior for several reactions including methanol electrooxidation and 2,2-dimethylpropane isomerization.[55-57] The observed similarities are strongly influenced by surface composition as samples with different atomic ratio or impurities result in disparate products.[58] With the goal in mind of revealing the fundamental attributes leading to similarities in catalytic behavior, molecular level investigations of electronic structure and reactive properties were undertaken by our group.[59, 60] Common electronic transitions were observed between the photoelectron spectra of Pt^- and WC^-, confirming similarities between bulk surfaces and the atomic scale.[61] Furthermore, similarities in the electronic structure of additional isovalent species including Ni^- with TiO^- and Pd^- with ZrO^- were found.[62] Such composite entities that mimic the properties of specific elements have come to be known as "superatoms".[59] Gas-phase reactivity experiments probing the interaction of ethane and propane with the isovalence ions Pd^+ and ZrO^+ resulted in common C-C and C-H bond breaking products.[63] The concept of "superatoms" is continually being examined and extended to systems of larger and varied composition that is highlighted by the similar oxidative properties observed between the isovalent systems NiO^+ with TiO_2^+ and PdO^+ with ZrO_2^+.[64] These initial studies of superatoms are paving the way for the development of less costly catalytic materials and processes through the replacement of expensive precious metals.

1.6 Synopsis

The following dissertation reports the findings of gas-phase reactivity investigations probing model catalytic active sites with the intention of developing further fundamental insights of reaction mechanisms. Activated oxygen species are essential to many catalytic processes; herein, several forms of activated oxygen are studied to identify differences in reactive nature as well as determine the influence the surrounding environment imparts. In particular, titanium oxide clusters containing an oxygen centered radical (O^-) are investigated and compared with radical oxygen containing zirconium oxide clusters that have been previously studied. Additionally, superoxide units (O_2^-) are identified on a series of zirconium oxide clusters and studies are performed to determine their reactive nature. These forms of activated oxygen are highly reactive but differ greatly in the oxidation processes they participate in.

Common electronic transitions between isovalent ions were observed through photoelectron spectroscopy. Reactivity investigations have explored several isovalent systems and similar reaction mechanisms are detailed in this dissertation. Of interest, early transition metal-oxide superatomic mimics are discussed as possible replacements for group 10 metal species in catalytic applications.

Chapter 2 describes the results of a combined GIB-MS and density functional study probing the interaction of stoichiometric titanium oxide cationic clusters with the molecules CO, C_2H_2, C_2H_4, and C_3H_6. An oxygen centered radical on $Ti_2O_4^+$ is responsible for selective oxidation of the reactants. The results of density functional theory (DFT) calculations are presented as energy profiles and MD simulations that reveal the mechanisms of the reactions.

Chapter 3 presents the structure and reactivity properties of a series of clusters $Zr_xO_{2x+1}^+$ ($x = 1 – 3$) that have been investigated using DFT calculations and guided-ion-beam mass spectrometry. This series of clusters are determined through DFT to contain a superoxide unit

(O_2^-) that is an active site for oxidation. Experiment and theory provide evidence that the size of the cluster has marked influence over the reactivity properties towards C_3H_6, C_4H_6, and C_2H_2.

Within Chapter 4, the superatomic concept is tested by comparing the reactivity of ZrO^+ with the isovalent ion Pd^+ in a synergistic study employing GIB-MS in conjunction with theoretical investigations. The findings reveal similar reactivity patterns for both ethane and propane with the scission of a C-C bond being the primary reaction mechanism for the interaction of both gases with ZrO^+ and Pd^+. Hydrogen abstraction is also observed with similar branching ratios for both ions. It is proposed that the similar reactivity is due to ZrO^+ having molecular orbitals with 4d components that participate in the reaction in a similar way as the 4d orbitals of Pd^+.

Chapter 5 further explores the reactivity of superatomic mimics through GIB-MS and DFT calculations of the isovalent pairs PdO^+ with ZrO_2^+ and NiO^+ with TiO_2^+. Branching ratios and calculated reaction profiles present enhanced oxidation mechanisms for the interaction of the ions with ethene while being unreactive towards CO. Of interest, the group 10 metal oxide congeners begin in the quartet state and undergo a spin-crossover to the doublet state, that increases the exothermicity of the process and provides a pathway with surmountable transitions for the creation of acetaldehyde. It is shown that the general concept of isovalent mimics can be extended to more complex systems in the frameworks of reactive characteristics and electronic properties.

Chapter 6 presents concluding remarks and discusses future directions of GIB-MS studies for the investigation of catalytic model systems.

1.7 References

1. van Santen, R. A.; Neurock, M. *Molecular Heterogeneous Catalysis* WILEY-VCH: Weinheim, 2006; 47-61.
2. Somorjai, G. A.; Li, Y. *Introduction to Surface Chemistry and Catalysis;* 2nd edition; John Wiley & Sons, Inc.: Hoboken, NY, 2010; 443-447.
3. Bell, R. C.; Zemski, K. A.; Justes, D. R.; Castleman, A. W., Jr. *J. Chem. Phys.* **2001**, *114*, 798.
4. Böhme, D. K.; Schwarz, H. *Angew. Chem. Int. Ed.* **2005**, *44*, 2336.
5. Johnson, G. E.; Mitrić, R.; Bonačić-Koutecký, V.; Castleman, A. W., Jr., *Chem. Phys. Lett.* **2009**, *475*, 1.
6. Muetterties, E. L. *Science* **1977**, *196*, 839.
7. Somorjai, G. A. *J. Phys. Chem.* **1990**, *94*, 1013.
8. Herzing, A. A.; Kiely, C. J.; Carley, A. F.; Landon, P.; Hutchings, G. J. *Science* **2008**, *321*, 1331.
9. Sterrer, M.; Risse, T.; Pozzoni, U. M.; Giordano, L.; Heyde, M.; Rust, H.-P.; Pacchioni, G.; Freund, H.-J. *Phys. Rev. Lett.* **2007**, *98*, 096107.
10. Giordano, L.; Pacchioni, G.; Goniakowski, J.; Nilius, N.; Rienks, E. D. L.; Freund, H.-J. *Phys. Rev. Lett.* **2008**, *101*, 026102.
11. Hagen, J.; Socaciu, L. D.; Le Roux, J.; Popolan, D.; Bernhardt, T. M.; Wöste, L.; Mitrić, R.; Noack, H.; Bonačić-Koutecký, V. *J. Am. Chem. Soc.* **2004**, *126*, 3442.
12. Johnson, G. E.; Mitrić, R.; Nößler, M.; Tyo, E. C.; Bonačić-Koutecký, V.; Castleman, A. W., Jr. *J. Am. Chem. Soc.* **2009**, *131*, 5460.
13. Johnson, G. E.; Mitrić, R.; Tyo, E. C.; Bonačić-Koutecký, V.; Castleman, A. W., Jr. *J. Am. Chem. Soc.* **2008**, *130*, 13912.

14. Lang, S. M.; Bernhardt, T. M.; Barnett, R. N.; Landman, U. *Angew. Chem. Int. Ed.* **2010**, *49*, 980.

15. Rothgeb, D. W.; Hossain, E.; Kuo, A. T.; Troyer, J. L.; Jarrold, C. C.; Mayhall, N. J.; Raghavachari, K. *J. Chem. Phys.* **2009**, *130*, 124314.

16. Lang, S. M.; Bernhardt, T. M. *J. Chem. Phys.* **2009**, *131*, 024310.

17. Lang, S. M.; Bernhardt, T. M.; Barnett, R. N.; Yoon, B.; Landman, U. *J. Am. Chem. Soc.* **2009**, *131*, 8939.

18. Shayesteh, A.; Lavrov, V. V.; Koyanagi, G. K.; Bohme, D. K. *J. Phys. Chem. A* **2009**, *113*, 5602.

19. Armentrout, P. B.; Ervin, K. M.; Rodgers, M. T. *J. Phys. Chem. A* **2008**, *112*, 10071.

20. Dong, F.; Heinbuch, S.; Xie, Y.; Rocca, J. J.; Bernstein, E. R.; Wang Z.-C.; Deng, K.; He, S.-G. *J. Am. Chem. Soc.* **2008**, *130*, 1932.

21. Nößler, M.; Mitrić, R.; Bonačić-Koutecký, V.; Johnson, G. E.; Tyo, E. C.; Castleman, A. W., Jr. *Angew. Chem. Int. Ed.* **2010**, *49*, 407.

22. Dietl, N.; Höckendorg, R. F.; Schlangen, M.; Lerch, M.; Beyer, M. K.; Schwarz, H. *Angew. Chem. Int. Ed.* **2011**, *50*, 1430.

23. Roach, P. J.; Woodward, W. H.; Castleman, A. W., Jr.; Reber, A. C.; Khanna, S. N. *Science* **2009**, *323*, 492.

24. Chemicals Industry Catalysis Workshop Report. http://www.ccrhq.org (accessed November 3, 2010).

25. Armor, J. N. *Catal. Today* **2011**, *163*, 3.

26. Ertl, G. *Angew. Chem.* **2008**, *47*, 3524.

27. Mahdi, W.; Schütze, J.; Weinberg, G.; Schoonmaker, R.; Schlögl, R.; Ertl, G. *Catal. Lett.* **1991**, *11*, 19.

28. Somorjai, G. A. *Introduction to Surface Chemisry and Catalysis*, John Wiley & Sons, Inc.: New York, **1994**; 485.

29. Swart, I.; de Groot, F. M. F.; Weckhuysen, B. M.; Gruene, P.; Meijer, G.; Fielicke, A. *J. Phys. Chem. A* **2008**, *112*, 1139.

30. Whette, R. L.; Cox, D. M.; Trevor, D. J.; Kaldor, A. *Phys. Rev. Lett.* **1985**, *54,* 1494.

31. Berces, A.; Hackett, P. A.; Lian, L.; Mitchell, S. A.; Rayner, D. M. *J. Chem. Phys.* **1998**, *108*, 5476.

32. Armentrout, P. B. *Annu. Rev. Phys. Chem.* **2001**, *52*, 423.

33. *Supported Metals in Catalysis*; Anderson, J. A., García, M. F., Eds.; Imperial College Press: Singapore, 2005.

34. Marcilly, C. *J. Catal.* **2003**, *216*, 47.

35. Oyama, S. T.; Middlebrook, A. M.; Somorjai, G. A. *J. Phys. Chem.* **1990**, *94*, 5029.

36. Čapek, L.; Adam, J.; Grygar, T.; Bulánek, R.; Vradman, L.; Košová-Kučerová, G.; Čičmanec, P.; Knotek, P. *Appl. Catal. A* **2008**, *342*, 99.

37. Moore, N. A.; Mitrić, R.; Justes, D R.; Bonačić-Koutecký, V.; Castleman, A. W., Jr. *J. Phys. Chem. B* **2006**, *110*, 3015.

38. Feyel, S.; Döbler, J.; Schröder, D.; Sauer, J.; Schwarz, H. *Angew. Chem. Int. Ed.* **2006**, *45*, 4681.

39. Van Devener, B.; Anderson, S. L. *Energy Fuels* **2006**, *20*, 1886.

40. Wickham, D. T.; Engel, J. R.; Hitch, B. D. Karpuk, M. E. *J. Propul. Power* **2001**, *17*, 1253.

41. Kim, J.; Van der Bruggen, B. *Environ. Pollut.* **2010**, *158*, 2335.

42. Zhang, X.; Du, A. J.; Lee, P.; Sun, D. D.; Leckie, J. O. *Appl. Catal. B* **2008**, *84*, 262.

43. Tyo, E. C.; Nößler, M.; Mitrić, R.; Bonačić-Koutecký, V.; Castleman, A. W., Jr. *Phys. Chem. Chem. Phys.* **2011**, *13*, 4243.

44. Choudhary, T. V.; Banergee, S.; Choudhary, V. R. *Appl. Catal. A* **2002**, *234*, 1.

45. Garcia, T.; Solsona, B.; Cazorla-Amorós, D.; Linares-Solano, Á.; Taylor, S. H. *Appl. Catal. B* **2006**, *62*, 66.

46. Socaciu, L.D.; Hagen, J.; Bernhardt, T. M.; Wöste, L.; Heiz, U.; Häkkinen, H.; Landman, U. *J. Am. Chem. Soc.* **2003**, *125*, 10437.

47. Bernhardt, T. M. *Int. J. Mass Spectrom.* **2005**, *243*, 1.

48. Rothenberg, G. *Catalysis: Concepts and Green Applications*, Wiley-VHC, Weinheim, **2008**.

49. Haruta, M.; Kobayashi, T.; Sano, H.; Yamada, N. *Chem. Lett.* **1987**, *2*, 405.

50. Haruta, M.; Yamada, N.; Kobayashi, T.; Iijima, S. *J. Catal*. **1989**, *115*, 301.

51. Popolan, D. M.; Bernhardt, T. M. *J. Chem. Phys.* **2011**, *134*, 091102.

52. Alayoglu, S.; Tao, F.; Altoe, V.; Specht, C.; Zhu, Z.; Aksoy, F.; Butcher, D. R.; Renzas, R. J.; Liu, Z.; Somorjai, G. A. *Catal. Lett.* **2011**, *141*, 633.

53. Vajda, S.; Pellin, M. J.; Greeley, J. P.; Marshall, C. L.; Curtiss, L. A.; Ballentine, G. A.; Elam, J. W.; Catillon-Mucherie, S.; Redfern, P. C.; Mehmood, F.; Zapol, P. *Nature Mater*. **2009**, *8*, 213.

54. Abbet, S.; Sanchez, A.; Heiz, U.; Schneider, W.-D.; Ferrari, A. M.; Pacchioni, G.; Rösch, N. *J. Am. Chem. Soc.* **2000**, *122*, 3453.

55. Levy, R. B.; Boudart, M. *Science* **1973**, *181*, 547.

56. Weigert, E. C.; Stottlemyer, A. L.; Zellner, M. B.; Chen, J. G. *J. Phys. Chem. C* **2007**, *111*, 14617.

57. Leclercq, L.; Imura, K.; Yoshida, S.; Barbee, T.; Boudart, M. "Preparation of Catalysis II" (B. Delmon, P. Grange, P. A. Jacobs, and G. Poncelet, Eds.), p. 627. Elsevier, Amsterdam, 1978.

58. Ross, P. N., Jr.; Stonehart, P. *J. Catal.* **1975**, *39*, 298.

59. Castleman, A. W., Jr. *J. Phys. Chem. Lett.* **2011**, *2*, 1062.

60. Castleman, A. W., Jr. *Catal. Lett.* **2011**, *141*, 1243.

61. Peppernick, S. J.; Gunaratne, K. D. D.; Castleman, A. W., Jr. *Chem. Phys. Lett.* **2010**, *489*, 1.

62. Peppernick, S. J.; Gunaratne, K. D. D.; Castleman, A. W., Jr. *PNAS* **2010**, *107*, 975.

63. Tyo, E. C.; Reber, A. C.; Khanna, S. N.; Castleman, A. W., Jr. *J. Phys. Chem. C.* **2011**, *115*, 16797.

64. Tyo, E. C.; Nößler, M.; Rabe, S.; Harmon, C. L.; Mitrić, R.; Bonačić-Koutecký, V.; Castleman, A. W., Jr. *Phys. Chem. Chem. Phys* (accepted 2011).

Chapter 2

Reactivity of Stoichiometric Titanium Oxide Cations

2.1 Introduction

Heterogeneous catalysts are widely used in the large majority of industrial chemical processes, playing an important role in improving efficiency and reducing energy requirements.[1] The latter is an issue of major importance to industrial nations. Furthermore, catalysts play an increasing role in energy production, particularly in the development of alternative energy sources, and in the area of environmental remediation as well.[2] Despite the importance of catalysis to modern society, the current approach to developing and improving catalytic materials is still largely phenomenological in nature.[3]

It has been recognized that a molecular level understanding of factors influencing catalytic reactions must be attained in order to enable the rational design of catalysts that exhibit improved activity and selectivity.[4] Especially important is the identification of species having highly active and selective reaction sites that enhance specific classes of reaction, nanocatalysts are increasingly recognized to be of particular value in controlling product selectivity due to their unique structure and electronic properties.[5-7]

There are numerous approaches to attaining the goal of elucidating the basic mechanisms by which catalysts function. One of these involves detailed investigation of chemical interactions of deposited species having selected size, composition and structure, that can serve to influence specific reaction mechanisms through the lowering of energy barriers to a particular reaction.[8,9]

The approach of studying isolated gas-phase cluster reactions is particularly valuable in this regard where the role of composition, structure and charge-state may be readily investigated experimentally and treated theoretically.[10-12]

A study of the interaction of mass selected gas-phase metal and metal-oxide cluster ions with selected molecules is a valuable approach as the reactions of such species can thereby be investigated under well-defined conditions. Hence the influence of impurities and ill-defined surface inhomogeneities often encountered in condensed phase experiments can be eliminated.[13,14] The versatility of gas-phase studies enables a determination of the effect that size, stoichiometry, charge state, oxidation state, and degree of coordinative saturation have upon reactivity with various organic molecules.[15] At the same time the individual gas-phase mechanisms are amenable to theoretical investigation of the operative structure-reactivity relationships as well as the energetics of the mechanisms responsible for oxidation reactions.[16] We acquire benefit from collaborative undertakings of experimental and theoretical groups[10,16,17], in order to elucidate processes of importance.

A recent experimental and theoretical study published by our laboratory identified a series of positively charged stoichiometric zirconium oxide clusters $(ZrO_2)^+_x$ (x= 1 – 4) that served to enhance important oxidation reactions involving carbon monoxide and hydrocarbons (ethene and acetylene).[17] The identified structure-reactivity relationships revealed, within the series of clusters, the presence of a radical oxygen center with an elongated zirconium–oxygen bond that functioned as a reactive site. Hence they were identified as potentially good candidates for incorporation into a nanocatalyst. A catalytic cycle could be acquired by employing a strong oxidizer to regenerate the active stoichiometric clusters. In this context, findings revealing the role of radical oxygen centers in influencing the reactivity of charged systems prompted us to extend this concept to a consideration of binary neutral metal oxides based on the same total

electron count[18] and to carry out further investigations to determine if other clusters might also display similar catalytic-like behavior.

The investigation of titanium oxide is important since it has been utilized for catalytic purposes as both a support and active material.[19,20] Findings from recent studies have reported that Au/TiO_2 promotes the synthesis of aromatic azo compounds[21] and that TiO_2 itself can cleave the N=N double bond of azobenzene.[22] Also, mass selected gas-phase experiments have found TiO_2^+ to be capable of abstracting an H atom from water and methane.[23] Due to titanium and zirconium being congeners, they contain similar valence electron shells (Ti: $4s^2 3d^2$, Zr: $5s^2 4d^2$) and hence it was an interesting open question if the series $(TiO_2)^+_x$ would also contain oxygen centered radical active sites and therefore display enhanced reactivity, as well.

This question prompted the current study designed to investigate the reactive mechanisms and products arising from the interaction of titanium oxide cationic clusters with CO, C_3H_6, C_2H_2, and C_2H_4. A particular objective is to discover species that are highly oxidative. Experimental findings are presented in the form of branching ratios that compare the normalized intensities of reactants and products vs. the concentration of reactants, thus identifying reactivity for selected clusters. Theoretical investigations of structures and energy profiles for oxidation reactions, together with molecular dynamics simulations, provide insight about responsible mechanisms.

The chapter is structured as follows: experimental and computational methods are first described, where after results are presented that focus primarily on $Ti_2O_4^+$ reactivity with CO and subsequently on the reactivity of the aforementioned hydrocarbons.

2.2 Experimental Methods

The reactivity of cationic titanium oxide clusters with CO, C_3H_6, C_2H_2, C_2H_4, and N_2O was studied utilizing a guided-ion-beam mass spectrometer that has been thoroughly described in

a publication[24] and depicted in Figure 2-1. Titanium oxide clusters were produced in a laser vaporization (LaVa) source via pulsing of a 13.2 atm expansion gas, composed of oxygen seeded in helium, into the plasma created via ablation of a 1/8" titanium rod (99.95%, Research and PVD Materials Corp.) by the second harmonic (532 nm) of a Nd:YAG laser (Specra-Physics, INDI-50) operating at 20 Hz. LaVa sources are a well established means of creating thermalized clusters over a wide range in sizes; reviews have been written on the topic.[25] The expansion gas is introduced to the LaVa source by a pulse valve (General Valve, Series 9, 28V) and composed of ultra high purity oxygen (99.993%, GT&S Welco) and high purity helium (99.99%, Praxair). A range of mixtures were tested having 1% to 10% oxygen contribution. The expansion gas composed of 5% oxygen seeded in helium created the clusters TiO_2^+ and $Ti_2O_4^+$ in the highest abundance. The reactant gases used in this investigation are CO (99.9%, GT&S Welco), C_3H_6 (99.0%, GT&S Welco), C_2H_2 (99.6%, GT&S Welco), C_2H_4 (99.9%, GT&S), N_2O (99.6%, MG Industries), and Xe (99.999%, GT&S Welco).

The clusters pass through a channel at the exit of the source and are cooled by supersonic expansion into vacuum.[26] The high pressure of the expansion gas (13.2 atm) passing into a low pressure field free region decreases the internal vibrational and rotational energy of the clusters through three body collisions. The addition of a nozzle at the exit of the source will influence the distribution of clusters created. The length and diameter of a nozzle will affect the number of collisions occurring between atoms in the high pressure source region and change the cluster distribution obtained. Typically a longer and narrower nozzle will create larger clusters as well as clusters with a higher oxygen concentration. In this experiment a broad distribution of clusters were created without the use of a nozzle. A pattern generator is also used to control the timing of events within the source region, adjusting the opening of the pulse valve in relation to interaction of the laser with the metal rod will influence the distribution of clusters created within the LaVa

source. Optimum conditions for this study are reached when the pulse valve opens at a delay of 10 μs and the laser is delayed by 5000 μs.

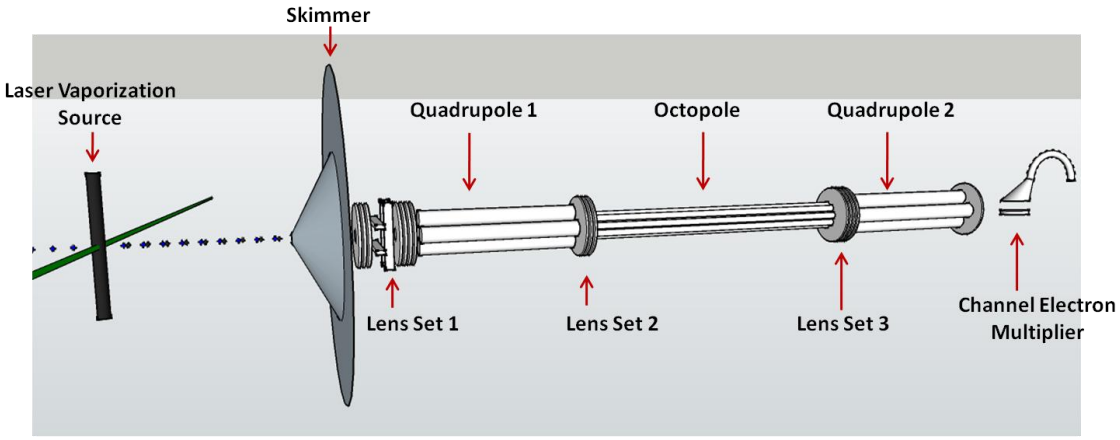

Figure 2-1. Guided-Ion-Beam Mass Spectrometer

The clusters proceed through a 3 mm skimmer creating a collimated molecular beam and are directed by a set of electrostatic lenses into a quadrupole mass filter. The voltage applied to each lens is adjusted before every experiment to optimize the ion current. The mass to charge (m/z) ratio differs as the size of a cluster is varied, thus a voltage will not have the same focusing effect for each cluster. All lenses in the instrument are powered by 205B-01 Bertan power supplies (0-1 kV, 0-30 mA). The quadrupole mass filter[27] (9.5mm, Extrel Inc.) permits clusters of a desired m/z ratio to pass into an octopole reaction cell (Extrel Inc.). A home-built rf generator based on the design of Anderson[28] supplies the rf and dc potentials to operate the octopole reaction cell.

At varying pressures the neutral reactants CO, C_3H_6, C_2H_2, C_2H_4, or N_2O are admitted to the reaction cell utilizing a low flow metering valve (Swagelok) to determine the reactivity and structural characteristics of the clusters. An MKS Baratron capacitance manometer is used to monitor the pressure of reactant introduced. A potential of zero volts is applied to the injection

lens before the collision cell and the dc float voltage applied to the octopole ion guide so the clusters react at thermal energies. The product ions are extracted from the octopole and flow into a second quadrupole mass filter (9.5mm Extrel Inc.) that scans a m/z range of 40-740 amu to perform product mass determination.

The resultant ions are detected by a channel electron multiplier (CEM) (Detector Technology, Inc., model XP-2145). The conversion dynode is powered by a Bertran Inc., High Voltage Power Supply (Model 210-10R) up to ± 8000 V. The electron multiplier is operated at a maximum voltage of -4000 V on the front of the cone to ground at the rear (John Fluke MFG. Co., Inc., Model 408A DC Power Supply). The ion signal is filtered and transferred to a TTL signal by a MIT Inc., F-100T Amplifier-Descriminator. The filtered signal is sent to a multichannel scalar card (Tennelec/Nucleus, Inc., MCS-II) to view mass spectra. The data is further analyzed with the Grams/32 software for integration of peak intensities.

A retarding potential analysis previously performed in our laboratory has determined that the energy imparted upon the clusters exiting the LaVa source is around 1 eV in the laboratory frame.[24] The supersonic expansion imparts nearly equivalent kinetic energy on all clusters exiting the source. The initial center of mass frame energy (E_{CM}) calculated for the reaction of CO, C_2H_2, and C_2H_4 with TiO_2^+ and $Ti_2O_4^+$ is roughly 0.26 eV and 0.15 eV, respectively. Interaction between propene and the ions TiO_2^+ and $Ti_2O_4^+$ is slightly more energetic, 0.35 eV and 0.21 eV, respectively.

$$E_{CM} = E_{LAB} \frac{Mass\,[Reactant\,Gas]}{Mass\,[Cluster] + Mass\,[Reactant\,Gas]} \qquad (2.1)$$

The E_{CM} is an estimated upper limit for the energy of interaction. As collisions dissipate the initial energy, subsequent interactions will occur at lower energy.

The experimental branching ratios presented in Section 2.4 depict the normalized ion intensities of products and reactants detected at increasing pressures of neutral reactant. It can be seen that for reactive species, an increase of neutral reactant in the collision cell results in a concomitant rise in products while the parent species decreases in intensity. Collision induced dissociation (CID) experiments are performed introducing inert xenon at varying pressures to the clusters of interest. CID investigations are performed to confirm that detected product ions are indeed due to chemical reactivity and not collisional fragmentation. The mass coincidence of three oxygen atoms and one titanium atom presents a problem when mass selecting clusters containing multiple titanium atoms. Our LaVa source is capable of creating clusters with high oxygen content for example TiO_7^+ that is coincident with $Ti_2O_4^+$. Interaction with xenon confirmed that multiple O_2 units were being lost for the initial studies of $Ti_2O_4^+$, thus the mass coincidence TiO_7^+ cluster was also being created as loss of multiple O_2 units from the stable $Ti_2O_4^+$ cluster is unfavorable. Through tailoring our source conditions the creation of TiO_7^+ has been limited to a negligible quantity. It is determined that low laser fluence (25.5 mW) promotes creation of TiO_7^+. Experiments are performed with a high laser fluence (155 mW) that is effective at limiting the quantity of TiO_7^+ created. Some reactions revealed minor O_2 loss products attributed to collisional dissociation of the TiO_7^+ cluster and are not discussed further.

2.3 Theoretical Calculations

Calculations are performed by the Bonačić-Koutecký group at the Humboldt Universität zu Berlin that compliment experimental results and provide mechanistic detail of reaction processes. The structural properties of the cationic $(TiO_2)_x^+$ (x = 1-2) clusters and their reactivity toward CO, C_3H_6, C_2H_2, C_2H_4 and N_2O are studied using DFT method with the hybrid B3LYP functional.[29-31] For the titanium atoms a triple-ζ-valence-plus-polarization (TZVP) atomic basis

set combined with the Stuttgart group 12-electron relativistic effective core potential (12e-RECP) is employed.[32-35] For the carbon, oxygen, hydrogen and nitrogen atoms the TZVP basis sets are used.[36] Previous studies of the reactivity of transition metal oxides have shown that such a combination of hybrid density functionals with triple zeta quality basis sets allow reliable prediction of the reaction energetics and mechanisms.[10,16-18,37] All structures presented are fully optimized using gradient minimization techniques and stationary points are characterized as minima or transition states by calculating the frequencies. Moreover, the reaction mechanisms are determined by calculating the energy profiles based on DFT energies. The proposed reaction mechanisms are also confirmed by performing ab-initio molecular dynamics (MD) simulations "on the fly" based on the DFT method. Newton's equations of motion are solved using the Verlet algorithm with time steps of 1 fs and the forces are calculated employing the analytical energy gradients in the framework of the TURBOMOLE program.[38] The MD simulations performed at constant energy or at constant temperature allow the rearrangements of bonds along the reaction pathways to be followed. For further details refer to the figure captions. In order to improve the efficiency of the calculations, the resolution of identity (RI)-DFT procedure[39,40] is employed involving the Perdew-Burke-Ernzerhof (PBE) functional.[40] In order to verify the accuracy of the functional, a previous comparison[16] is performed of the structural properties as well as energy profiles obtained from DFT calculations using the B3LYP and the PBE functional and found good agreement.

2.4 Results and Discussion

Titanium oxide cationic clusters containing one and two titanium atoms and up to six oxygen atoms have been experimentally and theoretically investigated and, according to the joint findings, $Ti_2O_4^+$ and to a lesser extent TiO_2^+ are highly oxidative. Theoretical findings from the

present study reveal that the most stable structure of $Ti_2O_4^+$ is comprised of a spin unpaired electron located on a peripheral oxygen atom that is presented in Figure 2-2. This leads to an elongation of a titanium oxygen bond and consequently a center effective for oxidation reactions. The oxidation state of the atoms of the cluster are as follows; the titanium atoms are in the +4 state, the bridging oxygen atoms are in the -2 state, one of the peripheral oxygen atoms is in the -2 state, and the peripheral oxygen with the localized spin unpaired electron is in the -1 state. Other isomers that do not contain pronounced radical centers are considerably higher in energy (cf. Figure 2-2) and therefore are not expected to be present under the experimental conditions. Analogous radical centers have been observed in vanadium[37, 42] and zirconium[17] oxide clusters.

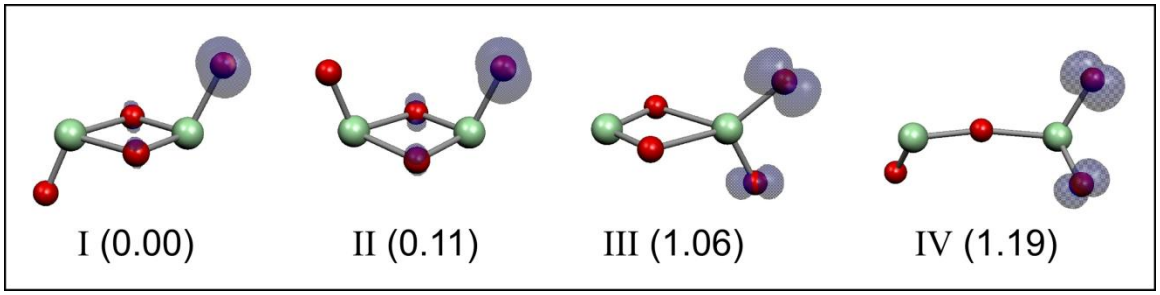

Figure 2-2. Calculated structural isomers for $Ti_2O_4^+$ given in eV. The gray isosurfaces indicate localized spin density. Reprinted from reference 43.

CO Oxidation

Combined experimental and theoretical investigations of the interaction of CO with mass selected $Ti_2O_4^+$ revealed the occurrence of an oxidation reaction in accordance with equation 2.2.

$$Ti_2O_4^+ + CO \rightarrow Ti_2O_3^+ + CO_2 \qquad (2.2)$$

As seen from the branching ratios presented in Figure 2-3a, an increase in the quantity of the oxygen loss product $Ti_2O_3^+$ is observed as the concentration of reactant is increased. The oxygen transfer product accounts for nearly 30% of the total ion intensity at the highest pressure

investigated. As neutral products can not be detected, it is assumed that the loss of oxygen from the reactant is due to the oxidation of CO to CO_2 as confirmed by theory. The branching ratios reveal that the interaction of $Ti_2O_4^+$ is highly active as well as selective toward oxidation of CO.

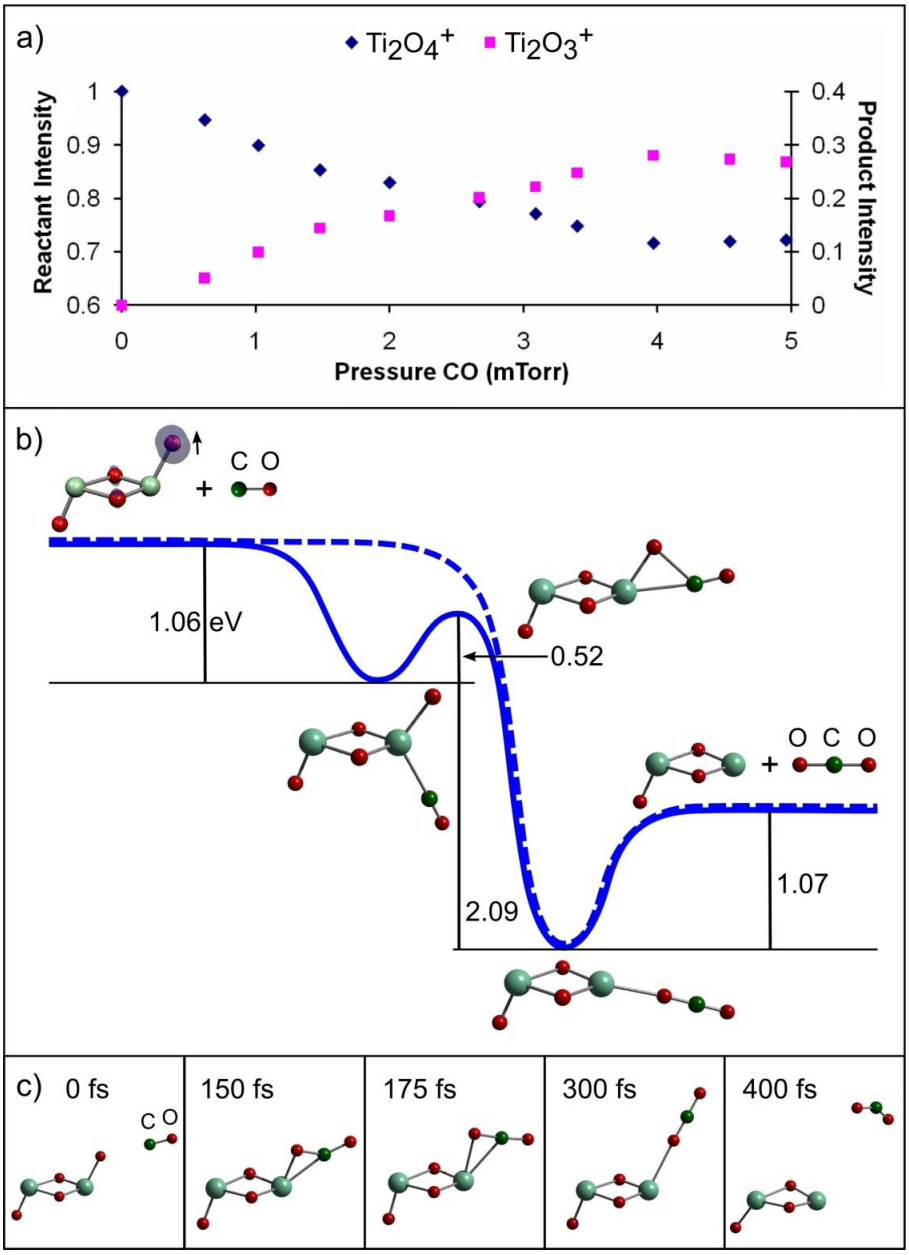

Figure 2-3. a) Branching ratios presented in normalized ion intensities for the reaction of $Ti_2O_4^+$ with CO. b) Calculated energy profile given in eV together with the structures and c) snapshots from the MD simulations performed at constant temperature (T = 1000 K) for reaction of $Ti_2O_4^+$ with CO. Reprinted from reference 43.

For the interaction of CO with $Ti_2O_4^+$, containing a radical center at one of the peripheral oxygen atoms as shown in Figure 2-3b, two possible reaction pathways that are essentially equally exothermic have been identified. The first of these pathways is presented as the dashed line in the energy profile of Figure 2-3b. The initial encounter involves the attachment of carbon to the peripheral oxygen containing the spin unpaired electron. The reactants settle into a potential well 3.15 eV lower in energy than the reactants with CO directly bound to the peripheral oxygen. The products $Ti_2O_3^+$ and CO_2 are released through cleavage of the titanium oxygen bond in a process that is exothermic by 2.08 eV. A second possible reaction pathway is displayed as the solid line whereby the mechanism proceeds through an initial encounter complex with carbon bound to the titanium as shown in Figure 2-3b. The pathway proceeds through a transition state 0.52 eV higher in energy, with the carbon bound to both the oxygen radical and titanium center. The remainder of the reaction profile follows the identical energetic pathway as in the first mechanism. Moreover the snapshots of the MD shown in Figure 2-3c illustrate the above described mechanism. Thus, our results reveal that $Ti_2O_4^+$ is active for the exothermic oxidation of carbon monoxide.

The reactive pathways for a series of zirconium oxide cationic clusters, $(ZrO_2)_x^+$ (x = 2–4), with the same stoichiometry as the titanium oxide clusters discussed currently, has been investigated previously[17]. The calculated structures for both species, $Ti_2O_4^+$ and $Zr_2O_4^+$, were found to be similar in geometry and contain a spin unpaired electron on a peripheral oxygen, creating a radical oxygen active site with an elongated metal oxygen bond. A common mechanism for the selective oxidation of CO has been found for both clusters, providing further support for the possible application of size selected clusters containing oxygen centered radicals as oxidation catalysts. To facilitate the comparison between the reactive species $Ti_2O_4^+$ and

$Zr_2O_4^+$, the phenomenological rate constants at the average lab frame energy of 1eV are presented. Assuming pseudo-first-order kinetics the rate constants are calculated using equation 2.3.

$$\ln\frac{I_r}{I_0} = -k[R]t \tag{2.3}$$

In equation 2.3, I_r represents the reactant ion intensity upon introduction of CO, I_0 the reactant ion intensity without introduction of CO, k the rate constant, R the concentration of reactant gas, and t the time the ion spends within the reaction cell. Calculation of the reaction time is accomplished by determining the velocity of an ion leaving the supersonic expansion using the equations of Anderson and Fenn[26] along with measuring the distance of the reaction cell (12.9 cm) through a trapezoidal pressure falloff approximation[44]. The velocity by supersonic expansion is provided in equation 2.4

$$v_s = M_T\left[\frac{\gamma RT}{m\left(1+\frac{\gamma-1}{2}\right)M_T}\right]^{1/2} \tag{2.4}$$

in which M_T is the mach number, γ is the specific heat capacity ratio, and m is the mass of the ion. The specific heat capacity ratio of helium is used as it is the major component of the expansion gas. This method of determining the rate constant takes into account the increased time larger ions spend within the reaction cell due to their slower velocity. The slope taken from the plot of $\ln I_r/I_0$ vs. R (Figure 2-4) is equivalent to –kt. An earlier investigation performed in our laboratory found good agreement between rate constants determined through the pseudo-first-order method and those determined through acquiring cross sections under single collision conditions[42]. The

rate constant value is on the order of 8.8 x 10^{-12} cm^3 s^{-1} for $Ti_2O_4^+$ and 2.4 x 10^{-12} cm^3 s^{-1} for $Zr_2O_4^+$. The error bars are estimated to be ± 30%. The branching ratios are comparable; however, the heavier $Zr_2O_4^+$ spends more time in the reaction cell thus the reaction rate for $Ti_2O_4^+$ is higher. In summation, both $Zr_2O_4^+$ and $Ti_2O_4^+$ exhibit similar radical oxygen sites and follow common reaction profiles when interacting with CO, yet $Ti_2O_4^+$ is the more active species.

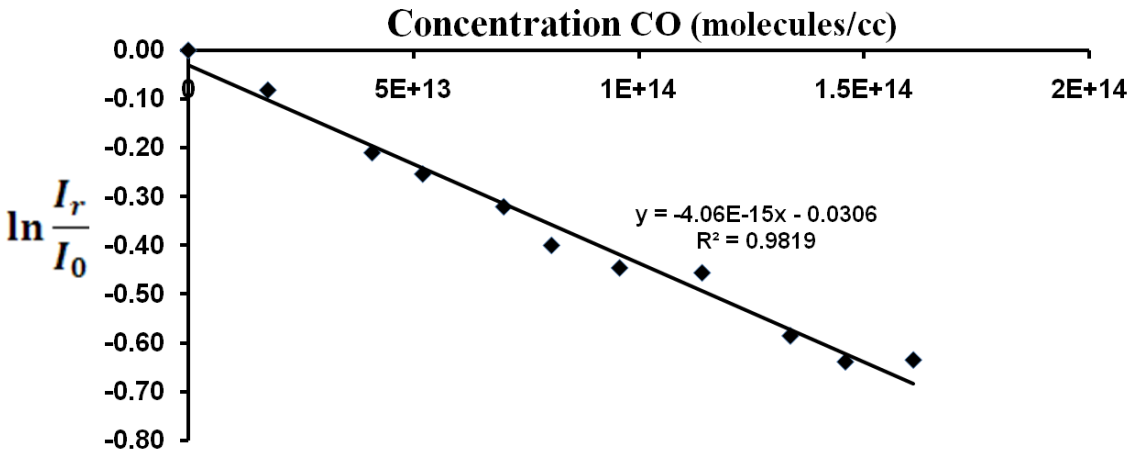

Figure 2-4. Plot of the logarithmic ratio of reactant ion intensity in the presence and absence of CO (ln I_r/I_0) vs. concentration of CO for $Ti_2O_4^+$.

Within the TiO_2^+ species, the spin density of the unpaired electron is delocalized equally over both oxygen atoms in the ground state structure (cf. Figure 2-5a). Upon interaction with CO, TiO_2^+ displays less than 2% of oxygen transfer according to the branching ratios presented in Figure 2-5b. Therefore, the active site represented by TiO_2^+ is less efficient for the oxidation of CO than the radical oxygen center represented by $Ti_2O_4^+$. Snapshots of the MD's shown in Figure 2-5a confirm that the oxidation reaction with TiO_2^+ can in principle occur. Similar delocalization of the spin density is calculated for the corresponding ZrO_2^+ explaining the decreased reactivity with CO as well. The remainder of the discussion is focused on $Ti_2O_4^+$ as it is the more reactive species.

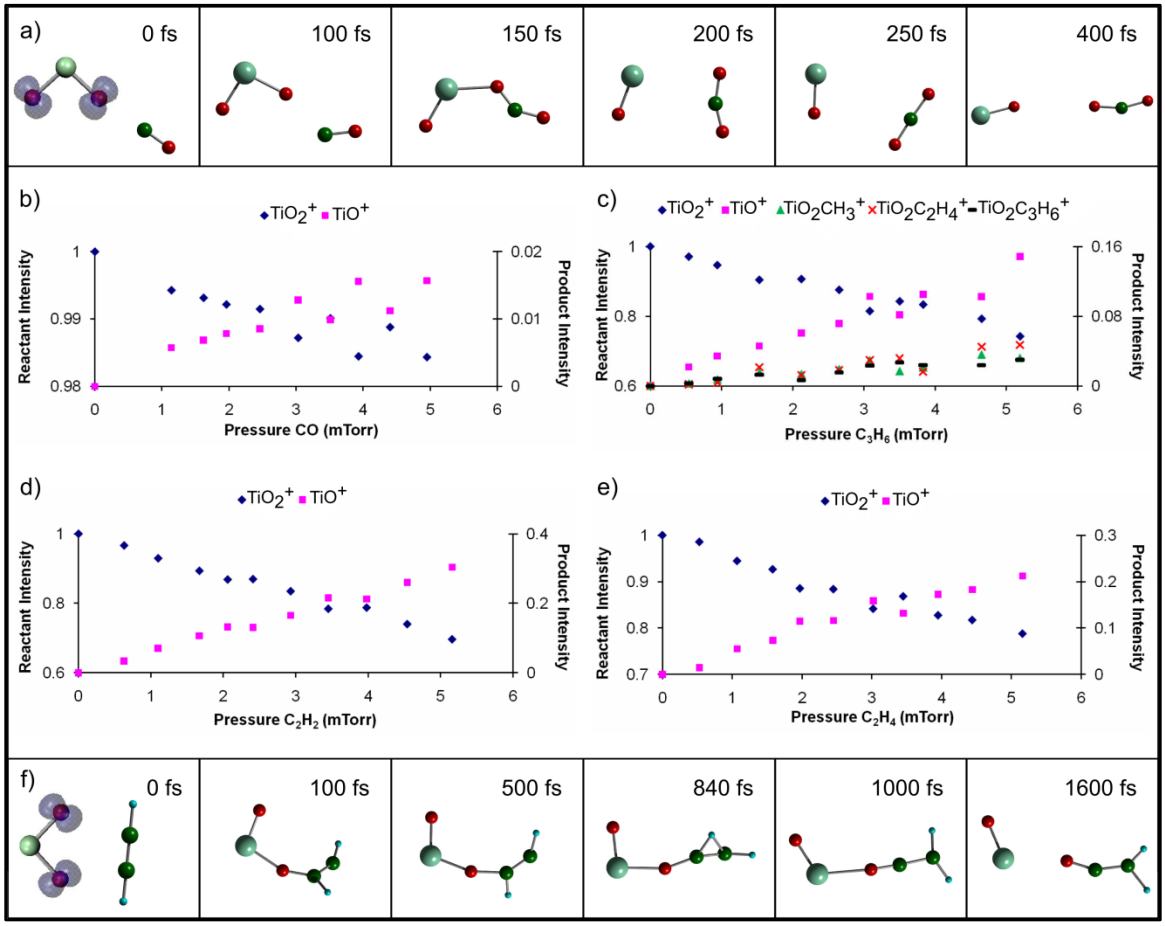

Figure 2-5. MD snapshots for the interaction of TiO_2^+ with a) CO and f) C_2H_2 exhibiting the spin unpaired electron delocalized over the peripheral oxygen. Presented are the branching ratio for the interaction of TiO_2^+ with b) CO, c) C_3H_6, d) C_2H_2, and e) C_2H_4. Reprinted from reference 43.

Propene Oxidation

The interaction of $Ti_2O_4^+$ with propene was found to display a primary oxygen transfer channel forming $Ti_2O_3^+$ in accordance with equation 2.5.

$$Ti_2O_4^+ + C_3H_6 \rightarrow Ti_2O_3^+ + C_3H_6O \qquad (2.5)$$

The oxygen transfer product accounts for around 25% of the total ion intensity as shown in Figure 2-6. In addition, three minor reaction products were identified for cracking and association upon reaction of $Ti_2O_4^+$ with C_3H_6. The minor reaction channels are detected in relatively similar quantities of roughly 2 – 3 %. $Ti_2O_4^+$ was determined to be a highly selective and active cluster for the oxidation of propene as there were only small quantities of cracking and association products formed.

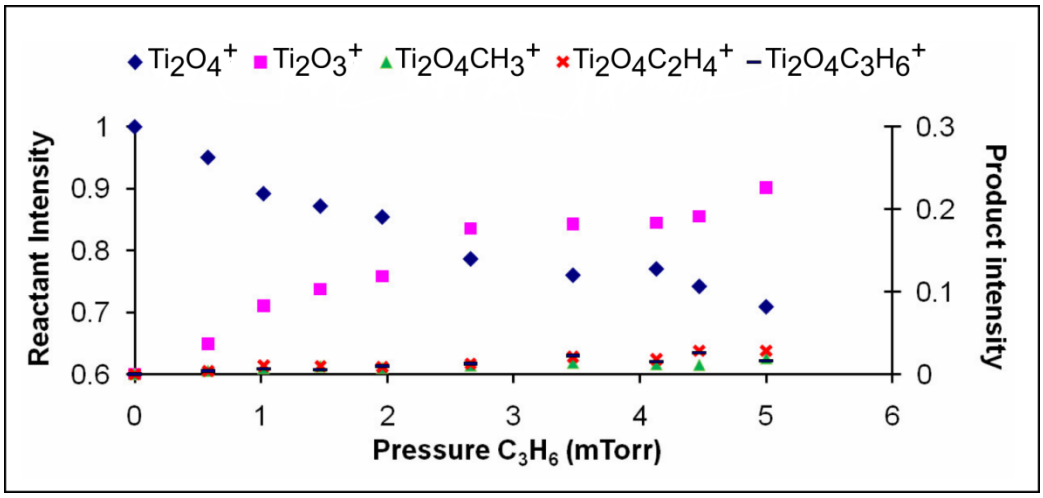

Figure 2-6. Branching ratios presented in normalized ion intensities for the reaction of $Ti_2O_4^+$ with C_3H_6. Reprinted from reference 43.

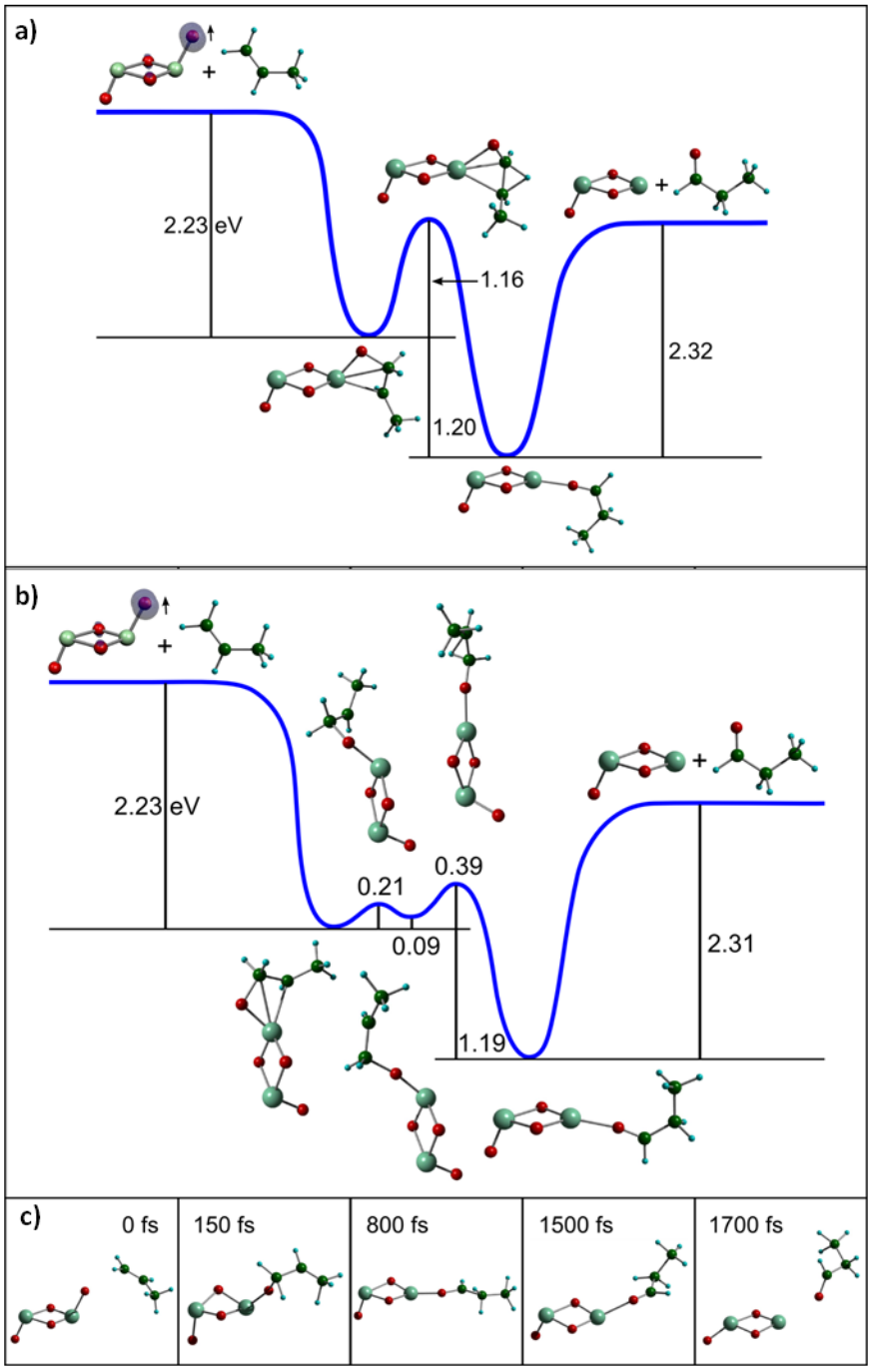

Figure 2-7. a) and b) Display the energy profiles for interaction of $Ti_2O_4^+$ with propene leading to the formation of propanal. Values are given in eV. c) MD simulations performed at constant temperature (T = 1500 K) for reaction of $Ti_2O_4^+$ with C_3H_6 forming propanal. Reprinted from reference 43.

Results of theoretical investigations presented in Figures 2-7 and 2-8 determined that two possible products, propanal and acetone, may be created from the transfer of oxygen between propene and $Ti_2O_4^+$ via processes that are effectively isoexothermic. The preferential bonding site for propene has the primary carbon bound to both the peripheral oxygen and titanium center while the secondary carbon also binds to titanium. As seen in Figure 2-7a this complex is 2.23 eV more stable than the free reactants. For the reaction to proceed to propanal, a hydrogen must be transferred from the primary to secondary carbon, followed by relaxation into a structure 3.43 eV lower in energy than the reactants. Cleavage of the titanium-oxygen bond requires 2.32 eV in energy, thus releasing neutral propanal and $Ti_2O_3^+$. The overall reaction is exothermic by 1.11 eV. Creation of propanal is also illustrated by the MD snapshots presented in Figure 2-7c. A related isoexothermic pathway for the formation of propanal involves an isomerization mechanism as shown in Figure 2-7b.

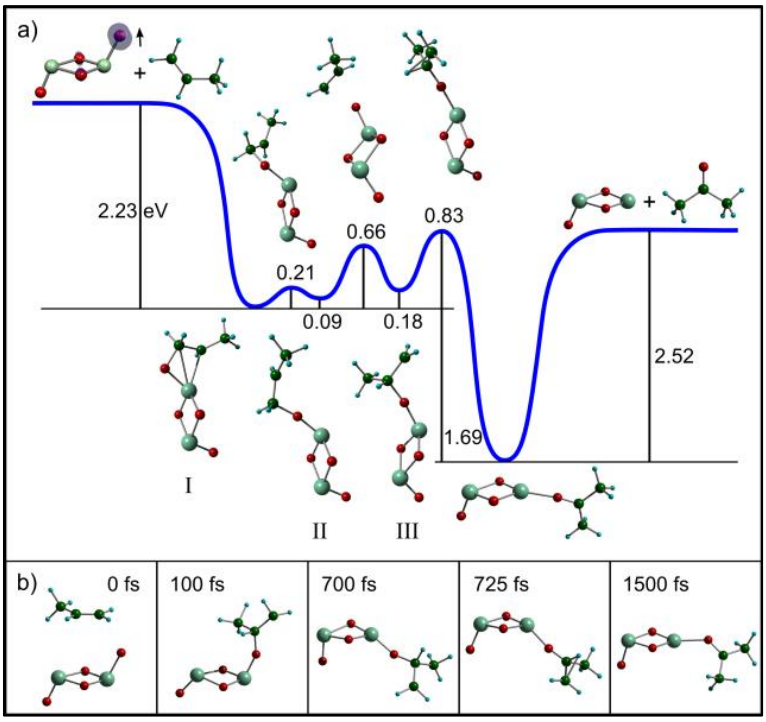

Figure 2-8. a) Calculated energy profile given in eV together with the structures and b) snapshots from the MD simulations performed at constant temperature (T = 1000 K) for reaction of $Ti_2O_4^+$ with C_3H_6 creating acetone. Reprinted from reference 43.

As seen in Figure 2-8a, the formation of acetone is a second possible product originating from the interaction of $Ti_2O_4^+$ with propene. An isomerization mechanism involving encounter complex I can occur, switching the bonding position from the first to the second carbon (compare isomer II to isomer III). The final transition toward the formation of acetone requires the transfer of hydrogen from the central carbon to the unsaturated terminal carbon. The exit channel for the release of acetone and $Ti_2O_3^+$ is 1.40 eV lower in energy than the reactant entrance channel. The MD snapshots shown in Figure 2-8b confirm the above described mechanism. The pathways for creation of acetone (-1.40 eV) and propanal (-1.11 eV) through the reaction of $Ti_2O_4^+$ with propene are both exothermic and thus a mixture of the two products is expected.

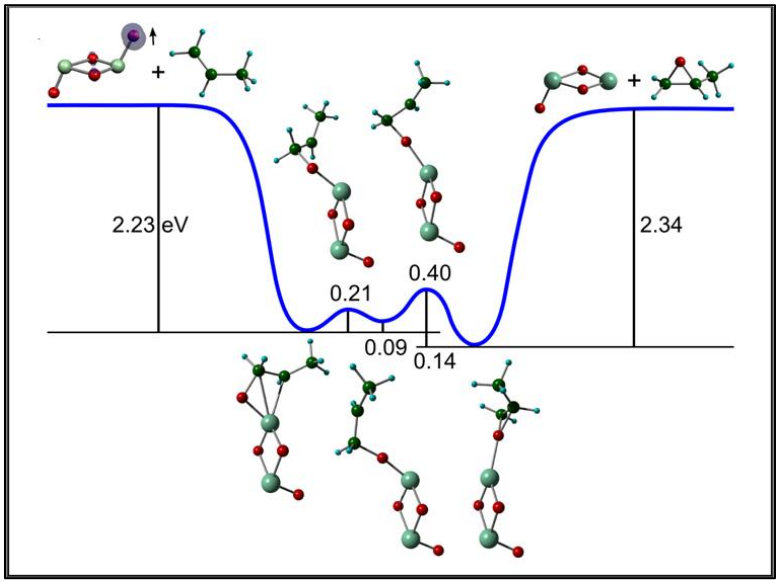

Figure 2-9. Calculated energy profile given in eV for reaction of $Ti_2O_4^+$ with C_3H_6 forming an epoxide in an endothermic mechanism. Reprinted from reference 43.

The creation of an epoxide product through interaction of $Ti_2O_4^+$ with propene has been considered. In Figure 2-9 the reaction mechanism for creation of an epoxide is presented. The

products are of nearly equal energy as the reactants, thus it is not expected to be a major product in the experimental investigations.

Using the earlier described method for determining the pseudo-first-order rate constant, it has been calculated that the rate constant value for oxygen transfer to propene from $Ti_2O_4^+$ is on the order of 3.1 x 10^{-12} cm^3 s^{-1}. Our earlier studies of $Zr_xO_{2x}^+$ clusters[17] did not investigate the reactivity with propene so there is no data for comparison between the species. The reaction of TiO_2^+ with propene leads to oxidation, as well as other channels at a lower intensity; see Figure 2-5c.

Regeneration of the Active Species

The catalytic cycle for the reaction of $Ti_2O_4^+$ with propene (depicted in Figure 2-10a) initiates by formation of two possible complexes I and II, the first leading to the production of propanal while the second results in the formation of acetone. With the aim of developing a full catalytic cycle, regeneration of the active species $Ti_2O_4^+$ is studied and the results are presented in Figure 2-10b and 2-10c. Reaction of the $Ti_2O_3^+$ cluster with N_2O is found to spontaneously regenerate $Ti_2O_4^+$ as shown in the branching ratios (Figure 2-10b) that is consistent with the MD simulations presented in Figure 2-10c. Compared to the earlier discussed oxidation reactions, the regeneration is lower in intensity with the product $Ti_2O_4^+$ being only 4 % of the total ion intensity at a total N_2O pressure of 5 mtorr. However, the findings show that the starting cluster has been regenerated and the catalytic cycle has been completed.

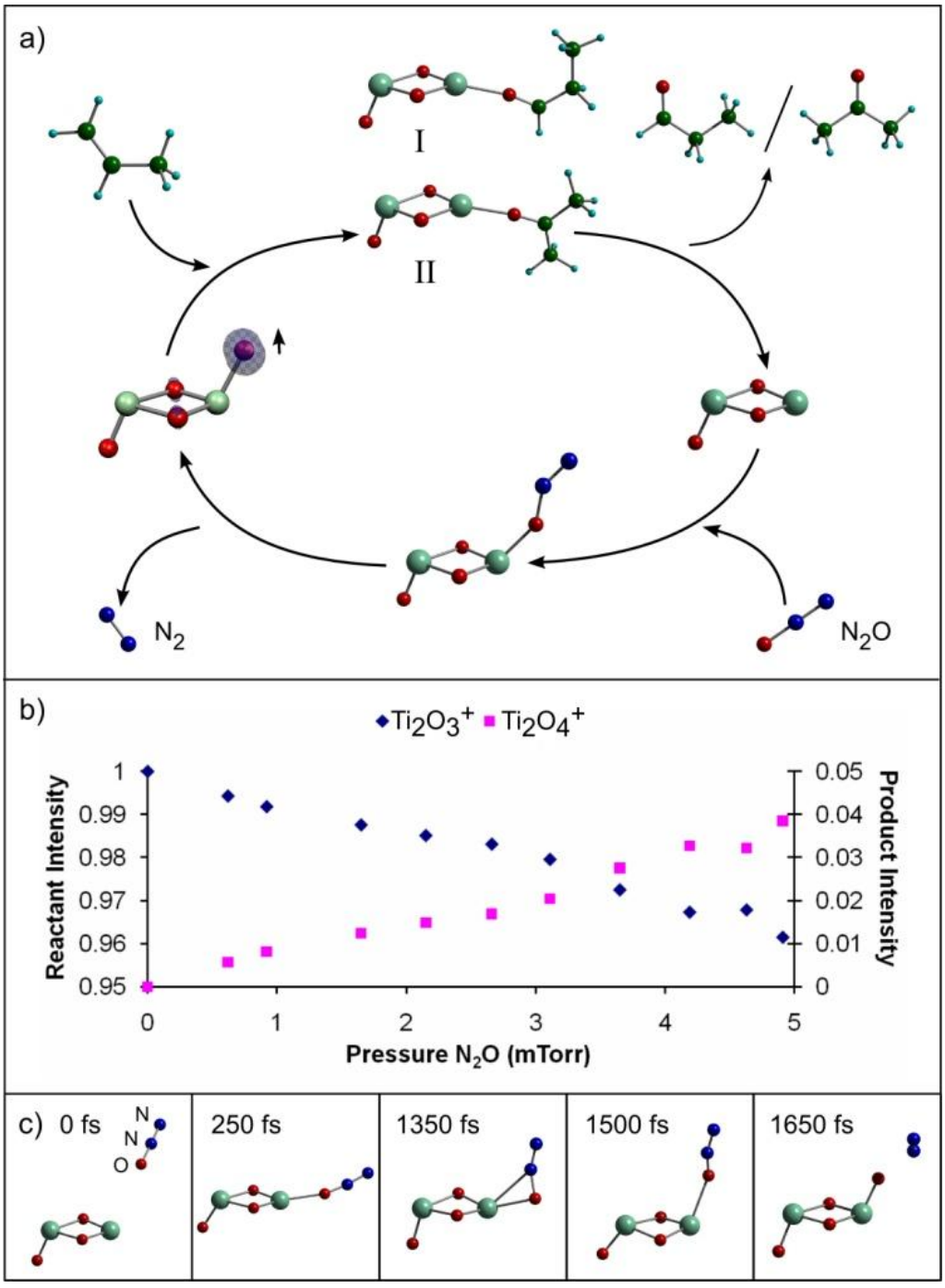

Figure 2-10. a) The full catalytic cycle is depicted for the oxidation of propene forming propanal (I) and acetone (II) followed by interaction with N_2O for regeneration of the active species $Ti_2O_4^+$. b) Branching ratios presented in normalized ion intensities for reaction of $Ti_2O_3^+$ with N_2O. c) Snapshots from MD simulations performed at constant energy (E = 0.1 eV) for the reaction of $Ti_2O_3^+$ with N_2O. The light green spheres are titanium, red spheres represent oxygen, dark green represent carbon, light blue represent hydrogen, and dark blue represent nitrogen. Reprinted from reference 43.

Reactions with C_2H_2 and C_2H_4

Experimental and theoretical investigations are undertaken to determine the reactivity of $Ti_2O_4^+$ with the reactants C_2H_2 and C_2H_4. The primary product for the interaction with acetylene is an oxygen transfer as described in equation 2.6.

$$Ti_2O_4^+ + C_2H_2 \rightarrow Ti_2O_3^+ + C_2H_2O \qquad (2.6)$$

The branching ratio and MD simulations for the interaction of $Ti_2O_4^+$ with acetylene creating $Ti_2O_3^+$ and ethenone are presented in Figure 2.11a and b. The quantity of oxygen transfer product, $Ti_2O_3^+$, is nearly 45 % relative to the total ion intensity as seen in Figure 2.11a with a 1% quantity of $Ti_2O_4C_2H_2^+$ resulting from the association of acetylene. Acetylene initially associates

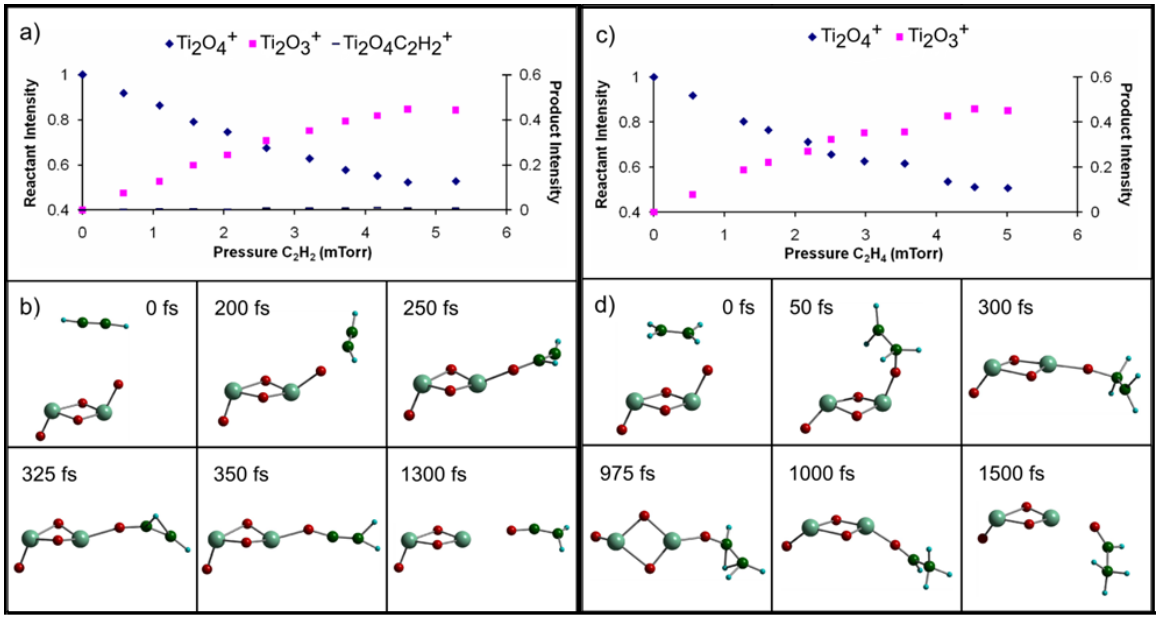

Figure 2-11. Branching ratios presented in normalized ion intensities for reaction of $Ti_2O_4^+$ with a) C_2H_2 and c) C_2H_4. Snapshots from MD simulations performed at constant temperature (T = 1000 K) of the reaction $Ti_2O_4^+$ with b) C_2H_2 and d) C_2H_4. Reprinted from reference 43.

to a peripheral oxygen of the $Ti_2O_4^+$ cluster, as shown in the MD simulations presented in Figure 2.11b; then the reaction proceeds through hydrogen transfer from the bound carbon to the adjacent carbon. The complex is then free to evolve into the products $Ti_2O_3^+$ and ethenone. This reaction is exothermic and spontaneous as revealed by our results.

The investigation, probing the reactivity of $Ti_2O_4^+$ with ethene is presented in Figure 2.11c and d. The sole product observed is the transfer of atomic oxygen creating $Ti_2O_3^+$ and C_2H_4O as described in equation 2.7.

$$Ti_2O_4^+ + C_2H_4 \rightarrow Ti_2O_3^+ + C_2H_4O \qquad (2.7)$$

The oxygen loss product accounts for greater than 45 % of the total ion intensity for the reaction of $Ti_2O_4^+$ with ethene as shown in Figure 2.11c. The MD simulations determine the major transition required is a hydrogen transfer from the associated carbon to the adjacent carbon, thus creating acetaldehyde as presented in Figure 2.11d. The catalytic oxidation of ethene to acetaldehyde is a valuable industrial reaction as are all of the oxidation reactions presented.

Additionally, interactions between the species $(Zr_xO_{2x})^+$ (x = 2–4) with acetylene and ethene[17] produced a primary oxidation pathway; thus confirming common reactivity behavior with $Ti_2O_4^+$. Pseudo-first-order rate constants were calculated for the oxygen transfer from $Ti_2O_4^+$ to ethene and acetylene to be on the order of 8.4×10^{-12} cm^3 s^{-1} and 8.8×10^{-12} cm^3 s^{-1}, respectively. The corresponding rate constants for oxygen transfer from $Zr_2O_4^+$ to ethene and acetylene [17] are 1.3×10^{-12} cm^3 s^{-1} and 5.9×10^{-12} cm^3 s^{-1}, respectively. Comparison between the selected clusters proves $Ti_2O_4^+$ to be the more active cluster for oxygen transfer to unsaturated hydrocarbons as well as CO. The observation that incorporation of group IV transition metals into a stoichiometic metal-oxide cluster creates an active site for the oxidation of CO, C_3H_6, C_2H_2, and C_2H_4 is the message of importance.

The interaction of TiO_2^+ with acetylene and ethene also resulted in an oxidation reaction as presented in Figure 2-5d-f, yet of lower intensity than $Ti_2O_4^+$. The delocalization of the spin density is again causing the decease in reactivity in comparison with $Ti_2O_4^+$. Due to delocalized spin density of ZrO_2^+ a similar decreased reactivity between ZrO_2^+ with acetylene and ethene was found and reported in an earlier publication[17].

2.5 Conclusion

The present study has examined the reactivity of titanium oxide cationic clusters with CO, C_2H_2, C_2H_4, and C_3H_6. Experimental and theoretical investigations have identified $Ti_2O_4^+$ and to a lesser extent TiO_2^+ to exhibit preferential oxygen loss when introduced to the reactants. Theoretical investigation determined that $Ti_2O_4^+$ contains a spin unpaired electron localized on a peripheral oxygen creating an oxygen centered radical with an elongated titanium oxygen bond. MD simulations determine that the clusters oxidize the considered reactants and the calculated energy profiles reveal the mechanisms of the reactions. Regeneration of the oxygen centered radical was achieved through the reaction of N_2O with $Ti_2O_3^+$. A rate constant comparison was also performed with the earlier published investigation of $Zr_2O_4^+$ for oxygen transfer to CO, C_2H_2, and C_2H_4. In all cases, $Ti_2O_4^+$ presented a higher rate constant suggesting it would be a better candidate for inclusion in a deposited catalyst.

In summary, considering the findings obtained through this study, it is evident that investigation of the interaction of selected molecules with clusters is a valuable approach to elucidate fundamental mechanisms of catalysis.

2.6 References

1. *Supported Metals in Catalysis*, ed. J. A. Anderson, M. F. Garcia, Imperial College Press: London, **2005**.
2. Somorjai, G. A.; Frei, H.; Park, J. Y. *J. Am. Chem. Soc.* **2009**, *131*, 16589.
3. *Theoretical Aspects of Heterogeneous Catalysis*, ed. M. A. C. Nascimento, Kluwer Academic Publishers: Boston, **2001**.
4. Tsang, S. C.; Cailuo, N.; Oduro, W.; Kong, A. S. T.; Clifton, L.; Yu, K. M. K.; Thiebaut, B.; Cookson, J.; Bishop, P. *ACS Nano* **2008**, *2*, 2547.
5. Lin, Y.; Somorjai, G. A. *Nano Lett.* **2010**, *10*, 2289.
6. Lei, Y.; Mehmood, F.; Lee, S.; Greeley, J.; Lee, B.; Seifert, S.; Winans, R. E.; Elam, J. W.; Meyer, R. J.; Redfern, P. C. et al. *Science* **2010**, *328*, 224.
7. Ishida, T.; Haruta, M. *Angew. Chem. Int. Ed.* **2007**, *46*, 7154.
8. Kaden, W. E.; Wu, T.; Kunkel, W. A.; Anderson, S. A. *Science* **2009**, *326*, 826.
9. Herzing, A. A.; Kiely, C. J.; Carley, A. F.; Landon, P.; Hutchings, G. J. *Science* **2008**, *321*, 1331.
10. Johnson, G. E.; Mitrić, R.; Bonačić-Koutecký, V.; Castleman, Jr., A. W. *Chem. Phys. Lett.* **2009**, *475*, 1.
11. van Koppen, P. A. M.; Bowers, M. T.; Haynes, C. L.; Armentrout, P. B. *J. Am. Chem. Soc.* **1998**, *120*, 5704.
12. Dong, F.; Heinbuch, S.; Xie, Y.; Rocca, J. J.; Bernstein, E. R.; Wang, Z.-C.; Deng, K.; He, S.-G. *J. Am. Chem. Soc.* **2008**, *130*, 1932.
13. Bohme, D. K.; Schwarz, H. *Angew. Chem. Int. Ed.* **2005**, *44*, 2336.
14. Lang, S. M.; Bernhardt, T. M.; Barnett, R. N.; Yoon, B.; Landman, U. *J. Am. Chem. Soc.* **2009**, *131*, 8939.

15. Zemski, K. A.; Justes, D. R.; Castleman Jr., A. W. *J. Phys. Chem. B* **2002**, *106*, 6136.
16. Johnson, G. E.; Mitrić, R.; Nößler, M.; Tyo, E. C.; Bonačić-Koutecký, V.; Castleman, Jr., A. W. *J. Am. Chem. Soc.* **2009**, *131*, 5460.
17. Johnson, G. E.; Mitrić, R.; Tyo, E. C.; Bonačić-Koutecký, V.; Castleman, Jr., A. W. *J. Am. Chem. Soc.* **2008**, *130*, 13912.
18. Nößler, M.; Mitrić, R.; Bonačić-Koutecký, V.; Johnson, G. E.; Tyo, E. C.; Castleman, Jr., A. W. *Angew. Chem. Int. Ed.* **2010**, *49*, 407.
19. Li, S.-C.; Diebold, U. *J. Am. Chem. Soc.* **2010**, *132*, 64.
20. Valden, M.; Lai, X.; Goodman, D. W. *Science* **1998**, *281*, 1647.
21. Grirrane, A.; Corma, A.; García, H. *Science* **2008**, *322*, 1661.
22. Li, S.-C.; Diebold, U. *J. Am. Chem. Soc* **2010**, *132*, 64.
23. Harvey, J. N.; Diefenbach, M.; Schröder, D.; Schwarz, H. *Int. J. Mass. Spectrom.* **1999**, *182*, 85.
24. Bell, R. C.; Castleman, Jr., A. W. *J. Phys. Chem. A* **2002**, *106*, 9893.
25. de Heer, W. A. *Rev. Mod. Phys.* **1993**, *65*, 611.
26. Anderson, J. B.; Fenn, J. B. *Phys. Fluids* **1965**, *8*, 780.
27. Miller, P. E.; Denton, M. B. *J. Chem. Ed.* **1986**, *63*, 617.
28. Jones, R. M.; Gerlich, D.; Anderson, S. L. *Rev. Sci. Instrum.* **1997**, *68*, 3357.
29. Becke, A. D. *Phys. Rev. A* **1988**, *38*, 3098.
30. Becke, A. D. *J. Chem. Phys* **1993**, *98*, 5648.
31. Lee, C.; Yang, W.; Parr, R. G. *Phys. Rev. B* **1998**, *37*, 785.
32. Dolg, M.; Stoll, H.; Preuss, H.; Pitzer, R. M. *J. Phys. Chem.* **1993**, *97*, 5852.
33. Andrea, D.; Haeussermann, U.; Dolg, M.; Stoll, H.; Preuss, H. *Theor. Chim. Acta* **1990**, *77*, 123.

34. Gilb, S.; Weis, P.; Furche, F.; Aldrichs, R.; Kappes, M. M. *J. Chem. Phys.* **2002**, *116*, 4094.

35. Cao, X. Y.; Dolg, M. *J. Chem. Phys.* **2001**, *115*, 7348.

36. Schaefer, A.; Huber, C.; Ahlrichs, R. *J. Chem. Phys.* **1994**, *100*, 5829.

37. Justes, D. R.; Mitrić, R.; Moore, N. A.; Bonačić-Koutecký, V.; Castleman, Jr., A. W. *J. Am. Chem. Soc.* **2003**, *125***,** 6289.

38. Ahlrichs, R.; Bär, M.; Häser, M.; Horn, H.; Kölmel, C. *Chem. Phys. Lett.*, **1989**, *162*, 165.

39. Dunlap, B. I.; Connolly, J. W. D.; Sabin, J. R. *J. Chem. Phys*. **1979**, *71*, 3396.

40. Eichkorn, K.; Treutler, O.; Ohm, H.; Haser, M.; Aldrichs, R. *Chem. Phys. Lett*. **1995**, *242*, 652.

41. Perdew, J. P.; Burke, K.; Ernzerhof, M. *Phys. Rev. Lett*. **1996**, *77*, 3865.

42. Moore, N. A.; Mitrić, R.; Justes, D. R.; Bonačić-Koutecký, V.; Castleman, Jr., A. W. *J. Phys. Chem. B* **2006**, *110*, 3015.

43. Tyo, E. C.; Nößler, M.; Mitrić, R.; Bonačić-Koutecký, V.; Castleman, Jr., A. W. *Phys. Chem. Chem. Phys.* **2011**, *13*, 4243.

44. Bell, R. C.; Zemski, K. A.; Justes, D. R.; Castleman, A. W., Jr. *J. Chem. Phys.* **2001**, *114*, 798.

Chapter 3

Investigating Reactive Superoxide Units Bound to Zirconium Oxide Cations

3.1 Introduction

Currently, considerable interest in catalytic research is focused on determining the active sites responsible for promotion of catalytic mechanisms. Relationships among the elemental composition, electronic structure, and geometric structure correlate to specific chemical transformations and catalytic processes.[1] The remarkable oxidative ability of selected catalytic materials is due to their capacity to activate oxygen on their surfaces. Findings from detailed investigations probing the reactivity of various forms of activated oxygen are expected to provide information that may enable the tailored design of highly selective and active oxidation catalysts.

Investigations have established the application of zirconium oxide as an active catalyst and support material.[2-5] Metal-oxide surfaces commonly host oxygen in three activated forms; radical oxygen, superoxide, and peroxide. The structure, formation, and reactivity of superoxide on zirconium oxide surfaces have been investigated to gain a better understanding of their character.[6-9] In particular, the catalytic combustion of propene and toluene occurs over zirconium oxide surfaces through oxidation at the superoxide site.[8,9] Alternatively, it is observed that the oxidation of CO and CH_4 is accomplished by lattice oxygen ions on the surface, thus illustrating the differences in reactivity for various forms of activated oxygen.[3,10] One of the major impediments in elucidating the mechanisms of catalytic reactions and utilizing the acquired information in designing new catalytic materials is that reactions usually involve defect-sites that

are difficult to duplicate and isolate.[11] Gas-phase ionic structures can yield reproducible sites, including charge density, providing a major benefit towards using clusters as models of catalytic centers.[12] Moreover, the ability to investigate structural aspects through the modeling of steps, ledges and other features is a major advantage of conducting catalysis research via cluster science.

Gas-phase studies of atomic ions provide fundamental understanding of reaction mechanisms while investigating the influence of chemical composition, coordination number, charge state, and oxidation state.[13-16] Various investigations have imparted detailed insight into oxidation, hydrogen abstraction, and C-C bond braking mechanisms. A collaborative effort between the experimental laboratory of Prof. A. W. Castleman Jr. and theoretical laboratory of Prof. Vlasta Bonačić-Koutecký identified an oxygen centered radical located on the series of clusters $Zr_xO_{2x}^+$ and $Zr_xO_{2x+1}^-$ (x = 1 – 4)[17,18] to be highly active for oxygen transfer. These studies also revealed how differences in charge state influenced reactivity. Other studies have identified that zirconium oxide clusters containing a radical oxygen unit are active for C-H bond cleavage.[19-21]

Through gas-phase spectroscopic studies, various clusters have been identified to contain bound superoxide units.[22,23] Such clusters will be investigated through mass spectrometric and theoretical means to provide insight into their activity and selectivity for oxidation reactions. Specifically, this investigation determines the reactivity of zirconium oxide cationic clusters containing superoxide structural units with propene, butadiene, acetylene, ethene, and CO.

The structures of cationic zirconium oxide clusters of stoichiometry $Zr_xO_{2x+1}^+$ (x = 1-3) are determined to contain the superoxide unit and are interacted with the reactants. Theoretical and experimental investigations identify the selective oxidation of propene and acetylene. Competitive products are found for interaction with butadiene with major pathways identified for

oxidation and the formation of formaldehyde. The significant findings and their implications are reported herein.

3.2 Experimental Methods

Experiments are performed through interaction of C_3H_6, C_4H_6, C_2H_2, C_2H_4, CO, and N_2O with mass selected cationic zirconium oxide clusters utilizing an in house built guided-ion-beam mass spectrometer.[24] The instrument has been described in Chapter 2 and is only briefly detailed here. Zirconium oxide clusters are produced in a laser vaporization (LaVa) source via pulsing of a 13.2 atm expansion gas, composed of oxygen seeded in helium, into the plasma created via ablation of a 1/8" zirconium rod (99.95%, Research and PVD Materials Corp.) by the second harmonic (532 nm) of a Nd:YAG laser (Specra-Physics, INDI-50) operating at 20 Hz. The expansion gas is introduced to the LaVa source by a pulse valve (General Valve, Series 9, 28V) and is composed of ultra high purity oxygen (99.993%, GT&S Welco) and high purity helium (99.99%, Praxair). A range of mixtures were tested having 1% to 10% oxygen contribution. The expansion gas composed of 5% oxygen seeded in helium created the clusters ZrO_3^+, $Zr_2O_5^+$ and $Zr_3O_7^+$ in the highest abundance. The reactant gases used in this investigation are C_3H_6 (99.0%, GT&S Welco), C_4H_6 (1,3-butadiene 99.5%, GT&S Welco), C_2H_2 (99.6%, GT&S Welco), C_2H_4 (99.9%, GT&S), CO (99.9%, GT&S Welco), N_2O (99.6%, MG Industries), and N_2 (99.9%, GT&S Welco).

The clusters exit the LaVa source and are cooled by supersonic expansion into vacuum. The high pressure of the expansion gas (13.2 atm) passing into a low pressure field free region decreases the internal vibrational and rotational energy of the clusters through three-body collisions. A retarding potential analysis previously performed in our laboratory determined that the energy imparted upon the clusters exiting the LaVa source is around 1 eV in the laboratory

frame.[24] The clusters progress through a 3 mm skimmer creating a collimated molecular beam and are directed by a set of electrostatic lenses into a quadrupole mass filter. The quadrupole mass filter permits clusters of a desired mass to charge (m/z) ratio to pass into an octopole collision cell. Varying pressures of the reactants are admitted to the collision cell utilizing a low flow metering valve to determine the reactivity and related structural characteristics of the clusters. An MKS Baratron capacitance manometer is used to monitor the pressure of reactant introduced. A potential of zero volts is applied to the injection lens before the collision cell and the dc float voltage applied to the octopole ion guide so the clusters react at thermal energies. The product ions are extracted from the octopole and flow into a second quadrupole mass filter that scans a (m/z) range of 40-740 amu to perform product mass determination. Lastly, resultant ions are detected by a channel electron multiplier (CEM) connected to a multichannel scalar card.

The experimental branching ratios presented in Chapter 3 depict the normalized ion intensities of products and reactants detected at increasing pressures of reactant. It can be seen that for reactive species, an increase of reactant in the collision cell results in a concomitant rise in products while the parent species decreases in intensity. Collision induced dissociation (CID) experiments are performed introducing inert N_2 at varying pressures to the clusters of interest. CID investigations are performed to confirm that detected product ions are indeed due to chemical reactivity and not collisional fragmentation.

3.3 Theoretical Methods

Calculations are performed by the Bonačić-Koutecký group at the Humboldt Universität zu Berlin that compliment experimental results and provide mechanistic detail of reaction processes. The structural properties of the cationic $Zr_xO_{2x+1}^+$ (x = 1-3) clusters and their reactivity toward C_3H_6, C_4H_6, C_2H_2 and N_2O are studied using the DFT method with the hybrid B3LYP

functional.[25-27] For the zirconium atoms a triple-ζ-valence-plus-polarization (TZVP) atomic basis set combined with the Stuttgart group 12-electron relativistic effective core potential (12e-RECP) is employed.[28-30] For the carbon, oxygen, hydrogen and nitrogen atoms the TZVP basis sets are used.[31] Previous studies of the reactivity of transition metal oxides have shown that such a combination of hybrid density functionals with triple zeta quality basis sets allow for the accurate prediction of the reaction energetics and mechanisms.[12-14,17,18,32] All structures presented are fully optimized using gradient minimization techniques and stationary points are characterized as minima or transition states by calculating the frequencies. Moreover, the reaction mechanisms are determined from the energy profiles based on DFT energies. The proposed reaction mechanisms are also confirmed by performing ab-initio molecular dynamics (MD) simulations "on the fly" based on the DFT method. Newton's equations of motion are solved using the Verlet algorithm with time steps of 1 fs and the forces are calculated employing the analytical energy gradients in the framework of the TURBOMOLE program.[33] The MD simulations performed at constant temperature allow the bonding rearrangements along the reaction pathways to be followed. In order to improve efficiency of MD simulations the resolution of identity (RI)-DFT procedure[34,35] is employed requiring the use of the Perdew-Burke-Ernzerhof (PBE) functional.[36] The accuracy of this functional has been verified previously[17] by comparing structural properties as well as energy profiles with those obtained by the B3LYP functional; good agreement is obtained.

3.4 Structural Characterization

A series of cationic zirconium oxide clusters have been identified to contain a superoxide unit, consisting of two oxygen atoms sharing an unpaired electron (O_2^-) and an elongated oxygen-oxygen bond of 1.33 Å in comparison to 1.21 Å of a normal O_2. The series of clusters, herein referred to as superoxides, have the stoichiometry $(Zr_xO_{2x+1})^+$. Theoretical structures for the

superoxide species ZrO_3^+, $Zr_2O_5^+$, and $Zr_3O_7^+$ are provided in Figure 3-1; gray spheres represent the spin density of the unpaired electron over the two oxygens.

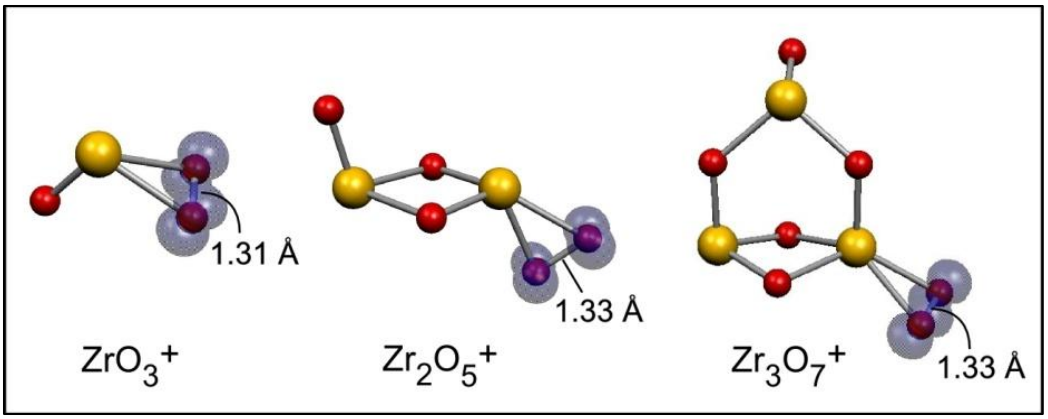

Figure 3-1. Calculated lowest-energy structures for ZrO_3^+, $Zr_2O_5^+$, and $Zr_3O_7^+$. The gray isosurfaces indicate localized spin density. Reprinted from reference 37.

Additional structures, including the three most energetically stable isomers, are presented in Figure 3-2 for comparison. Low lying isomers are found for $Zr_2O_5^+$ and $Zr_3O_7^+$ that additionally contain the superoxide unit. $Zr_3O_7^+$ isomers consisting of terminal oxygen atoms on all three zirconium atoms are significantly higher in energy than isomers containing a superoxide unit (Figure 3-2). Reactivity investigations, both experimental and theoretical, are performed through introduction of various hydrocarbon molecules to the aforementioned clusters. Interaction of the $Zr_2O_5^+$ clusters with propene, butadiene, and acetylene results in a strong oxidation of the hydrocarbons. Additionally, interaction with butadiene results in the creation of formaldehyde as a major product channel. Many earlier studies have determined the reactivity of gas-phase clusters containing a radical oxygen center while the current investigation is among the first to study the reactivity of clusters containing isolated superoxide units. In the following, the interaction of $Zr_2O_5^+$ with propene, butadiene, and acetylene is presented first. Followed by a discussion of the interactions of ZrO_3^+ and $Zr_3O_7^+$ with the reactants.

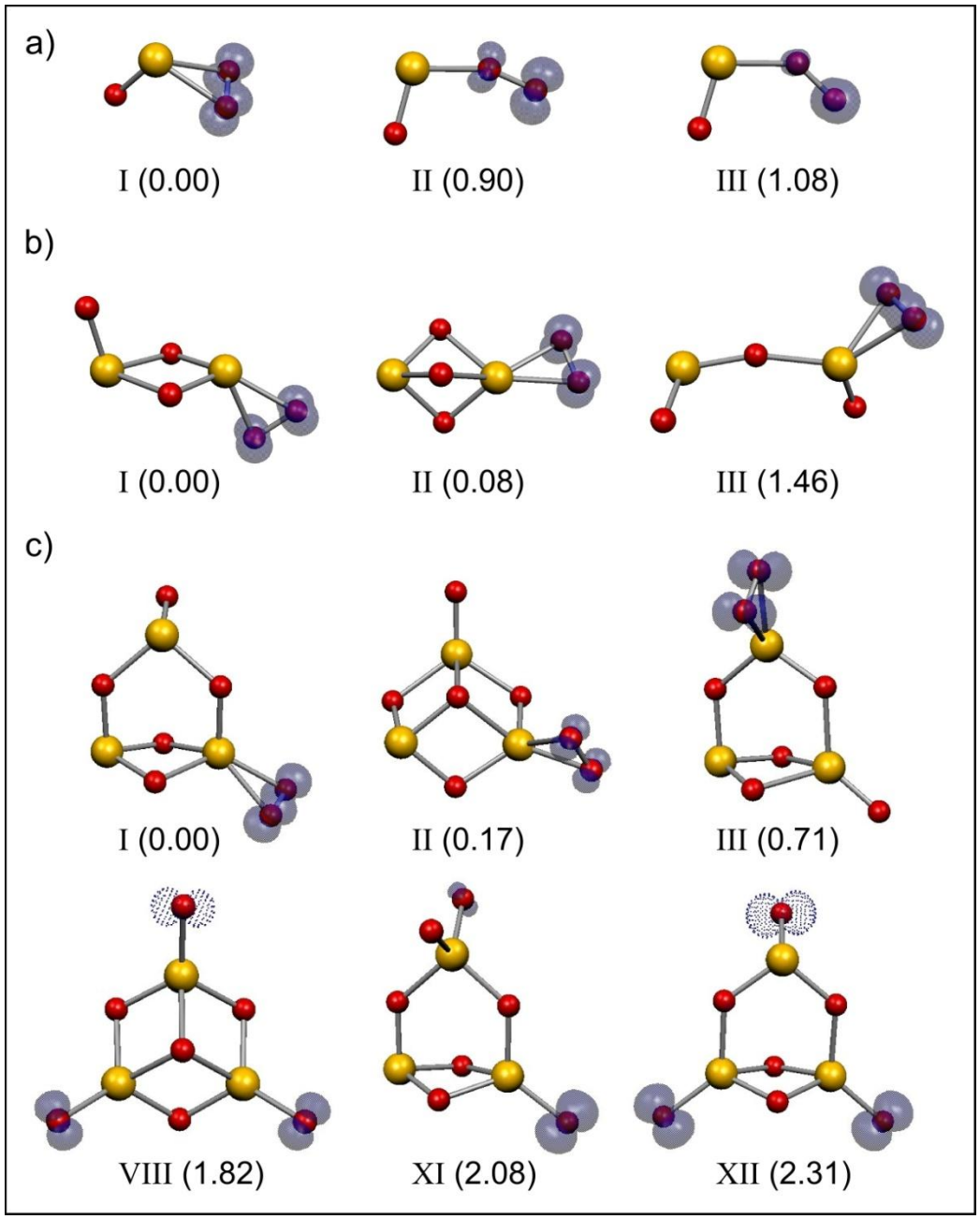

Figure 3-2. Calculated structural isomers for a) ZrO_3^+, b) $Zr_2O_5^+$, and c) $Zr_3O_7^+$ given in eV. The gray isosurfaces indicate localized spin density. Reprinted from reference 37.

3.5 Interaction of $Zr_2O_5^+$ with Reactants

Propene Oxidation

Combined experimental and theoretical investigations reveal the occurrence of an oxidation reaction upon the interaction of the superoxide cluster $Zr_2O_5^+$ and propene in accordance with equation 3.1.

$$Zr_2O_5^+ + C_3H_6 \rightarrow Zr_2O_4^+ + C_3H_6O \qquad (3.1)$$

Oxidation of propene by $Zr_2O_5^+$ is observed as a major reaction channel. The branching ratio presented in Figure 3-3a displays the experimental results for the reaction. The oxygen loss product, $Zr_2O_4^+$, accounts for nearly 30% of the total ion current when roughly 5 mTorr of propene is introduced. The experimental technique that is utilized enables detection of the ionic species so it is assumed that the neutral product has been oxidized; loss of a single oxygen through collisional dissociation is unlikely as investigations with inert N_2 did not display atomic oxygen loss. However, $Zr_2O_3^+$ is observed and accounts for 2% of the total ion signal at 5 mTorr propene; its presence is attributed to the collisional dissociation of O_2 that is confirmed through interaction with inert N_2. Various co-products including association and cracking of the reactant are detected in low intensity of 2% and are presented in the branching ratio plot. The branching ratios display that the superoxide unit contained on $Zr_2O_5^+$ is active for the preferential oxidation of propene.

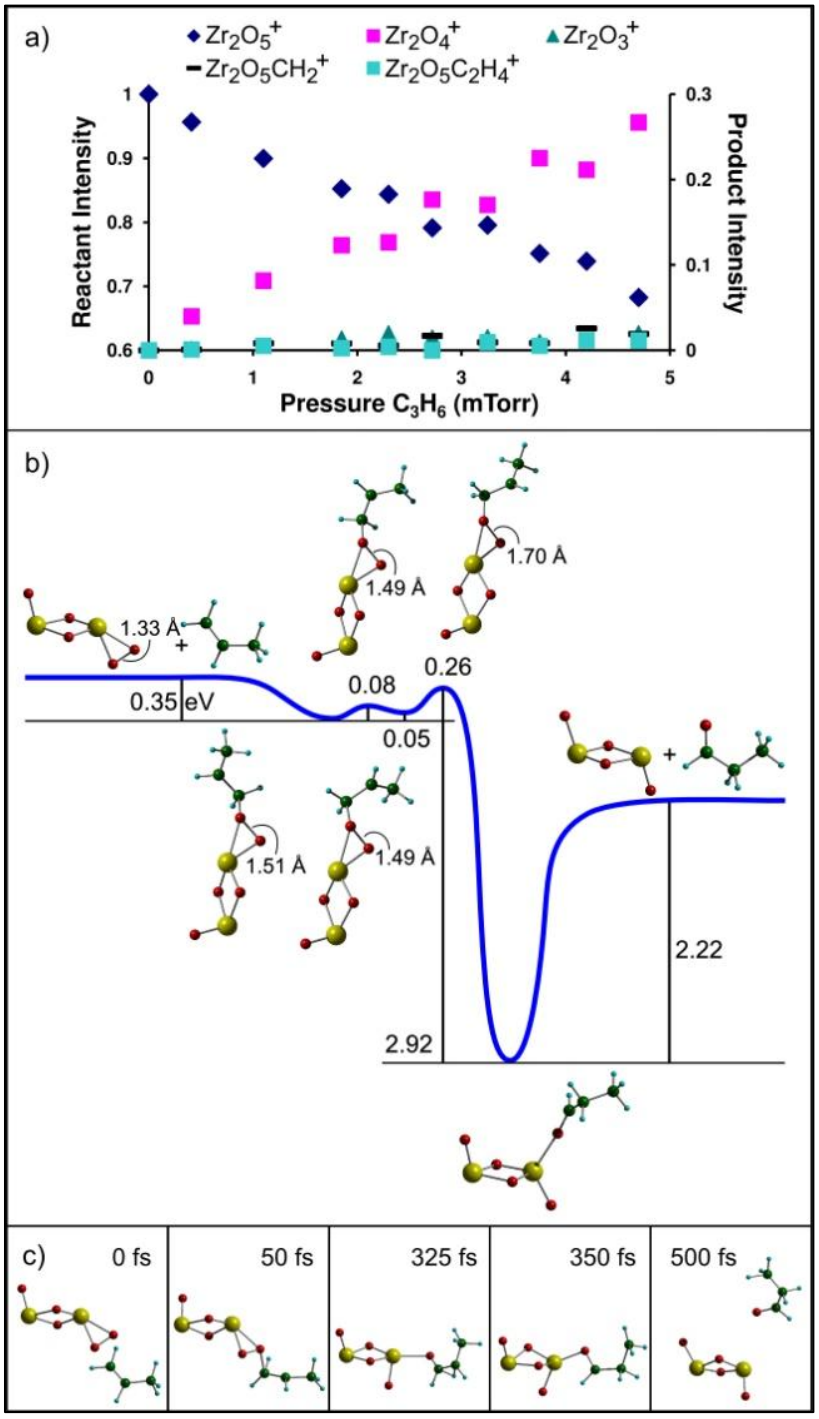

Figure 3-3. a) Branching ratios presented in normalized ion intensities for the reaction of $Zr_2O_5^+$ with C_3H_6. b) Calculated energy profile given in eV together with the structures and c) snapshots from the MD simulations performed at constant temperature (T = 1000 K) for reaction of $Zr_2O_5^+$ with C_3H_6 creating propanal. Reprinted from reference 37.

The energy profile presented in Figure 3-3b depicts the reaction mechanism for formation of propanal through oxidation of propene by $Zr_2O_5^+$. The binding of a terminal carbon in propene to an oxygen of the superoxide unit creates a stable complex 0.35 eV lower in energy than the reactants. The mechanism proceeds through the transfer of a hydrogen atom from the primary carbon to the central carbon with a concomitant scission of the superoxide bond. This step is followed by relaxation into a complex that is 3.27 eV more stable than the initial reactants. The overall formation of propanal and $Zr_2O_4^+$ through the interaction of propene and $Zr_2O_5^+$ is 1.05 eV exothermic. Creation of propanal is also illustrated by MD snapshots in Figure 3-3c. Formation of the isomer acetone has been calculated to be exothermic by 1.32 eV yet a barrier within the mechanism (Figure 3-4a) points to the creation of acetone being unlikely. The mechanism for the creation of an epoxide (Figure 3-4b) has also been calculated and the resulting products are of nearly the same energy as the reactants; thus creation of this product is not favorable. The oxidative nature of O_2^- when incorporated in the $Zr_2O_5^+$ cluster for the creation of the isomer propanal has been presented.

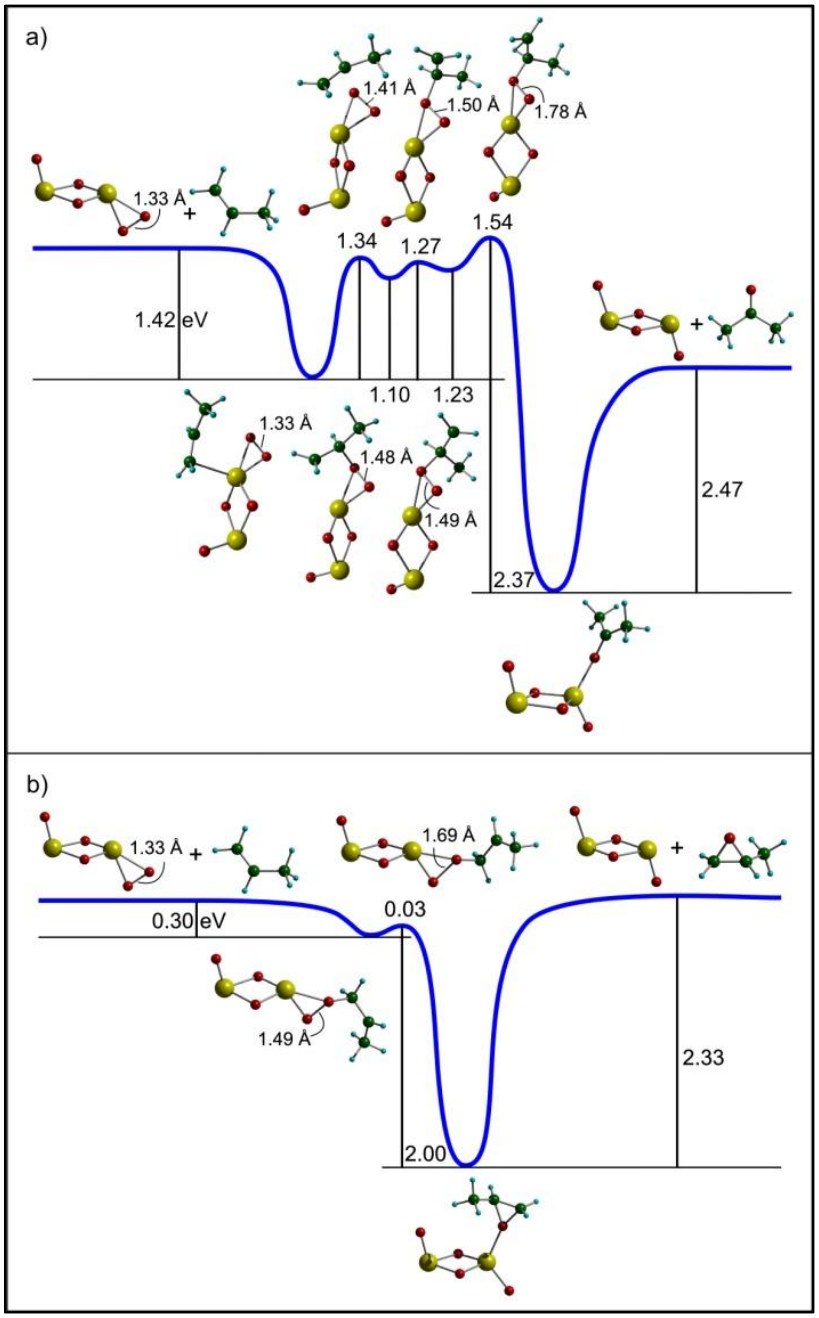

Figure 3-4. a) A calculated energy profile given in eV for reaction of $Zr_2O_5^+$ with C_3H_6 forming acetone. b) An additional calculated energy profile given in eV for reaction of $Zr_2O_5^+$ with C_3H_6 forming an epoxide. Reprinted from reference 37.

Butadiene Reactivity

Continuing the investigation into the reactivity properties of cationic zirconium superoxide clusters, the species $Zr_2O_5^+$ is interacted with butadiene. The primary products for the interaction between $Zr_2O_5^+$ and butadiene are described in equations 3.2 and 3.3.

$$Zr_2O_5^+ + C_4H_6 \rightarrow Zr_2O_4^+ + C_4H_6O \quad (3.2)$$

$$Zr_2O_5^+ + C_4H_6 \rightarrow Zr_2O_4C_3H_4^+ + OCH_2 \quad (3.3)$$

As seen in the branching ratio of Figure 3-5a oxidation of butadiene is a major reaction channel for the interaction with $Zr_2O_5^+$ accounting for 25% of the ions detected when 4.5 mTorr butadiene is introduced. Another significant reaction product is the $Zr_2O_4C_3H_4^+$ ion with the concomitant loss of the neutral product OCH_2. The $Zr_2O_4C_3H_4^+$ ion intensity is roughly 27% of the total ions detected, slightly higher than the $Zr_2O_4^+$ product. Other products attributed to association, cracking, and O_2 dissociation are detected, each accounting for 2-3% of the detected ions. The product $Zr_2O_5C_4H_6^+$ is due to association of the reactant to the ion while $Zr_2O_4C_4H_6^+$ is formed as energy gained through association of the reactant is great enough to release an oxygen atom. The formation of $Zr_2O_4C_2H_3^+$ results in a concomitant release of the neutral product OC_2H_3. Finally, the $Zr_2O_3^+$ ion is a collisional product that was also seen during the interaction with C_3H_6. The experimental results determine that the preferential oxidation of butadiene along with a competitive reaction channel for the loss of OCH_2 are the significant products in the interaction of $Zr_2O_5^+$ with butadiene.

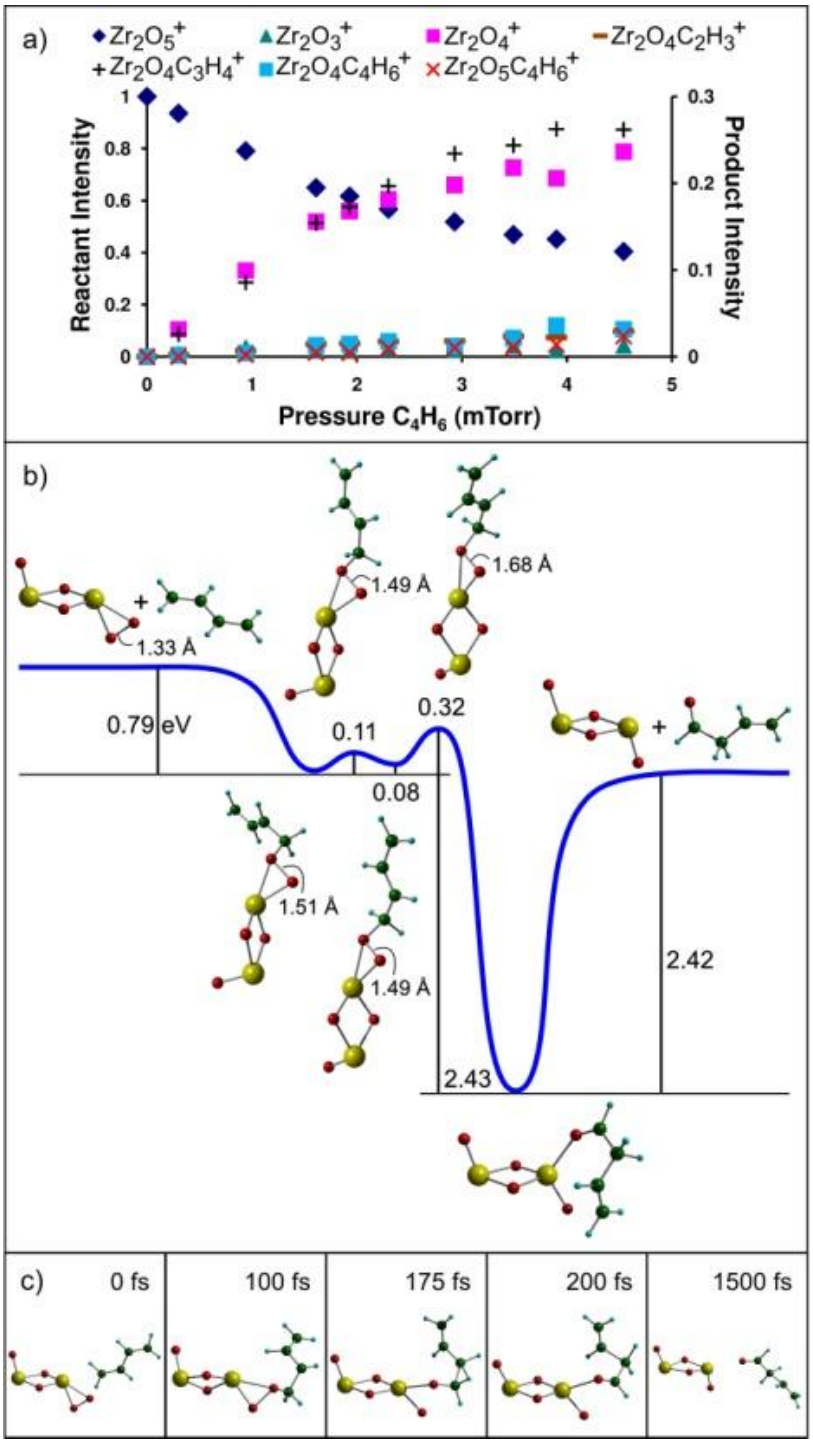

Figure 3-5. a) Branching ratios presented in normalized ion intensities for the reaction of $Zr_2O_5^+$ with C_4H_6. b) Calculated energy profile given in eV together with the structures and c) snapshots from the MD simulations performed at constant temperature (T = 1000 K) for reaction of $Zr_2O_5^+$ with C_4H_6 creating butenal. Reprinted from reference 37.

Theoretical methods have been employed to investigate the formation of butenal as well as OCH_2 upon interaction of $Zr_2O_5^+$ with butadiene. The reaction profile for the oxidation of butadiene, presented in Figure 3-5b, displays an encounter complex 0.79 eV more stable than the reactants with a structure similar to the encounter complex between propene and $Zr_2O_5^+$. The reaction proceeds through the simultaneous transfer of hydrogen and splitting of the O-O bond to form butenal in a process that is 0.80 eV exothermic overall. The MD Snapshots of Figure 3-5c display the steps required to accomplish the oxidation of butadiene and the dissociation of the products $Zr_2O_4^+$ and butenal.

The formation of OCH_2 has also been investigated theoretically and the MD snapshots are presented in Figure 3-6. Two pathways have been identified in the creation of OCH_2, both interacting initially with the superoxide unit. The pathway depicted in Figure 3-6a proceeds by formation of an aldehyde through hydrogen transfer from the bound carbon to the adjacent carbon. At this point the terminal end of the molecule connects with the remaining oxygen from the superoxide, thereby forming a ring structure. Subsequent cleavage of a carbon-carbon bond results in the release of neutral formaldehyde. Another viable pathway, presented in Figure 3-6b, ensues by initial formation of an epoxide. The terminal end of the hydrocarbon binds to the peripheral oxygen that was not part of the superoxide forming a ring structure. A carbon-carbon bond breaks, followed by isomerization, and ultimately the formaldehyde unit is released from the cluster. The calculations present the creation of formaldehyde in an exothermic process that does not require overcoming transitions that are higher in energy than the initial reactants. The interaction of butadiene and $Zr_2O_5^+$ has been investigated and found to create comparable amounts of butenal as well as formaldehyde.

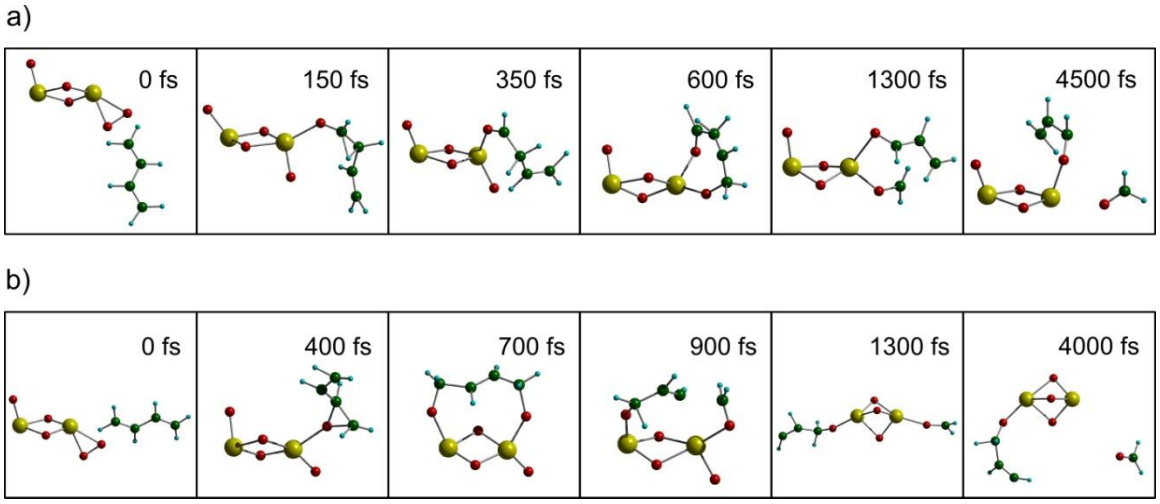

Figure 3-6. a) Snapshots from the MD simulation interacting $Zr_2O_5^+$ with C_4H_6, proceeding by formation of an aldehyde, towards the final product formaldehyde. b) Additional snapshots from the MD simulation proceeding by formation of an epoxide, towards the final product formaldehyde. Simulations conducted at constant temperature (T = 1500 K). Reprinted from reference 37.

Acetylene Oxidation

The interaction of $Zr_2O_5^+$ with acetylene further demonstrates the capacity for oxidation by the superoxide unit. The experimental results presented in branching ratio form (Figure 3-7a) display a preferential oxidation channel as described in equation 3.4.

$$Zr_2O_5^+ + C_2H_2 \rightarrow Zr_2O_4^+ + C_2H_2O \qquad (3.4)$$

The previously described reactions of cationic zirconium oxide clusters involved the interaction of a superoxide unit with an alkene; reaction with an alkyne hydrocarbon is now investigated. As mentioned, the primary reaction channel for oxidation of acetylene, accounting for 13% of the detected ions, is observed while additional channels for association of acetylene (3%) to the cluster and loss of two oxygen atoms (9%) are detected upon introduction of 5 mTorr of acetylene. Of note is the increased loss of two oxygen atoms (9%) from the cluster in

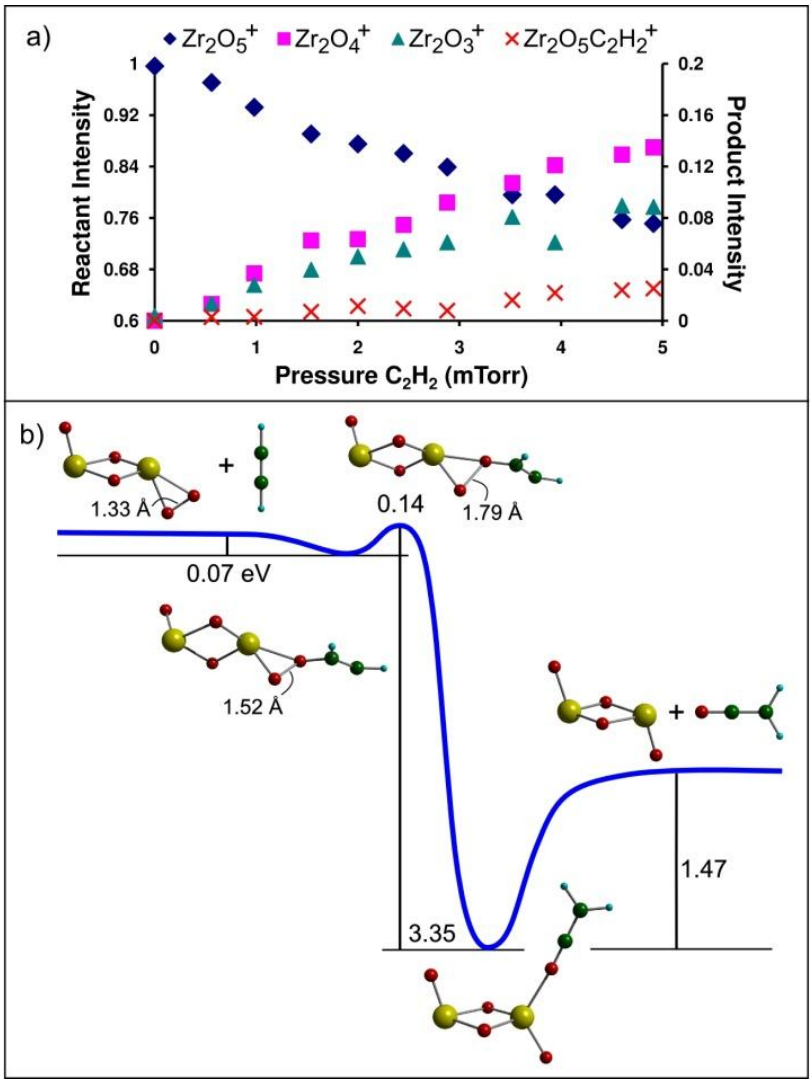

Figure 3-7. a) Branching ratios presented in normalized ion intensities for the reaction of $Zr_2O_5^+$ with C_2H_2. b) Calculated energy profile given in eV for reaction of $Zr_2O_5^+$ with C_2H_2 creating ethenone. Reprinted from reference 37.

comparison with the branching ratios for reaction with propene and butadiene (roughly 2%). The loss of two oxygen atoms discussed earlier during interaction with propene is attributed to the collisional dissociation of the superoxide unit from the cluster. In the present case, it is believed that the oxygen loss product $Zr_2O_4^+$ reacts with a second acetylene in the reaction cell transferring another oxygen atom, as multiple collision conditions are being employed. A previously

performed study revealed a strong oxidation mechanism during the reaction between $Zr_2O_4^+$, containing a radical oxygen active site, and acetylene leading to the second oxidation product. This investigation has further revealed the importance of the superoxide active site in catalysis, as after the primary reaction occurs an equally significant active site is created.

Theoretical calculations have determined ethenone to be the favorable isomer produced from the oxidation of acetone by $Zr_2O_5^+$. The reaction profile presented in Figure 3-7b displays the energetics and transition states for the oxidation of acetylene with a hydrogen transfer presenting a slight barrier toward the oxidation process. The association channel observed in the branching ratio is a result of interactions that may not have proceeded past the hydrogen transfer step and settled into the potential well. The overall process is the most exothermic of all mechanisms presented in this study with the desorbed products being 1.95 eV lower in energy than the reactants.

The interaction of propene, butadiene, and acetylene with the most active cluster, $Zr_2O_5^+$, has been discussed to detail the reactive nature of superoxide. The cluster displays superior oxidation toward the three reactants as presented in the branching ratios while energy profiles and MD simulations have provided detailed reaction mechanisms as well as determined the most favorable product isomers. Unexpected results are the energetically favorable formation of formaldehyde as a co-product in the oxidation of butadiene as well as identification of a secondary oxidation reaction during the interaction of $Zr_2O_5^+$ and acetylene. Insight into the reactive nature of superoxide units bound to zirconium has been developed through this investigation.

3.6 Interaction of ZrO_3^+ with Reactants

The interaction of ZrO_3^+ with butadiene appears to be very similar to the interaction with $Zr_2O_5^+$ as seen in the branching ratio of Figure 3-8a. The primary reaction channels are oxidation of butadiene and release of OCH_2 as described in equations 3.5 and 3.6.

$$ZrO_3^+ + C_4H_6 \rightarrow ZrO_2^+ + C_4H_6O \quad (3.5)$$

$$ZrO_3^+ + C_4H_6 \rightarrow ZrO_2C_3H_4^+ + OCH_2 \quad (3.6)$$

The oxygen transfer channel forming ZrO_2^+ is 14% of the ions detected with introduction of roughly 5 mTorr of butadiene and the $ZrO_2C_3H_4^+$ product accounts for 16%. It is also shown in the branching ratios that products attributed to association, replacement, and cracking are detected. With the introduction of 5 mTorr butadiene, the association product $ZrO_3C_4H_6^+$ and replacement product $ZrO_2C_4H_6^+$ results in 5% and 9% of the detected ions, respectively. At equivalent pressure, the product $ZrO_2C_2H_3^+$ accounts for roughly 5% of the ions detected. It is observed that the superoxide unit supported on ZrO_3^+ primarily reacts through the oxidation of butadiene and competitive creation of OCH_2.

Mechanistic aspects for the interaction between butadiene and the ZrO_3^+ cluster have been gained through theoretical calculations presented as energy profiles and MD snapshots. The energy profile for interaction of ZrO_3^+ (Figure 3-8b) with butadiene displays an association of the hydrocarbon to the superoxide unit with a binding energy of 0.95 eV; subsequent steps of the mechanism are analogous to those observed in the $Zr_2O_5^+$ profile creating butenal. An additional energetically stable interaction between butadiene and ZrO_3^+ is found to occur at the zirconium (Figure 3-9a) with both double bonds taking part in the association to zirconium (2.02 eV).

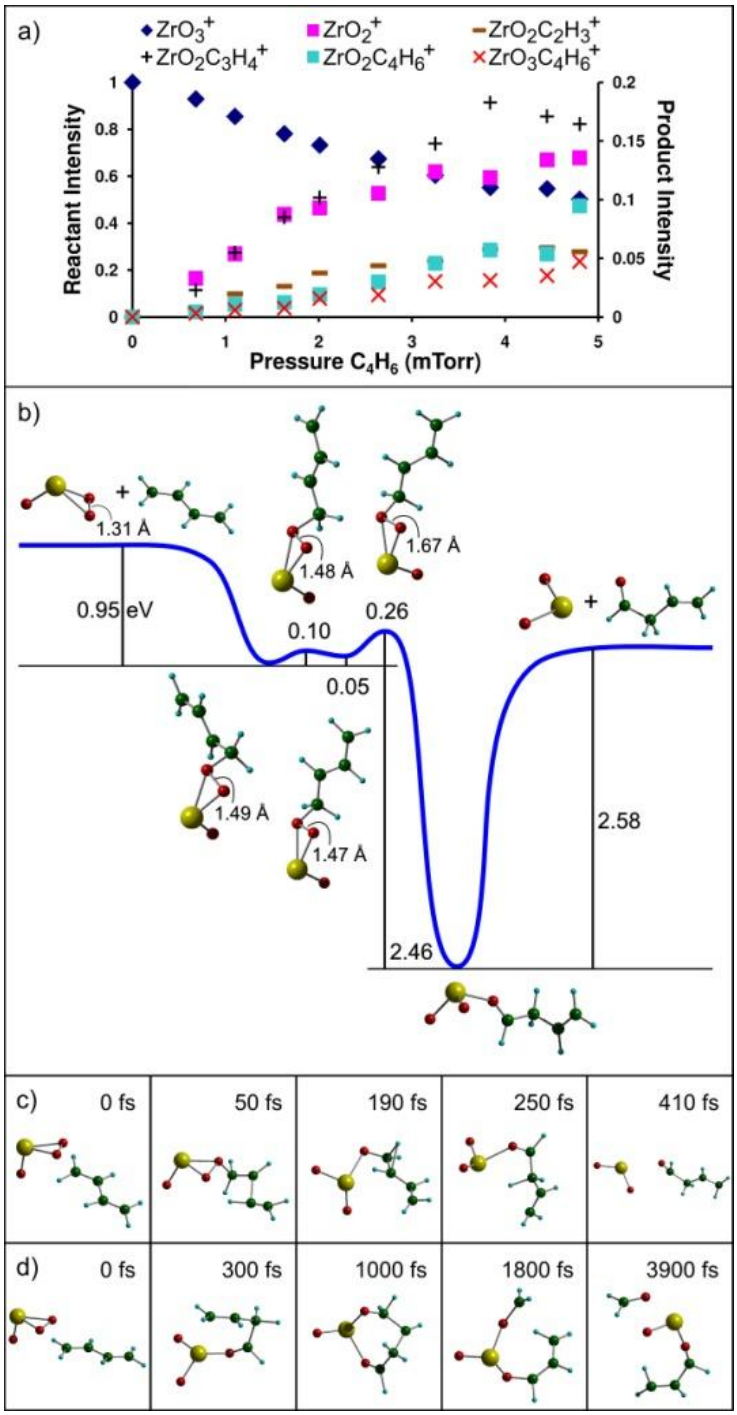

Figure 3-8. a) Branching ratios presented in normalized ion intensities for the reaction of ZrO_3^+ with C_4H_6. b) Calculated energy profile given in eV together with the structures and c) snapshots from the MD simulations performed at constant temperature (T = 1200 K) for reaction of ZrO_3^+ with C_4H_6 creating butenal. d) Snapshots from the MD simulation proceeding by formation of an aldehyde, towards the final product formaldehyde conducted at constant temperature (T = 1500 K). Reprinted from reference 37.

The transition that allows a terminal carbon to interact with the superoxide is 0.75 eV below the reactants, therefore being favorable for the oxidation of butadiene as well. The MD snapshots in Figure 3-8c and d display the steps for oxidation of butadiene and formation of formaldehyde, respectively and show similarity in the mechanism that is operative for the reaction of butadiene with $Zr_2O_5^+$.

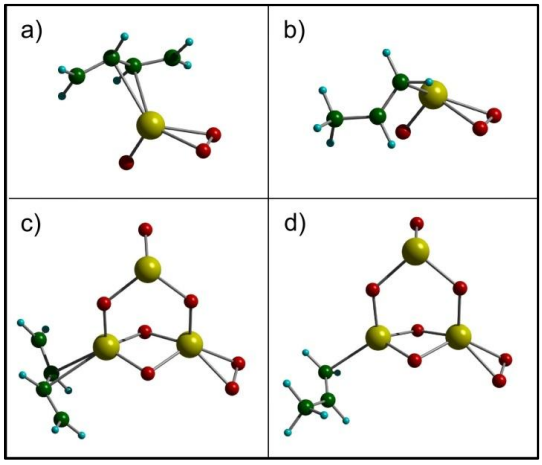

Figure 3-9. Depicted are the most energetically stable binding arrangements, occurring at the zirconium atom, for a) ZrO_3^+ with C_4H_6, b) ZrO_3^+ with C_3H_6, c) $Zr_3O_7^+$ with C_4H_6 and d) $Zr_3O_7^+$ with C_3H_6. Reprinted from reference 37.

Interaction of ZrO_3^+ with propene does not result in high reactivity or a primary reaction channel (Figure 3-10a). Oxidation, association, and cracking products (less than 5%) are detected in comparison to reactions with butadiene. Interaction between the doubly bound terminal carbon and zirconium (Figure 3-9b) results in the most stable association complex (1.70 eV); while interaction at the superoxide is less favorable (0.51 eV). A transition, 0.12 eV below the reactants, must be overcome to enable the propene to interact with the superoxide unit while still attached to the zirconium. The transition state is likely hindering the oxidation of propene. Additionally, the interaction of acetylene with ZrO_3^+ displays less reactivity than propene and hence is not discussed. In summary ZrO_3^+ is reactive towards butadiene while being relatively unreactive towards propene and acetylene.

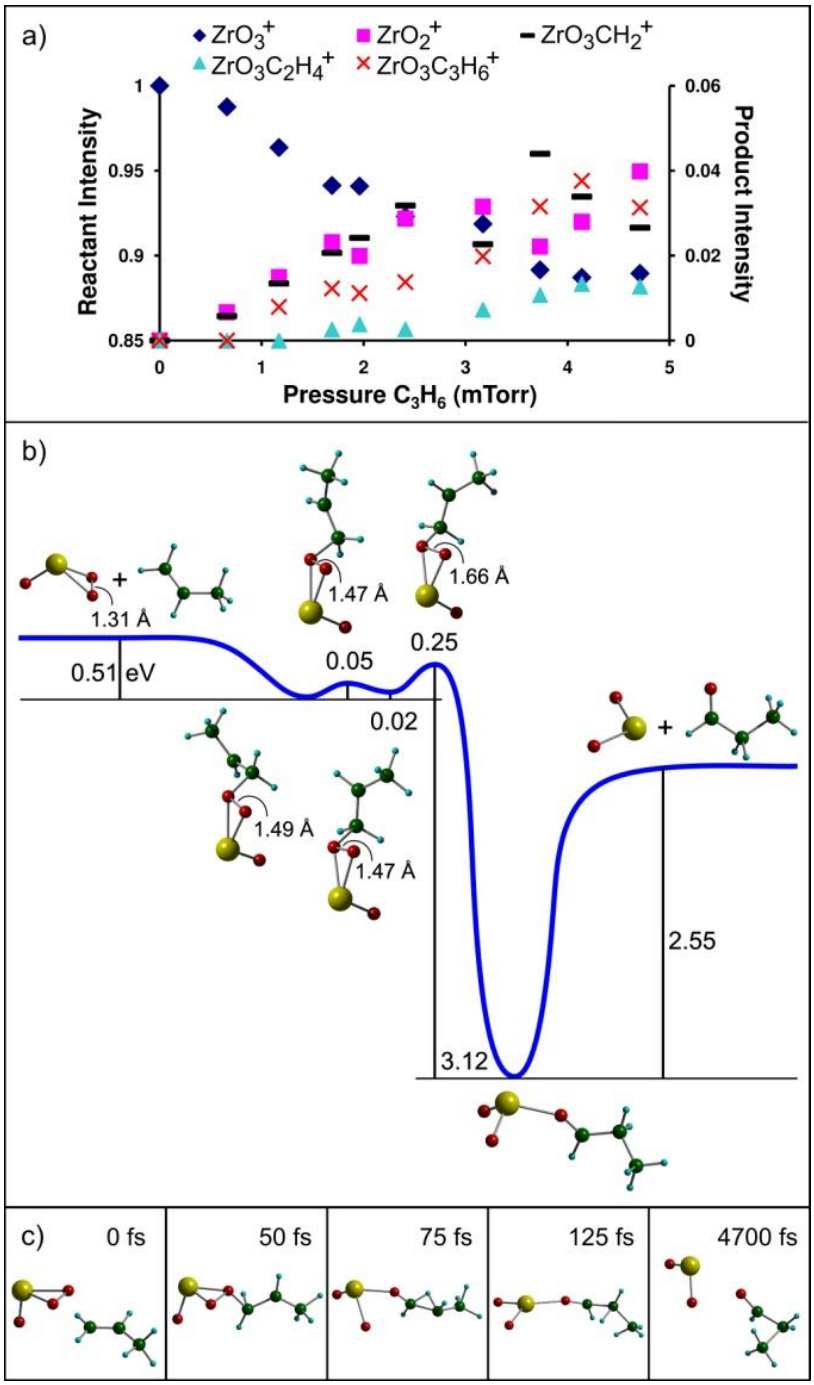

Figure 3-10. a) Branching ratios presented in normalized ion intensities for the reaction of ZrO_3^+ with C_3H_6. b) Calculated energy profile given in eV together with the structures and c) snapshots from the MD simulations performed at constant temperature (T = 1200 K) for reaction of ZrO_3^+ with C_3H_6 creating propanal. Reprinted from reference 37.

3.7 Interaction of $Zr_3O_7^+$ with Reactants

Oxidation is a minor channel in the branching ratios for interactions of $Zr_3O_7^+$ with butadiene and propene (Figure 3-11a and c). Although the oxidation reactions are exothermic (Figure 3-11b and d) the presence of barriers in the reaction mechanism are limiting the progression of the reaction (at ground energy) and causing the detected intensity for oxidation products to be low. Association is the major product for interaction of butadiene with $Zr_3O_7^+$. The association channel is linked to a strong interaction between the reactant and a zirconium atom that does not host the superoxide as seen in Figure 3-9c. The binding energy for association of butadiene to this zirconium center is 1.37 eV consisting of a structure in which all carbons

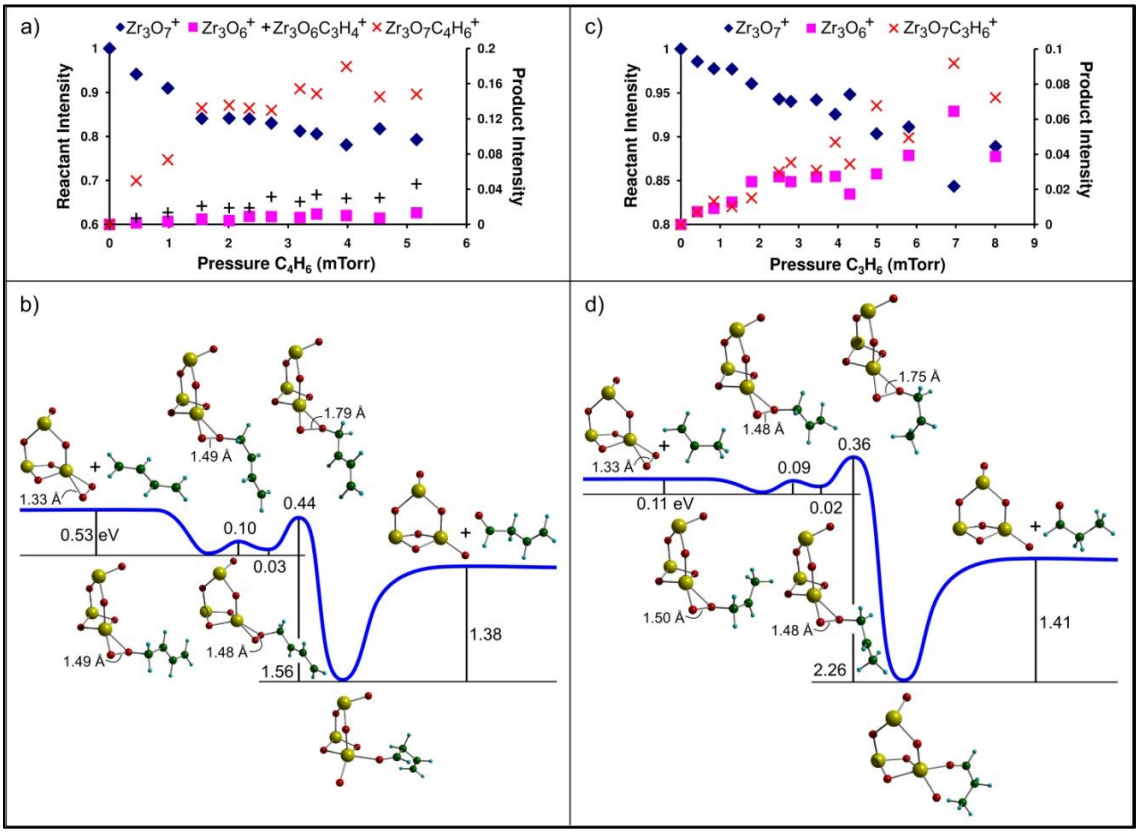

Figure 3-11. Branching ratios presented in normalized ion intensities for the reaction of $Zr_3O_7^+$ with a) C_4H_6 and c) C_3H_6. Calculated energy profile given in eV for reaction of $Zr_3O_7^+$ with b) C_4H_6 creating butenal and d) C_3H_6 creating propanal. Reprinted from reference 37.

interact with the zirconium atom. A transition 0.28 eV below the reactants must be overcome so that butadiene can interact with the superoxide unit. It is likely that the binding energy is distributed through the rotational/ vibrational modes of the cluster and the complex does not have enough energy to overcome the barrier for rearrangement.

In a similar fashion, association of propene to $Zr_3O_7^+$ is the primary product for interaction. Oxidation of propene is also observed as a reaction channel but of a lesser intensity. The binding energy of propene to a zirconium atom not attached to the superoxide unit (Figure 3-9d) is 1.24 eV while interaction between propene and the superoxide unit is 0.11 eV (Figure 3-11d). A rearrangement of the complex, similar to that for butadiene, would be required for propene to interact with the superoxide and is attributed as the cause for the larger association product and minor oxidation observed. Interaction between $Zr_3O_7^+$ and acetylene creates an association product with a minor oxidation similar to the reactivity of propene. The present study has demonstrated the importance that the surrounding environment plays in a reaction process. A reactant will bind to a cluster at the most energetically favorable site, in some cases this arrangement will hinder reaction as the distance between active site and associated reactant is too great. Thus catalysts must be designed with binding site and active site in reasonable proximity to one another.

3.8 Active Site Regeneration

Previous investigations performed by our laboratories were successful in regenerating the radical oxygen active site through introduction of the oxidizer N_2O to a mass selected cluster having one less oxygen. In the present study regeneration of the superoxide ($Zr_2O_5^+$) was attempted by interaction of $Zr_2O_3^+$ with O_2 and $Zr_2O_4^+$ with N_2O. Calculations determine that the oxidation of $Zr_2O_4^+$ by N_2O is unfeasible due to a barrier for the concerted breaking of an O—N

bond and simultaneous O—O bond formation. The regeneration of the superoxide is feasible through binding of an O_2 unit to the $Zr_2O_3^+$ species according to theory. Experimental methods were unable to regenerate the superoxide through either pathway. Although the active site has not been experimentally regenerated in the gas-phase, superoxide has been formed and characterized on zirconium oxide surfaces through the interaction of O_2 with the surface.[6-9] Thus, superoxide units on zirconium catalysts are appealing active sites as they oxidize various hydrocarbons and their formation mechanism on surfaces has previously been studied.

3.9 Comparing Activated Oxygen Species

The current work has provided a detailed analysis into the reactive nature of cationic zirconium oxide clusters containing superoxide units. A previous publication[18] investigated the reactivity of cationic zirconium oxide clusters containing a radical oxygen site, thus, a comparison between both forms of activated oxygen is in order. The discussion focuses on the clusters containing two zirconium atoms as they are the most active species. The $Zr_2O_4^+$ species (containing a radical oxygen) is active for oxygen transfer to CO and acetylene while reaction with ethene results in oxygen transfer and association products. In contrast, $Zr_2O_5^+$ (containing a superoxide unit) is unreactive toward CO and ethene while active for oxygen transfer and association with acetylene. Using the method described in Chapter 2, the pseudo-first order rate constant for oxygen transfer to acetylene is calculated to be more than twice as great for $Zr_2O_4^+$ (5.9×10^{-12} cm^3 s^{-1}) than $Zr_2O_5^+$ (2.7×10^{-12} cm^3 s^{-1}). $Zr_2O_5^+$ is active towards propene and butadiene; however it is likely that $Zr_2O_4^+$ will only display minor, if any, oxygen transfer toward these hydrocarbons as no excess O_2 loss was observed beyond CID levels. As mentioned earlier, an increased quantity of O_2 loss was detected upon reaction of $Zr_2O_5^+$ with acetylene as the $Zr_2O_4^+$ product from the initial oxygen transfer process undergoes a second oxygen transfer. As

an increased quantity of O_2 loss is not observed for the interaction of $Zr_2O_5^+$ with propene or butadiene it is unlikely that $Zr_2O_4^+$ will transfer oxygen to these reactants. In summation, $Zr_2O_4^+$ has a higher rate constant than $Zr_2O_5^+$ for oxygen transfer to acetylene yet both clusters present oxygen transfer towards reactants that the other does not.

3.10 Conclusion

Superoxide is a form of activated oxygen that has been identified on zirconium oxide surfaces. Theoretical and experimental means have been utilized to study the structure and reactivity of a series of clusters $Zr_xO_{2x+1}^+$ (x = 1 – 3) in the gas-phase that contain a superoxide. The species $Zr_2O_5^+$ is found to be highly oxidative during interaction with propene and acetylene as confirmed through MD simulations and the calculated energy profiles reveal the mechanisms of the reactions. Competitive mechanisms for formation of the oxidation product butenal and the creation of formaldehyde are determined for the interaction of $Zr_2O_5^+$ with butadiene. The reaction of ZrO_3^+ with butadiene also proceeds through energetically favorable mechanisms for the formation of formaldehyde and butenal while minimal reactivity is observed when propene and acetylene are introduced to ZrO_3^+. In contrast, association products result upon interaction of the reactants with $Zr_3O_7^+$. The prevalence in association products is attributed to barriers in the oxidation reaction mechanism as well as the most energetically stable binding site being located at a zirconium not attached to the superoxide unit. On the basis of these findings, we highlight the influence that the surrounding environment of a superoxide unit has toward reactivity properties and propose that future studies be performed to further this concept in catalytic materials.

3.11 References

1. Meier, D. C.; Lai, X.; Goodman, D. W. Surface Chemistry of Model Oxide-Supported Metal Catalysis: An Overview of Gold on Titania. In *Surface Chemistry and Catalysis*, Carley, A. F., Davies, P. R., Hutchings, G. J., Spencer, M. S., Eds.; Kluwer Acedemic/Plenum Publishers: New York, 2002; pp 147-189. Somorjai, G. A.; Li, Y. *Introduction to Surface Chemistry and Catalysis*, 2nd ed.; John Wiley and Sons. Inc.: Hoboken, New Jersey, 2010.
2. Yamaguchi, T. *Catal. Today* **1994**, *20*, 199.
3. Zhu, J.; van Ommen, J. G.; Bouwmeester, H. J. M.; Lefferts, L. *J. Catal.* **2005**, *233*, 434.
4. Berkstresser, G. W.; Brook, R. J.; Whelan, J. M. *J. Mater. Sci.* **1974**, *9*, 491.
5. Tidahy, H. L.; Hossein, M.; Siffert, S.; Cousin, R.; Lamonier, J.-F.; Aboukaïs, A.; Su, B.-L.; Giraudon, J.-M.; Leclercq, G. *Catal. Today* **2008**, *137*, 335.
6. Bedilo, A. F.; Poltnikov, M. A.; Mezentseva, N. V.; Volodin, A. M.; Zhidomirov, G. M.; Rybkin,I. M.; Klabunde, K. J. *Phys. Chem. Chem. Phys.* **2005**, *7*, 3059.
7. Zhao, Q.; Wang, X.; Cai, T. *Appl. Surf. Sci.* **2004**, *225*, 7.
8. Labaki, M.; Siffert, S.; Lamonier, J.-F.; Zhilinshaya, E. A.; Aboukaïs, A. *Appl. Catal. B-Environ.* **2003**, *43*, 261.
9. Lamonier, J.-F.; Labaki, M.; Wyrwalski, F.; Siffert, S.; Aboukaïs, A. *J. Anal. Appl. Pyrol.* **2008**, *81*, 20.
10. Zhu, J.; van Ommen, J. G.; Lefferts, L. *Catal. Today* **2006**, *112*, 82.
11. Bohme, D. K.; Schwarz, H. *Angew. Chem. Int. Ed.* **2005**, *44*, 2336.
12. Johnson, G. E.; Mitrić, R.; Bonačić-Koutecký, V.; Castleman, A. W., Jr. *Chem. Phys. Lett.*, **2009**, *475*, 1.

13. Tyo, E. C.; Nößler, M.; Mitrić, R.; Bonačić-Koutecký, V.; Castleman, A. W., Jr. *Phys. Chem. Chem. Phys.* **2011**, *13*, 4243.

14. Nößler, M.; Mitrić, R.; Bonačić-Koutecký, V.; Johnson, G. E.; Tyo, E. C.; Castleman, A. W., Jr. *Angew. Chem. Int. Ed.* **2010**, *49*, 407.

15. Dong, F.; Heinbuch, S.; Xie, Y.; Rocca, J. J.; Bernstein, E. R.; Wang, Z.-C.; Keng, K.; He, S.-G. *J. Am. Chem. Soc.*, **2008**, *130*, 1932.

16. Rothgeb, D. W.; Hossain, E.; Kuo, A. T.; Troyer, J. L.; Jarrold, C. C.; Mayhall, N. J.; Raghavachari, K. *J. Chem. Phys.*, **2009**, *130*, 124314.

17. Johnson, G. E.; Mitrić, R.; Nößler, M.; Tyo, E. C.; Bonačić-Koutecký, V.; Castleman, A. W., Jr. *J. Am. Chem. Soc.* **2009**, *131*, 5460.

18. Johnson, G. E.; Mitrić, R.; Tyo, E. C.; Bonačić-Koutecký, V.; Castleman, A. W., Jr. *J. Am. Chem. Soc.* **2008**, *130*, 13912.

19. Wu, X.-n.; Zhao, Y.-x.; He, S.-g. Ding, X.-l. *Chin. J. Chem. Phys.* **2009**, *22*, 635.

20. Ma, J.-b.; Wu, X.-n. Zhao, Y.-x. Ding, X.-l.; He, S.-g. *Chin. J. Chem. Phys.* **2010**, *23*, 133.

21. Ma, J.-b.; Wu, X.-n. Zhao, Y.-x. Ding, X.-l.; He, S.-g. *J. Phys. Chem. A* **2010**, *114*, 10024.

22. Huang, X.; Zhai, H.-J.; Waters, T.; Li, J.; Wang, L.-S. *Angew. Chem. Int. Ed.* **2006**, *46*, 657.

23. Zhai, H.-J.; Kiran, B.; Cui, L.-F.; Li, X.; Dixon, D. A.; Wang, L.-S. *J. Am. Chem. Soc.* **2004**, *126*, 16134.

24. Bell R. C.; Castleman, A. W., Jr. *J. Phys. Chem. A*, **2002**, *106*, 9893.

25. Becke, A. D. *Phys. Rev. A* **1988**, *38*, 3098-3100.

26. Becke, A. D. *J. Chem. Phys* **1993**, *98*, 5648-5652.

27. Lee, C.; Yang, W.; Parr, R. G.; *Phys. Rev. B* **1998**, *37*, 785-789.

28. Dolg, M.; Stoll, H.; Preuss, H.; Pitzer, R. M.; *J. Phys. Chem.* **1993**, *97*, 5852.

29. Andrea, D.; Haeussermann, U.; Dolg, M.; Stoll, H.; Preuss, H. *Theor. Chim. Acta* **1990**, *77*, 123-141.

30. Gilb, S.; Weis, P.; Furche, F.; Aldrichs, R.; Kappes, M. M. *J. Chem. Phys.* **2002**, *116*, 4094-4101.

31. Schaefer, A.; Huber, C.; Ahlrichs, R. *J. Chem. Phys.* **1994**, *100*, 5829.

32. Justes, D. R.; Mitrić, R.; Moore, N. A.; Bonačić-Koutecký, V.; Castleman, A. W., Jr. *J. Am. Chem. Soc.* **2003**, *125*, 6289.

33. Ahlrichs, R.; Bär, M.; Häser, M.; Horn H.; Kölmel, C. *Chem. Phys. Lett.*, **1989**, *162*, 165-169.

34. Dunlap, B. I.; Connolly, J. W. D.; Sabin, J. R. *J. Chem. Phys.* **1979**, *71*, 3396-3402.

35. Eichkorn, K.; Treutler, O.; Ohm, H.; Haser, M.; Aldrichs, R. *Chem. Phys. Lett*. **1995**, *242*, 652-660.

36. Perdew, J. P.; Burke, K.; Ernzerhof, M. *Phys. Rev. Lett*. **1996**, *77*, 3865-3868.

37. Tyo, E. C.; Nößler, M.; Harmon, C. L.; Mitrić, R.; Bonačić-Koutecký, V.; Castleman, A. W., Jr. *J. Phys. Chem. C* **2011**, *115*, 21559.

Chapter 4

Analogous Reactivity of Pd+ and ZrO+: Comparing the Reactivity with Small Hydrocarbons

4.1 Introduction

The group 10 metals, Ni, Pd, and Pt, have filled or nearly filled d shells and are widely used as catalysts due to their high activity for a number of reactions.[1-7] Limited quantities of these precious metals exist that motivates attempts to identify inexpensive replacement catalysts with comparable efficiency. Early transition metals are generally too reactive to be effective catalysts, however it has been proposed that by incorporating nonmetallic elements, e.g., carbon or oxygen, into an early transition metal, the surface reactivity of the metal can be moderated to produce an effective catalyst. The non-metal changes the electron density of the metal, and modulates the position of the d states near the Fermi energy.[8] Research in this vein has demonstrated that tungsten carbide and molybdenum carbide surfaces display chemical reactivity similar to platinum and ruthenium surfaces, respectively.[8-10] Extensive studies have been conducted to determine if further comparisons can be found[11-13] and investigations have shown that the coordination of non-metal atoms around metal atoms has a large influence upon catalytic activity as does the presence of impurities including excess carbon or oxygen.[14,15] Studies probing the reactivity of isolated gas-phase ions with simple alkanes provide the opportunity to identify the potential microscopic origins of the observed reactivity similarities.

Spectroscopic investigations have been undertaken in our laboratory to determine if similar valence electronic structures are observed between heteroatomic molecules and group 10 metal ions.[16] Photoelectron studies using 532 nm light were performed on WC^- and Pt^-, revealing comparable electronic transitions and orbital symmetry. Subsequent studies of the pairs Ni^-/TiO^- and Pd^-/ZrO^- revealed commonality in their electronic spectrum. Based on these experimental findings, Peppernick *et al.* proposed that ZrO^- can be viewed as the superatomic form of Pd^-, or at least they have similar electronic structures within 2.33 eV of the Highest Occupied Molecular Orbital (HOMO) of the anion.[16] The intentions of the present study are to investigate the reaction of ZrO^+ and Pd^+ with ethane and propane through gas-phase experimental and theoretical investigations. Thus determining if the similarities of electronic structure in anions can be extended to cations and result in similar reactivity. Interest in palladium arises due to its high cost and use as an effective combustion catalyst. The identification of an alternative less expensive catalyst will be economically beneficial.

Gas-phase guided-ion-beam mass spectrometry studies enable the investigation of reactions between mass selected ionic clusters and small hydrocarbons. Mechanistic details of heterogeneous catalytic processes, as well as bond energies for transition metal ion-ligand complexes, can be determined.[17-21] Theoretical calculations provide detailed insights of reaction profiles including transition states, energy barriers and chemical transformations occurring during a catalytic processes. Through such experimental and theoretical investigations, specific clusters have been identified that are highly oxidative in nature as well as others that are proficient for activation of O_2.[22-26] It is believed that knowledge gained through such investigations may find use towards the directed design of highly active and selective catalysts.

Earlier thermochemical studies conducted by Armentrout and coworkers investigated the activation of C_2H_6 and C_3H_8 by Pd^+. The findings revealed the existence of channels for the cleavage of C-C and C-H bonds at high kinetic energy (10-30 eV in the lab frame).[17] Similar

studies were performed for the reaction of Zr^+ with C_2H_6 and C_3H_8 that resulted in quite different kinetic energy dependent reactivity than Pd^+, the dominant process for reaction with Zr^+ being dehydrogenation at low energy (less than 5 eV in the lab frame).[21] The findings reported herein provide the opportunity to compare the reactivity of various ionic species with Pd^+. Specifically, studies are performed to investigate C-H and C-C bond breaking processes when reacting ethane and propane with Pd^+ and ZrO^+ under comparable energetic conditions. In order to ascertain whether the reactions are ion specific, or merely involved transition metal oxide ions, reactions are undertaken interacting VO^+ with ethane and propane to determine if C-H and C-C bond cleavage are unique reaction channels to Pd^+ and ZrO^+.

4.2 Experimental Methods

The reactivity of cationic Pd^+ and ZrO^+ with C_2H_6 (99%, Specialty Gas Co.) and C_3H_8 (99%, GT&S Welco) is studied utilizing a guided-ion-beam mass spectrometer that has been described in Chapter 2. Ions are produced in a laser vaporization (LaVa) source via pulsing an expansion gas, composed of 2.5% oxygen (99.993%, GT&S Welco) seeded in helium (99.99%, GT&S Welco), into the plasma created through ablation of a palladium (99.9%, Alfa Aesar) or zirconium (99.95%, Research and PVD Materials Corp.) rod by the second harmonic (532 nm) of a Nd:YAG laser. Expansion gas mixtures consisting of 1-10% oxygen were tested. To create endothermic reaction conditions, a negative potential is applied to the reaction cell during experimentation. A range of energies from 0 to 30 eV in the lab frame has been studied and the most reactive conditions for the interaction of Pd^+ with both C_2H_6 and C_3H_8 is at 20 eV in the lab frame. The center of mass frame energy (E_{CM}) for interaction of Pd^+ and ZrO^+ with the reactant molecules at 20 eV in the lab frame (E_{Lab}) is calculated using equation 4.1.

$$E_{CM} = E_{LAB} \frac{Mass\,[Reactant\,Gas]}{Mass\,[Cluster] + Mass\,[Reactant\,Gas]} \quad (4.1)$$

The mass of Pd^+ (106.42 amu) and ZrO^+ (107.22) are nearly the same so their E_{CM} is essentially the same. The E_{CM} is 4.4 eV and 5.9 eV for interaction with ethane and propane, respectively.

To extract the ions from the octopole collision cell a potential of nearly -90 V is applied to the electrostatic lenses following the octopole. A high potential is necessary as the positive ions are strongly attracted to the octopole rods and many do not leave the reaction cell. The product ions flow into a second quadrupole mass filter that scans a (m/z) range of 40-740 amu for product mass determination. Lastly, resultant ions are detected by a channel electron multiplier (CEM) connected to a multichannel scalar card.

The experimental branching ratios presented in Section 4.4 depict the normalized ion intensities of products and reactants detected at increasing pressures of reactant. The pressure of reactant introduced to the collision cell varied from 0 to 5 mtorr. The threshold between single and multiple collision conditions within the experiment is roughly 1 mTorr. Working under both single and multiple collision conditions assists in identifying reaction mechanisms.[25] As the potential applied to the reaction cell is a uniform field, the energy of the primary and subsequent interactions will be nearly the same. It can be seen that for reactive species, an increase of reactant in the collision cell results in a concomitant rise in products while the parent species decreases in intensity. Presentation of pressure dependent branching ratios provides the ability to observe reaction channels due to secondary collisions as well as competing mechanisms that appear at higher pressures. The interaction with deuterated ethane (98% D_6 Ethane, Cambridge Isotope) has also been studied under the same reaction conditions to confirm hydrogen abstraction products.

4.3 Theoretical Calculations

Calculations are performed by the Khanna group at the Virginia Commonwealth University that compliment experimental results by providing mechanistic detail of reaction processes and electronic structures. First-principles electronic structure studies of the ions have been performed within a gradient corrected density functional formalism. The calculations are carried out using the ADF[28] set of codes while using the PBE generalized gradient approximation[29] for exchange and correlation. For all elements a Triple-ζ2P basis is employed with an all electron calculation that incorporates the Zeroth Order Regular Approximation for relativistic effects.[30] Transition states are determined using a linear transit approach.

4.4 Results and Discussion

The reaction of Pd^+ and ZrO^+ with C_2H_6 and C_3H_8 has been conducted at 20 eV in the lab frame over the 0 to 5 mTorr range of pressure. The reactivity observed under these conditions is cracking of C-C bonds as well as C-H bond cleavage. Theoretical findings from the present study have determined the intermediate states as well as associated energetic barriers for the experimentally detected bond cleavages. The following chemical formula detail the masses detected through mass spectrometry; structural detail of the product ions is presented within the theoretically determined reaction profiles. Following is a detailed analysis of the activity observed for Pd^+ and ZrO^+.

Identifying Products

The spectra for interaction of Pd^+ and ZrO^+ with C_3H_8 at 20 eV in the lab frame are presented in Figure 4-1a and 4-1b, respectively. Major products observed in the Pd^+ spectrum

(Figure 4-1a) for the 40 – 740 amu mass range are CH_3Pd^+, $C_2H_3Pd^+$, and $C_3H_5Pd^+$. The ZrO^+ spectrum (Figure 4-1b) presents products of the intensity $CH_3ZrO^+ > C_2H_3ZrO^+ > C_3H_5ZrO^+$, the same ordering as Pd^+. The reported products are those that are discernable under our reaction conditions and experimental capabilities. Spectra for the interaction of Pd^+ and ZrO^+ with ethane also present products for C-C and C-H bond breaking.

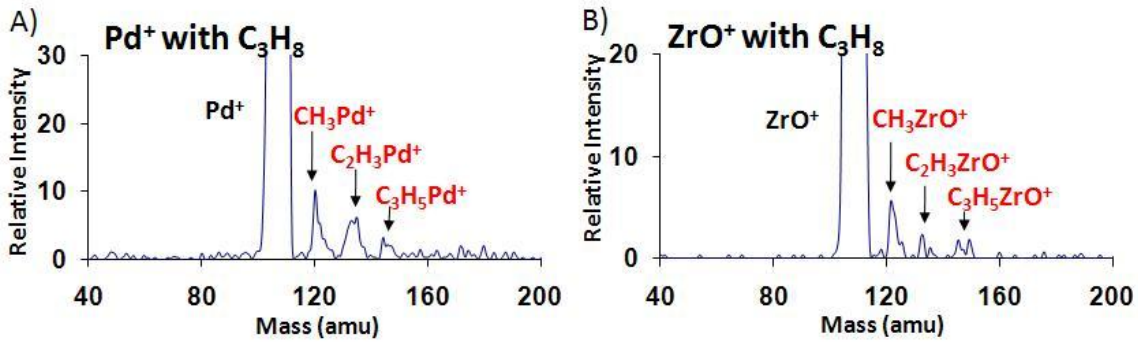

Figure 4-1. Spectra for the interaction of a) Pd^+ with 3.50 mTorr C_3H_8 and b) ZrO^+ with 3.90 mTorr C_3H_8 both occurring at 20 eV in the lab frame. Reproduced from reference 31.

Ethane Reactivity

Having presented the raw experimental data for interaction of ions with propane, the reaction with ethane will first be discussed followed by the analysis of propane reactivity. The major product detected for the interaction of the ions with ethane comprises a CH_3 unit bound to the ion, resulting in CH_3Pd^+ (or CH_3ZrO^+). This reaction is due to the activation and cracking of the C-C bond with release of a CH_3 neutral product as shown in equation 4.2. Another detected reaction product is $C_2H_4Pd^+$ (or $C_2H_4ZrO^+$) that is due to the activation of C-H bonds with the release of H_2 from ethane in accord with equation 4.3.

$$Pd^+ + C_2H_6 \rightarrow CH_3Pd^+ + CH_3 \quad (4.2)$$

$$Pd^+ + C_2H_6 \rightarrow C_2H_4Pd^+ + H_2 \quad (4.3)$$

The branching ratios in Figure 4-2 show that as the pressure of ethane is increased within the reaction cell, the relative intensity of products increases for both Pd^+ and ZrO^+. C-C cracking is the most active reaction channel presented in the branching ratios for the reactions of Pd^+ and ZrO^+ with ethane. Cleavage of C-H bonds is detected to a lesser extent. Furthermore, studies are performed using C_2D_6 as the reactant gas, under the same conditions, for confirmation of the products. Results from the deuterated studies support the mass assignments and the mechanisms in equations 4.2 and 4.3.

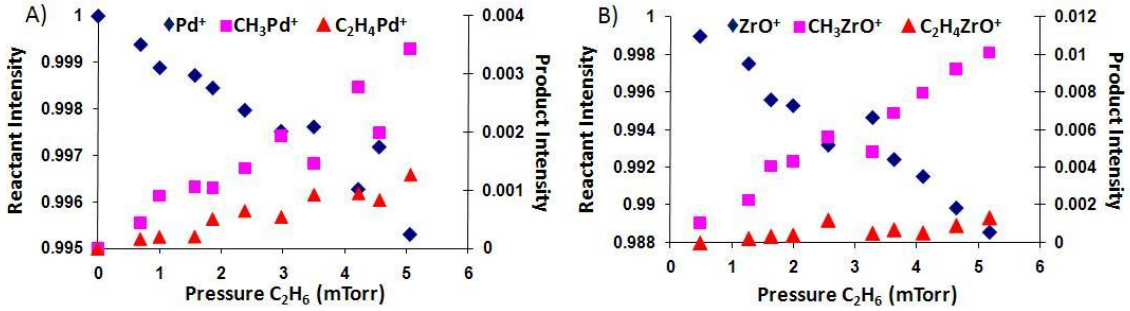

Figure 4-2. a) Pd^+ and b) ZrO^+ are reacted with 0 – 5 mTorr C_2H_6 at 20 eV in the lab frame. The branching ratios display the decrease in reactant intensity with the concomitant rise in product intensity as the pressure of gas in the reaction cell is increased. Reproduced from reference 31.

Calculation of the phenomenological rate constants is performed to aid in the comparison of the reactivity of ethane with the ions Pd^+ and ZrO^+. In similar fashion to the method used in Chapter 2, assuming pseudo-first-order kinetics the rate constants are calculated using equation 4.4.

$$\ln \frac{I_r}{I_0} = -k[R]t \qquad (4.4)$$

In equation 4.4, I_r represents the reactant ion intensity upon introduction of ethane, I_0 the reactant ion intensity without introduction of ethane, k the rate constant, R the concentration of reactant

gas, and t is the time the ion spends within the reaction cell. The previous calculation of the reaction time in Chapter 2 was accomplished by determining the velocity of an ion leaving the supersonic expansion using the equations of Anderson and Fenn[32] along with measuring the distance of the reaction cell (12.9 cm) through a trapezoidal pressure falloff approximation.[27a] In this experiment the contribution of velocity due to the supersonic expansion is minor in comparison to the velocity gained by the high potential applied to the octopole.[27b] The velocity (v) of 6010 m/s due to the voltage applied to the octopole is calculated using equation 4.5.

$$v = (2qE_{Lab}/m)^{1/2} \tag{4.5}$$

The charge of the ion is q and the mass is m. The reaction cell is still 12.9 cm in length. The slope taken from the plot of ln I_r/I_0 vs. R (Figure 4-3) is equivalent to –kt. An earlier investigation performed in our laboratory found good agreement between rate constants determined through the pseudo-first-order method and those determined through acquiring cross sections under single collision conditions.[27b] The rate constant value is on the order of 1.1 x 10^{-12} cm^3 s^{-1} for Pd^+ and 3.0 x 10^{-12} cm^3 s^{-1} for ZrO^+. The error bars are estimated to be ± 30%. Through experimental analysis it is determined that Pd^+ and ZrO^+ react with ethane in a similar nature creating common products while ZrO^+ reacts at a slightly higher rate.

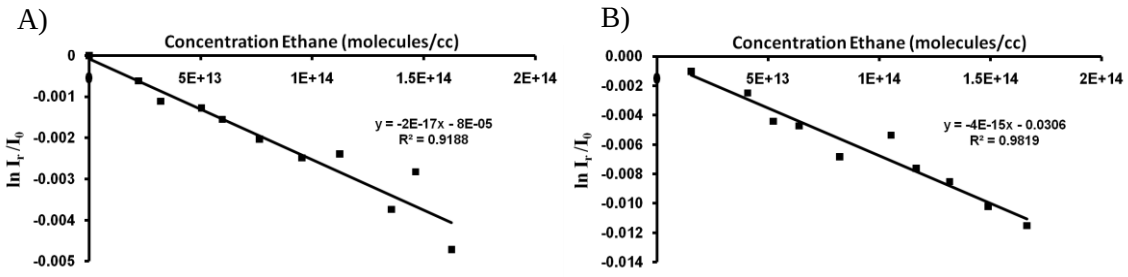

Figure 4-3. Plot of the logarithmic ratios of reactant intensity in the presence and absence of ethane (ln I_r/I_0) vs. concentration of ethane for a) Pd^+ and b) ZrO^+.

To better understand the observed reactivity, density functional theory is used to calculate energy profiles for the reactions of interest. As seen in Figure 4-4a and 4-4b, the insertion of Pd^+ into the C-C bond of ethane requires 0.97 eV while the barrier for ZrO^+ to insert into the C-C bond of ethane requires 1.33 eV. The complexes relax into an intermediate species with cleaved C-C bonds. The intermediate for Pd^+ is more stable than that for ZrO^+, lying 0.76 eV below the transition state for Pd^+, while only 0.14 eV below the transition state for ZrO^+. The removal of the methyl radical results in a process that is endothermic by 1.12 eV for Pd^+, and 0.85 eV for ZrO^+. For comparison, the cleavage of the C-C bond by Zr^+ is shown in Figure 4-4c. A transition for Zr^+ to insert into the C-C bonds is 0.81 eV above the association complex. The relaxed product, where the C-C bond is cleaved, is 3.52 eV below the reactants. Note the different scale in Figure 4-4c versus Figure 4-4a and 4-4b. The lower transition for C-C bond cleavage and the much stronger bonding between the methyl groups and Zr^+ show that to adjust the reactivity to be more like Pd^+, the strength of association must be reduced. Further, the strong binding of the methyl groups indicate that zirconium is likely to result in a reactive but rapidly poisoned "catalyst". This demonstrates that the addition of an oxygen atom reduces the reactivity of zirconium and makes the reaction profile closer to that of palladium.

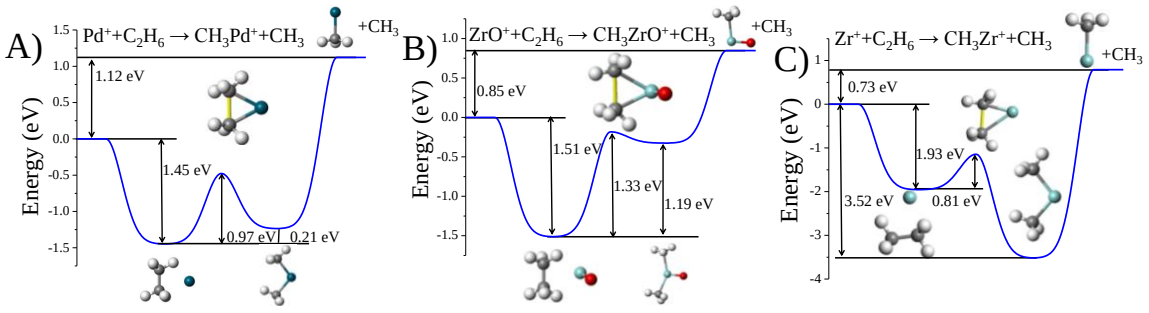

Figure 4-4. Energy profiles for the reaction of a) Pd^+, b) ZrO^+, and c) Zr^+ with ethane to form CH_3Pd^+, CH_3ZrO^+, and CH_3Zr^+ respectively. Reproduced from reference 31.

Reaction pathways in which the C-H bond is cleaved, resulting in the loss of H_2 by Pd^+ and ZrO^+ are shown in Figure 4-5a and 4-5b respectively. Initial interaction between C_2H_6 and the ions Pd^+ and ZrO^+ are roughly -1.45 eV and -1.30 eV, respectively; however density functional theory overestimates the binding energy of ions with molecules due to delocalization error.[33] The energy required to cleave the first C-H bond with Pd^+ is 0.65 eV, while it is 1.38 eV with ZrO^+. The intermediate state with the C-H bond cleaved by ZrO^+ is barely a local minimum in the energy landscape. The instability of intermediates versus products is a positive trait for catalysts, as trapping the complex in a stable intermediate may poison the catalyst. In fact, the energy landscape for the proton moving on the surface of ZrO^+ is unusually flat as shown in Figure 4-5b, and the barrier for H_2 formation once the C-H bond has been cleaved is only 0.03 eV. In the Pd^+ reaction pathway of Figure 4-5a, the primary barrier that needs to be overcome is the cleaving of the second C-H bond while forming H_2. In both reaction pathways, the H atom abstracted in the first step helps to cleave the second C-H bond by forming H_2.[34,35] The complex remaining after creation of H_2 contains an ethene bound to Pd^+ or ZrO^+. In the reaction pathways with both Pd^+ and ZrO^+, the complex with ethene is quite stable, and the release of H_2 requires 0.55 and 0.51 eV for Pd^+ and ZrO^+, respectively. It has been established through our experiment that the loss of H_2 occurs at an increased energy of 20 eV in the lab frame. The binding energy of Pd^+ and C_2H_6 in the reaction profile is overestimated through delocalization error and thus the transition states become barriers for the dehydrogenation process at thermal energies.

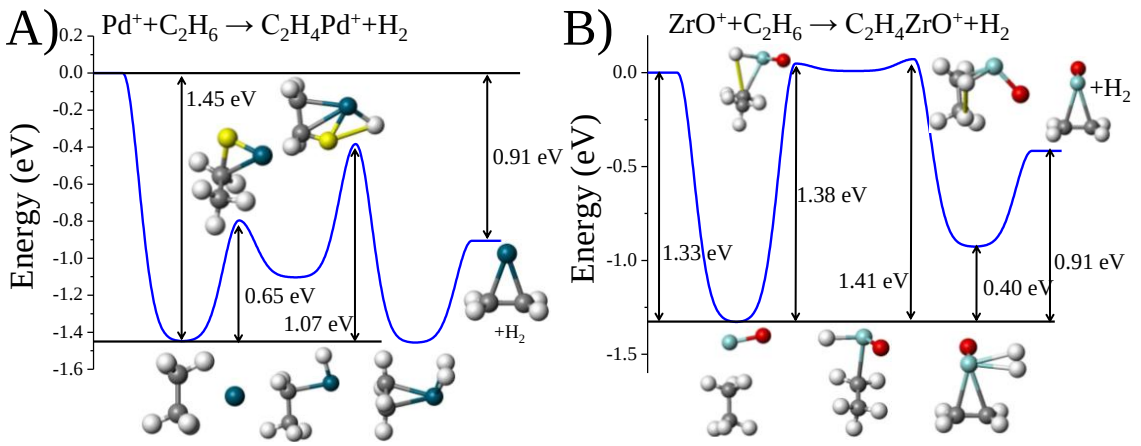

Figure 4-5. Energy profiles for the reaction of a) Pd^+ and b) ZrO^+ with ethane to form $C_2H_4Pd^+$ and $C_2H_4ZrO^+$. Reproduced from reference 31.

In Figure 4-6, the electronic structure of Pd^+, ZrO^+, and Zr^+ are plotted at the transition state for C-C bond cleavage in ethane. The molecular orbitals of the three transition states show the role of O on the coupling between the ions and ethane. Pd^+ has a nearly filled 4d manifold, so part of the reason for the similarity is that molecular orbitals with 4d Zr components in ZrO^+ are occupied, primarily as a result of hybridization between Zr and O orbitals. Additionally, one of the nonbonding delta molecular orbitals that are perpendicular to the Zr-O bond is stabilized and becomes occupied upon interaction with the stretched C-C bond. In the transition state for Zr^+, the electronic structure is quite different, as the singly occupied molecular orbital (red level) is a 4d orbital, and the HOMO-2 and HOMO (maroon levels) are a linear combination of 4d, 5s, and ethane orbitals. The addition of O to Zr populates the molecular orbitals with significant 4d components bringing the electronic structure closer to that of Pd that moderates the reactivity.

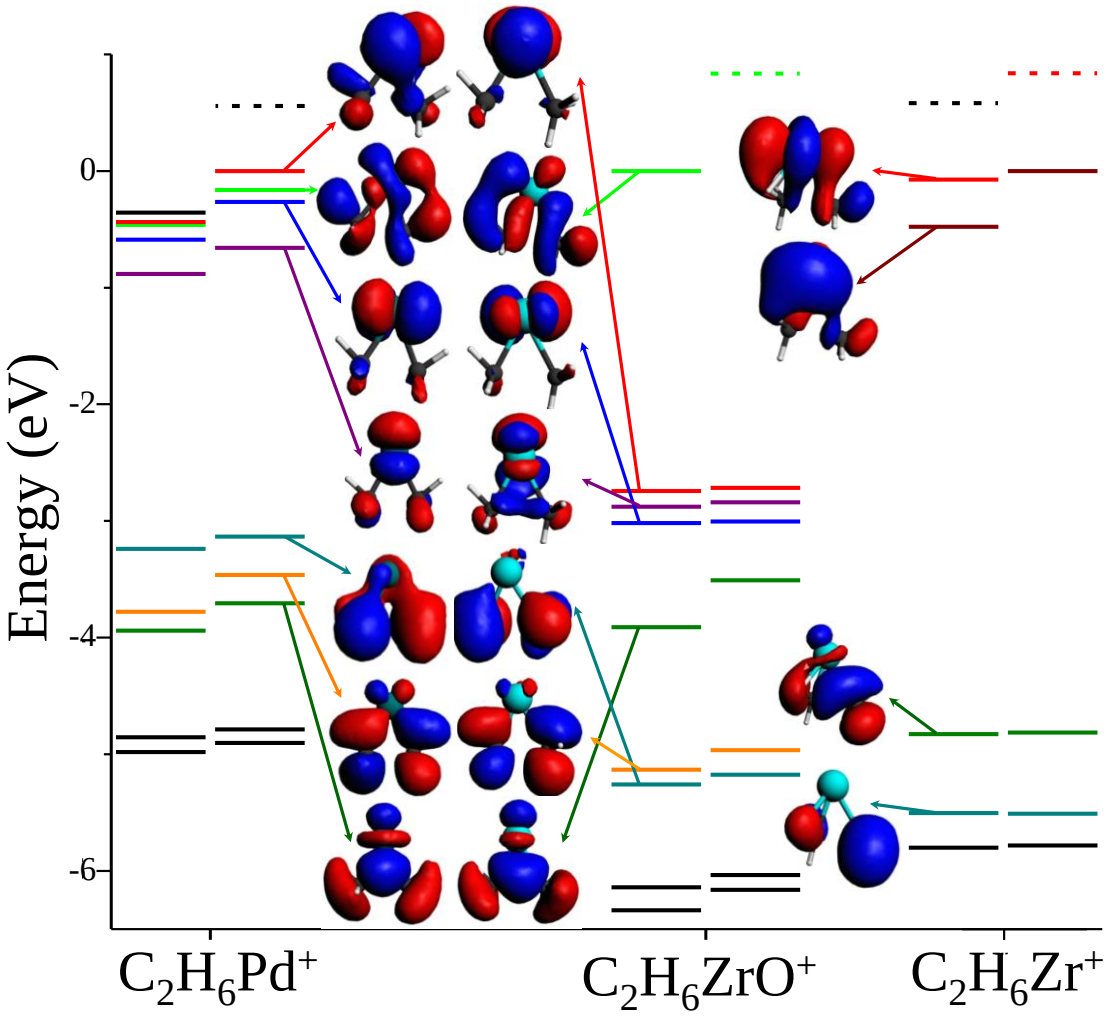

Figure 4-6. Electronic structure of $C_2H_6Pd^+$, $C_2H_6ZrO^+$, and $C_2H_6Zr^+$ at the transition state for the cleavage of the C-C bond. The color coding corresponds to analogous orbitals. Solid lines are occupied, dashed are unoccupied orbitals. Reproduced from reference 31.

Propane Reactivity

The reactive nature of Pd^+ and ZrO^+ is investigated further through interaction with C_3H_8 under parallel conditions. The energy of interaction is again 20 eV in the lab frame and the pressure of reactant gas is varied from 0 to 5 mTorr. The major reaction mechanism identified is the activation of the C-C bond which is also the major product for ethane. In this case there are two products resulting from C-C bond scission, the CH_3M^+ and $C_2H_3M^+$ (M = Pd, ZrO) products shown in equations 4.6 and 4.7.

$$Pd^+ + C_3H_8 \rightarrow CH_3Pd^+ + C_2H_5 \quad (4.6)$$

$$Pd^+ + C_3H_8 \rightarrow C_2H_3Pd^+ + H_2 + CH_3 \quad (4.7)$$

$$Pd^+ + C_3H_8 \rightarrow C_3H_5Pd^+ + H_2 + H \quad (4.8)$$

Figure 4-7a displays comparable intensity of CH_3Pd^+ and $C_2H_3Pd^+$ products upon reaction with Pd^+ while CH_3ZrO^+ dominates in the reaction with ZrO^+ as seen in Figure 4-7b. This small difference in reactivity may be advantageous as ZrO^+ exhibits a higher selectivity for a primary product that is usually desirable for a catalytic mechanism. The final product detected is the liberation of H_2 and a hydrogen atom with the concomitant bonding of the remaining hydrocarbon to the ion as described in equation 4.8.

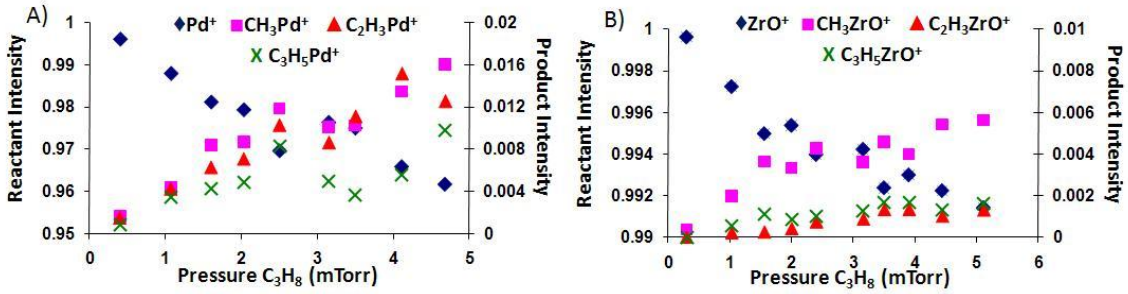

Figure 4-7. a) Pd^+ and b) ZrO^+ are reacted with 0 – 5 mTorr C_3H_8 at 20 eV in the lab frame. The branching ratios display a decrease in reactant intensity with the concomitant rise in product intensity as the pressure of gas in the reaction cell is increased. Reproduced from reference 31.

The reaction rate constants for interaction with propane are calculated utilizing a method described earlier in this chapter that assumes pseudo first order kinetics and derives the reaction time from the velocity gained by the potential placed on the octopole. The plot of ln I_r/I_0 vs. R is presented in Figure 4-8 where the slope of the best fit line is equivalent to –kt. The rate constant value is on the order of 1.0 x 10^{-11} cm^3 s^{-1} for Pd^+ and 2.2 x 10^{-12} cm^3 s^{-1} for ZrO^+. Through experimental analysis it is determined that Pd^+ and ZrO^+ react with propane in a similar nature creating common products. However a greater rate of reaction is observed for the reaction between propane and ZrO^+.

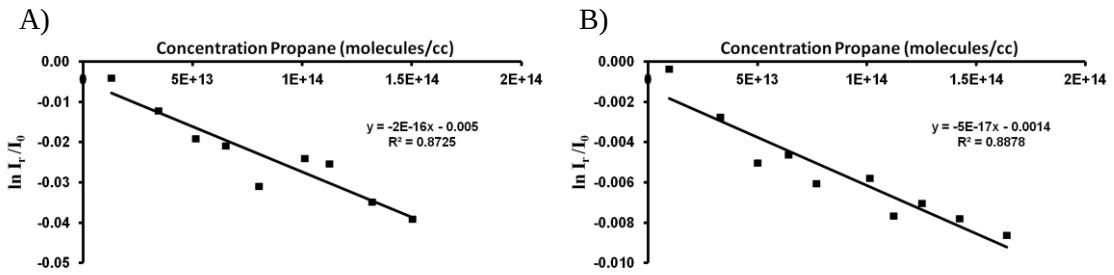

Figure 4-8. Plot of the logarithmic ratios of reactant intensity in the presence and absence of propane (ln I_r/I_0) vs. concentration of propane for a) Pd^+ and b) ZrO^+.

The energy profiles for the reactions of propane with Pd^+ and ZrO^+ are shown in Figure 4-9. Figures 4-9a and 4-9b show the reaction profile for C-C bond cleavage of propane in accordance with equation 4.5. The binding energies of propane to Pd^+ and ZrO^+ are 1.79 and 1.61 eV and the barrier to C-C cleavage is 1.08 and 1.09 eV, respectively. The final product in this reaction profile is the loss of an ethyl radical that is a net endothermal product of 0.96 eV for Pd^+ and 0.68 eV for ZrO^+. Figure 4-9c and 4-9d show the energy profile for producing $C_2H_3Pd^+$ and $C_2H_3ZrO^+$ (equation 4.7). The cleavage of the central CH bond in the Pd^+ reaction profile has a barrier of only 0.48 eV after a binding energy of 1.78 eV; the intermediate containing a hydrogen bound to Pd is 0.19 eV below the barrier. The barriers for cleaving terminal C-H bonds are larger than the central C-H bonds, so a mechanism where the central C-H is cleaved is considered. The cleavage of the central C-H bond in propane via ZrO^+ does not have a stable intermediate; the potential energy surface for motion of the H atom is quite flat at 1.11 eV, but the C-H bond is quite stretched at this point, 2.55 Å. The higher energy barrier is the formation of the H-H bond, which is 0.90 eV above the complex in Pd^+ and 1.52 eV above the complex in ZrO^+. The complex where C_3H_6 and H_2 are bound to the metals is quite stable, at 2.07 eV and 1.30 eV below the initial energy. Following H_2 loss, the Pd^+ and ZrO^+ may insert into the C-C bond, preferably between the methyl and C-H facilitating the loss of the methyl radical. The barrier is noticeably lower for Pd^+ to insert into the C-C bond than ZrO^+, 0.52 eV versus 1.38 eV, however the energies of the final complex are 2.23 eV and 2.18 eV. A second mechanism following C-H insertion is the release of an H radical as shown in Figure 4-9e and 4-9f. The insertion of ZrO^+ into an additional C-H bond does not result in a stable intermediate, while it does in Pd^+. The total energy of the reactions is 0.98 eV in Pd^+ and 1.44 eV in ZrO^+. The cleavage of the C-C bond in propane is energetically similar in both Pd^+ and ZrO^+. The barrier to cleaving the C-H bond is higher in ZrO^+ than Pd^+, suggesting that ZrO^+ may be a more selective reactant for some cracking reactions.

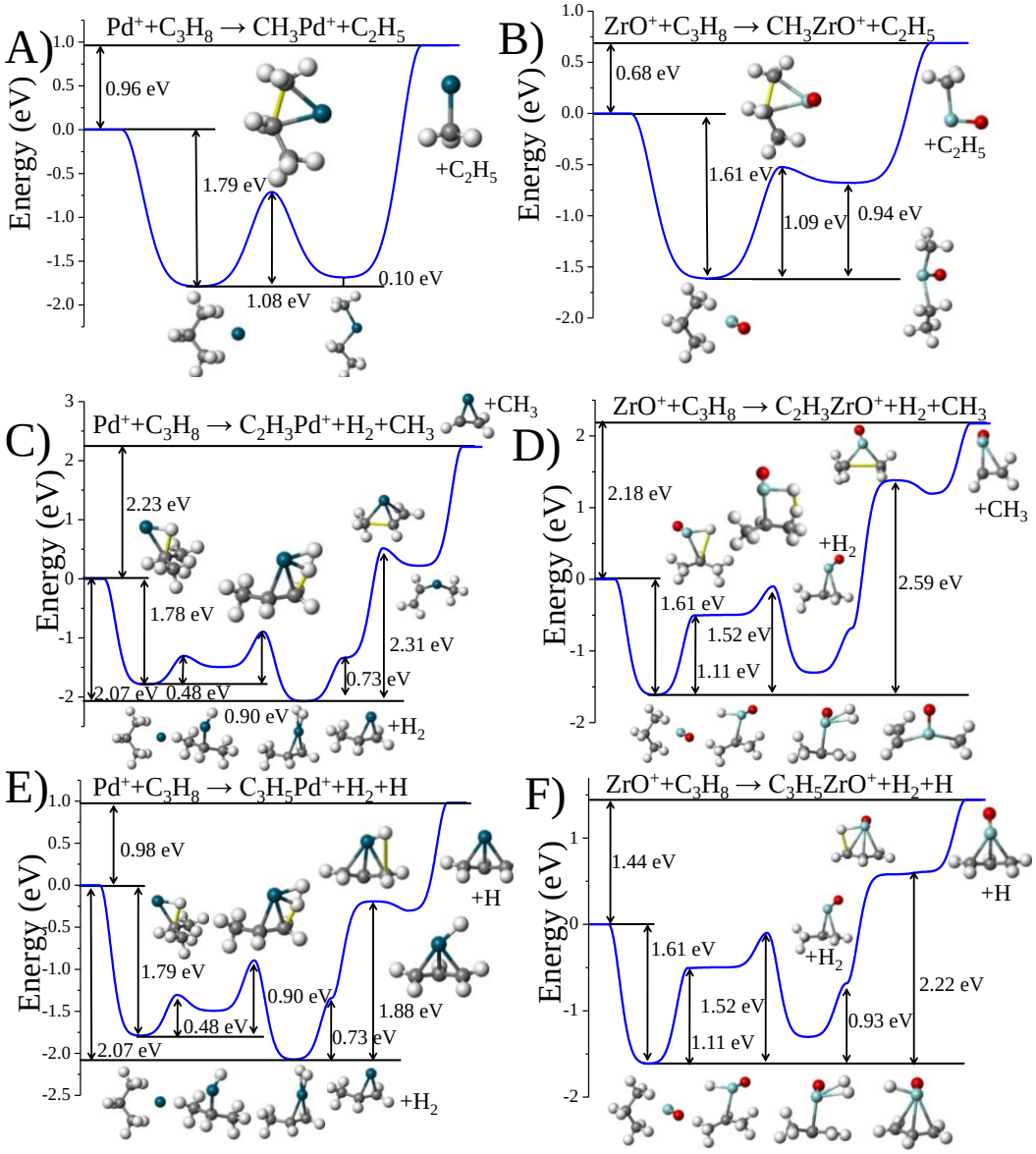

Figure 4-9. Reaction profiles for a) Pd^+ and b) ZrO^+ forming CH_3M^+, c) Pd^+ and d) ZrO^+ forming $C_2H_3M^+$, and e) Pd^+, f) ZrO^+ forming $C_3H_5M^+$. Reproduced from reference 31.

Further investigation with other transition metal ions, specifically VO^+, is performed to determine if the reactive similarities observed between Pd^+ and ZrO^+ are unique or a global trend for all transition metal cations at similar energetic conditions. Investigations previously conducted in our laboratory on group 5 metal oxide species determined that similarities in reactivity are

observed for congener ions of matching stoichiometry[22]. Vanadium is chosen as the species for comparison as it is not a congener of zirconium. The interaction of VO^+ with C_2H_6 and C_3H_8 at 14.5 eV did not result in the detection of reaction products. As VO^+ is lighter than Pd^+ and ZrO^+, the lab frame energy of 14.5 eV is the appropriate reaction condition to match the center of mass frame energy of the Pd^+ and ZrO^+ experiments. Additionally, studies found in the literature probing the interaction of MoO^+ with ethane at thermal energy resulted in the release of $2H_2$ and H_2.[36] As these reaction mechanisms occur at thermal energy and are exothermic in nature it is not expected that H_2 release would be observed at 20 eV in the lab frame. These examples illustrate that the reactivity of the species Pd^+ and ZrO^+ when interacted with ethane and propane is not observed for all early transition metal oxides.

4.5 Conclusion

The advancement of catalytic processes relies on the development of alternative materials for the replacement of expensive precious metal combustion catalysts. The current investigation provides evidence for the similarity in reactivity of the pair Pd^+ and ZrO^+ with ethane and propane. The primary reaction products for the interaction with ethane and propane are the scission of the C-C bond. Additionally, hydrogen abstraction is identified and confirmed through the comparison with deuterated ethane. The origin of this similarity is due to the hybridization between Zr and O that increases the occupation of the molecular orbitals with 4d components in ZrO^+ making the electronic structure at the transition state quite different from Zr^+. It will be interesting to examine if the resemblance displayed here can be extended to larger clusters and nanoparticles, eventually leading to the design of new catalysts.

4.6 References

1. Engel, T.; Ertl, G. *J. Chem. Phys.* **1978**, *69*, 1267.
2. Somorjai, G. A. *Science* **2008**, *322*, 932.
3. Chen, M.; Kumar, D.; Yi, C-W.; Goodman, D. W. *Science* **2005**, *310*, 291.
4. Xai, Y. *Science* **2009**, *324*, 1302.
5. Judai, K.; Abbet, S.; Wörz, A. S.; Heiz, U.; Henry, C. R. *J. Am. Chem. Soc.* **2004**, *126*, 2732.
6. Kaden, W.E.; Wu, T.P.; Kunkel, W.A.; Anderson, S.L. *Science* **2009**, *326*, 826.
7. Robles, R.; Khanna, S.N. *Phys Rev. B* **2010**, *82*, 085428.
8. Leclercq, L.; Imura, K.; Yoshida, S.; Barbee, T.; Boudart, M. "Preparation of Catalysis II" (B. Delmon, P. Grange, P. A. Jacobs, and G. Poncelet, Eds.), p. 627. Elsevier, Amsterdam, 1978.
9. Levy, R. B.; Boudart, M. *Science* **1973**, *181*, 547.
10. Weigert, E. C.; Stottlemyer, A. L.; Zellner, M. B.; Chen, J. G. *J. Phys. Chem. C* **2007**, *111*, 14617.
11. Kuznetsov, B. N.; Yermakov, Y. I.; Boudart, M.; Collman, J. P. *J. Mol. Catal.* **1978**, *4*, 49.
12. Lee, J. S.; Boudart, M. *Catal. Lett.* **1991**, *8*, 107.
13. Rodrigues, J. A. J.; Cruz, G. M.; Bugli, G.; Boudart, M.; Djéga-Mariadassou, G. *Catal. Lett.* **1997**, *45*, 1.
14. Ross, P. N., Jr.; Stonehart, P. *J. Catal.* **1975**, *39*, 298.
15. Boudart, M.; Lee, J. S.; Imura, K.; Yoshida, S. *J. Catal.* **1987**, *103*, 30.

16. a) Peppernick, S. J.; Gunaratne, K. D. D.; Castleman, A. W., Jr. *PNAS* **2010**, *107*, 975. b) Peppernick, S. J.; Gunaratne, K. D. D.; Castleman, A. W., Jr. *Chem. Phys. Lett.* **2010**, *489*, 1.
17. Chen, Y-M.; Sievers, M. R.; Armentrout, P. B. *Int. J. Mass. Spectrom.* **1997**, *167*, 195.
18. Dong, F.; Heinbuch, S.; Yan, X.; Rocca, J. J.; Bernstein, E. R.; Wang, Z-C.; Deng, K.; He, S-G. *J. Am. Chem. Soc.* **2008**, *130*, 1932.
19. Tyo, E. C.; Castleman, A. W., Jr.; Schröder, D.; Milko, P.; Roithova, J.; Ortega, J. M.; Cinellu, M. A.; Cocco, F.; Minghetti, G. *J. Am. Chem. Soc.* **2009**, *131*, 13009.
20. Schlangen, M.; Schwarz, H. *Angew. Chem. Int. Ed.* **2007**, *46*, 5614.
21. Sievers, M. R.; Armentrout, P. B. *Organometallics* **2003**, *22*, 2599.
22. Zemski, K. A.; Justes, D. R.; Castleman, A. W., Jr. *J. Phys. Chem. A* **2001**, *105*, 10237.
23. Johnson, G. E.; Mitrić, R.; Nössler, M.; Tyo, E. C.; Bonačić-Koutecký, V.; Castleman, A. W.; Jr. *J. Am. Chem. Soc.* **2009**, *131*, 5460.
24. Johnson, G. E.; Mitrić, R.; Tyo, E. C.; Bonačić-Koutecký, V.; Castleman, A. W.; Jr. *J. Am. Chem. Soc.* **2008**, *130*, 13912.
25. a. Lang, S. M.; Bernhardt, T. M.; Barnett, R. N.; Yoon, B.; Landman, U. *J. Am. Chem. Soc.* **2009**, *131*, 8939. b. Lang, S. M.; Bernhardt, T. M.; Barnett, R. N.; Landman, U. *Angew. Chem. Int. Ed.* **2010**, *49*, 980.
26. Wöste, L. *J. Am. Chem. Soc.* **2004**, *126*, 3442.
27. a. Bell, R. C.; Zemski, K. A.; Justes, D. R.; Castleman, A. W., Jr. *J. Chem. Phys.* **2001**, *114*, 798-811. b. Moore, N. A.; Mitrić, R.; Justes, D. R.; Bonačić-Koutecký, V.; Castleman, A. W., Jr. *J. Phys. Chem. B* **2006**, *110*, 3015.
28. te Velde, G.; Bickelhaupt, F.M; Baerends, E.J.; Fonseca Guerra, C.; van Gisbergen, S.J.A.; Snijders, J.G.; and Ziegler, T. J. *Comput. Chem.* **2001** *22*, 931.
29. Perdew, J.P.; Burke, K.; Enzerhof, M. *Phys. Rev. Lett.* **1996**, *77*, 3865.

30. Van Lenthe, E.; Baerends, E.J.; Snijders, J.G. *J. Chem. Phys.* **1993** *99*, 4597.

31. Tyo, E. C.; Castleman, Jr. A. W.; Reber, A. C.; Khanna, S. N. *J. Phys. Chem. C* **2011**, *115*, 16797.

32. Anderson, J. B.; Fenn, J. B. *Phys. Fluids* **1965**, *8*, 780.

33. Cohen, A.J.; Mori-Sánchez, P.; Yang, W. *Science* **2008**, *321*, 792.

34. Roach, P.J.; Woodward, W.H.; Castleman, Jr. A.W.; Reber, A.C.; Khanna, S.N. *Science* **2009**, *323*, 492.

35. Reber, A.C.; Khanna, S.N.; Roach, P. J.; Woodward, W. H.; Castleman, Jr. A. W. *J. Phys. Chem. A* **2010**, *114*, 6071.

36. Cassady, C. J.; McElvany, S. W. *Organometallics*, **1992**, *11*, 2367.

Chapter 5

Exploring Similarities in Reactivity of Isovalent Species: A Combined Theoretical and Experimental Investigation

5.1 Introduction

Late transition metals are active catalysts for a myriad of processes but unfortunately these precious metals are in limited supply and catalytic materials based on group 10 metals are exceptionally expensive. Hence the finding of alternative catalysts can potentially have important economic consequences.[1-3] Recent investigations have revealed that selected species of isovalent character display similar electronic behavior, raising a question whether their catalytic reactivity would also be similar and thereby serve to identify useful replacements.[4,5] In the quest to find suitable replacements our group undertook a study of similarities in chemistry between group 10 metals and early transition metal species through density functional theory, photoelectron spectroscopy, velocity map imaging, and gas-phase reactivity studies.[4-6] Velocity map imaging studies[4,5] provided information on comparable electronic transitions and orbital symmetry between the "isovalent" pairs Ni^-/TiO^- and Pd^-/ZrO^-. Describe in Chapter 4, a prior joint experimental and theoretical study determined analogous reactivity for the interaction of Pd^+ and ZrO^+ with both ethane and propane[6] whereupon the addition of an oxygen atom to Zr^+ changes the electron distribution resulting in a "superatom" with reactivity properties similar to Pd^+. The question can be raised whether the isovalent concept can be extended to reactivity of larger systems and hence point the way to find approaches in tailoring the design of nanoscale catalysts.

Herein I report an investigation combining experiment and theory to determine the reactivity of C_2H_4, C_2H_2, and CO with the diatomic/triatomic pairs NiO^+/TiO_2^+ and PdO^+/ZrO_2^+ in

order to further explore the concept[7] of superatomic mimics. Reactions of TiO_2^+ and ZrO_2^+ with C_2H_4, C_2H_2, and CO have been investigated previously,[8,9] showing that both species readily oxidize C_2H_4 and C_2H_2 while exhibiting minimal reactivity towards CO. Since TiO_2^+ and ZrO_2^+ are isovalent with NiO^+ and PdO^+, respectively, according to the criterion of mimics we expect to observe oxidation of C_2H_4 and C_2H_2 for both species, but minimal reactivity occurring upon interaction with CO.

In order to ascertain whether the elemental mimics concept can be extended to larger systems, the structural properties of the cationic species and mechanistic aspects of their reactivity are theoretically investigated employing the DFT method with the hybrid B3LYP functional.[10-12] Simultaneously, experiments are conducted in which the ions are created utilizing a Laser Vaporization (LaVa) source in concert with a tandem mass spectrometer to investigate the reactivity of the cationic species of interest.[13] The chapter is structured as follows; experimental and theoretical methods are described first, followed by a comparison and discussion of the experimental and theoretical results for interaction of NiO^+ and TiO_2^+ with C_2H_4, C_2H_2, and CO. Subsequently, a similar analysis of the interaction of PdO^+ and ZrO_2^+ with the three molecules is performed. Finally, conclusions are drawn from the investigation that considers the application of isovalent species as replacements for precious metals in catalytic processes.

5.2 Experimental Methods

The various ionic species are created utilizing a laser vaporization (LaVa) source coupled to a tandem mass spectrometer with QOQ configuration (Q: quadrupole, O: octopole) that has been described in Chapter 2 and publications.[13,14] In brief, thermalized metal oxide ions are created through the supersonic expansion of ions formed in the LaVa source. The ablation rods used for creation of ions are palladium (99.9%, Alfa Aesar), zirconium (99.95%, Research and

PVD Materials Corp.), nickel (99.95%, Research and PVD Materials Corp.), and titanium (99.95%, Research and PVD Materials Corp.). A retarding potential analysis previously performed in our laboratory determined that the energy imparted upon the clusters exiting the source is around 1 eV in the laboratory frame (E_{LAB}).[13] A potential of zero volts is applied to the injection lens before the collision cell and the dc float voltage applied to the octopole ion guide so the clusters react at thermal energies. Varying pressures of the reactants C_2H_4 (99.9%, GT&S Welco), C_2H_2 (99.6%, GT&S Welco), and CO (99.9%, GT&S Welco) are admitted into the octopole reaction cell to determine the reactive properties of the ions. The initial center of mass frame energies (E_{CM}) for the reaction of C_2H_4, C_2H_2 and CO with PdO^+, ZrO_2^+, NiO^+ and TiO_2^+ are calculated to be roughly 0.19 eV, 0.19 eV, 0.27 eV, and 0.26 eV respectively.

The experimental branching ratios presented in Section 5.4 depict the normalized ion intensities of products and reactants detected at increasing pressures of reactant. It can be seen that for reactive species, an increase of reactant in the reaction cell results in a concomitant rise in products while the parent species decreases in intensity.

5.3 Theoretical Methods

Calculations are performed by the Bonačić-Koutecký group at the Humboldt Universität zu Berlin that compliment experimental results and provide mechanistic detail of reaction processes. The structural properties of the investigated species and their reactivity are studied using the DFT method with the hybrid B3LYP functional.[10-12] The triple-zeta-valence-plus-polarization (def2-TZVP) atomic basis set[15] is used for all atoms combined with the Stuttgart group relativistic effective core potential in the case of Zr and Pd.[16] Previous studies of the reactivity of transition metal oxides have shown that such a combination of hybrid density functionals with triple zeta quality basis sets allow the accurate prediction of the reaction energetics and mechanisms.[8,9,17] All

structures presented are fully optimized using gradient minimization techniques and stationary points are characterized as minima or transition states by calculating the vibrational frequencies. Moreover, from the energy profiles based on energies obtained from DFT calculations the reaction mechanisms are deduced.

5.4 Results and Discussion

To begin evaluating the chemistry of NiO^+ vs. TiO_2^+ I studied the interaction of NiO^+ with C_2H_4 (Figure 5-1a) finding that the reaction results in a primary oxygen loss product as described by equation 5.1.

$$NiO^+ + C_2H_4 \rightarrow Ni^+ + \text{neutral products} \quad (5.1)$$

The branching ratios reveal a pronounced decrease in the reactant ion intensity, NiO^+, with a concomitant increase in the oxygen transfer product, Ni^+ (Figure 5-1a). As neutral products are not observed, it is inferred that the creation of the Ni^+ product corresponds with the transfer of oxygen to the reactant molecule C_2H_4. A minor channel, of less than 5%, corresponding to the replacement of oxygen by an associated C_2H_4 is also identified. In this case, the energy gained by association of C_2H_4 to the ion is likely enough to break the nickel oxygen bond releasing the oxygen atom. Comparison with the branching ratios for interaction between TiO_2^+ and C_2H_4 (Figure 5-1b) shows a similar primary oxygen transfer channel. Both ions are interacted with C_2H_4 at a high pressure of roughly 5 mTorr. The TiO_2^+ branching ratio (Figure 5-1b) presents slightly higher oxidative activity as 20% of the detected ion at 5 mTorr is the oxygen loss product while at nearly the same pressure the reaction of NiO^+ with C_2H_4 produces an oxygen loss product of only 15%. The identification of oxidative activity for both species provides support toward the concept that TiO_2^+ fulfills the criterion for being a mimic of NiO^+.

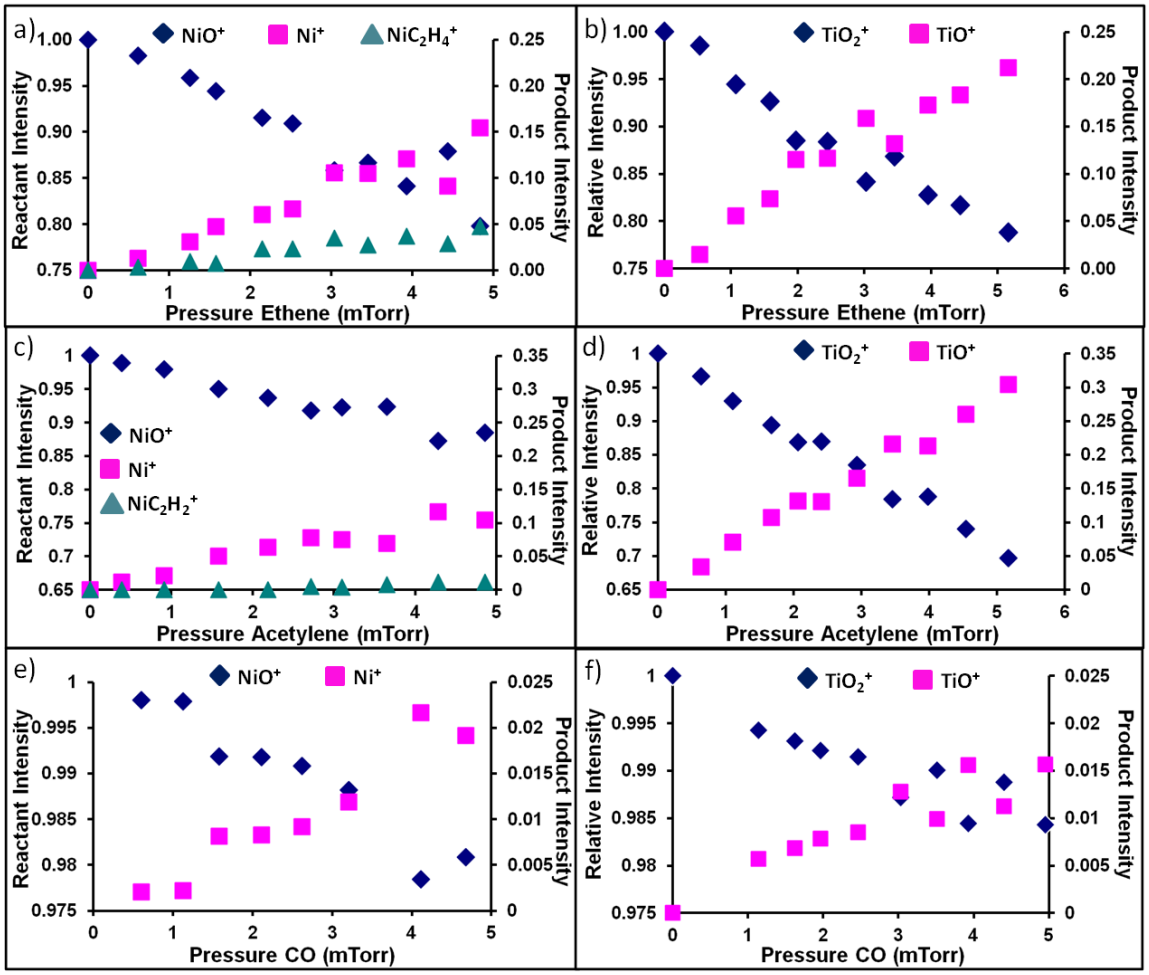

Figure 5-1. Branching ratios presented in normalized ion intensities for the reaction of a) NiO^+ and b) TiO_2^+ with 0-5 mTorr of C_2H_4, c) NiO^+ and d) TiO_2^+ with 0-5 mTorr of C_2H_2, and e) NiO^+ and f) TiO_2^+ with 0-5 mTorr of CO.

Investigations are performed to determine if further similarities in reactivity can be identified between NiO^+ and TiO_2^+ when interacted with C_2H_2 and CO. Through comparison of the branching ratios in Figure 5-1c-d it is seen that both NiO^+ and TiO_2^+ primarily undergo an oxygen transfer when C_2H_2 is introduced. In a similar fashion to the reactivity with C_2H_4, a minor product for a replacement reaction is observed in the NiO^+ branching ratio while TiO_2^+ presents a higher percentage of oxygen transfer product than NiO^+ during reaction with C_2H_2. A marked difference in reactivity is observed when CO is introduced to the ions as can be seen in Figure 5-1e and f.

The only observed product for introduction of CO to NiO^+ and TiO_2^+ is a minor quantity of oxygen loss at less than 2% of detected ions. Chapter 2 explains the minor reactivity of TiO_2^+ with CO as due to the spin-unpaired electron being delocalized equally over both oxygen atoms creating an active site that is not preferential for oxidation of CO. Overall, NiO^+ and TiO_2^+ represent catalytic active sites that are active for the transfer of oxygen to unsaturated hydrocarbons while being rather inactive towards CO. These experiments provide further support of the similarities in reactivity between isovalent ions.

To continue the comparison of reactivity between NiO^+ and TiO_2^+, reaction rate constants have been calculated. The reaction rate constants are calculated utilizing the method described in Chapter 2.4 that assumes pseudo first order kinetics. The slope taken from the plot of $\ln I_r/I_0$ vs. R is equivalent to –kt. The reaction rate constants for oxygen transfer between the ions NiO^+ and TiO_2^+ and the reactants C_2H_4, C_2H_2, and CO are presented in Table 5-1.

Table 5-1 Reaction Rate Constants for NiO^+ and TiO_2^+

Reactant	*NiO^+*	*TiO_2^+*
C_2H_4	1.71×10^{-12} cm^3 s^{-1}	2.42×10^{-12} cm^3 s^{-1}
C_2H_2	1.30×10^{-12} cm^3 s^{-1}	3.56×10^{-12} cm^3 s^{-1}
CO	2.63×10^{-13} cm^3 s^{-1}	1.50×10^{-13} cm^3 s^{-1}

The rate constants for oxygen transfer from TiO_2^+ to C_2H_4 and C_2H_2 are higher than NiO^+ in both cases. The evidence supports TiO_2^+ as being a more effective oxidation catalyst than NiO^+ as TiO_2^+ has a higher rate constant and no co-products. The rate constants for oxygen transfer from NiO^+ and TiO_2^+ to CO are roughly an order of magnitude lower than the interaction with the studied hydrocarbons. Although there are differences in the rate constants between NiO^+ and

TiO_2^+, both species show significant oxygen transfer to the hydrocarbons of interest while presenting limited oxidation of CO.

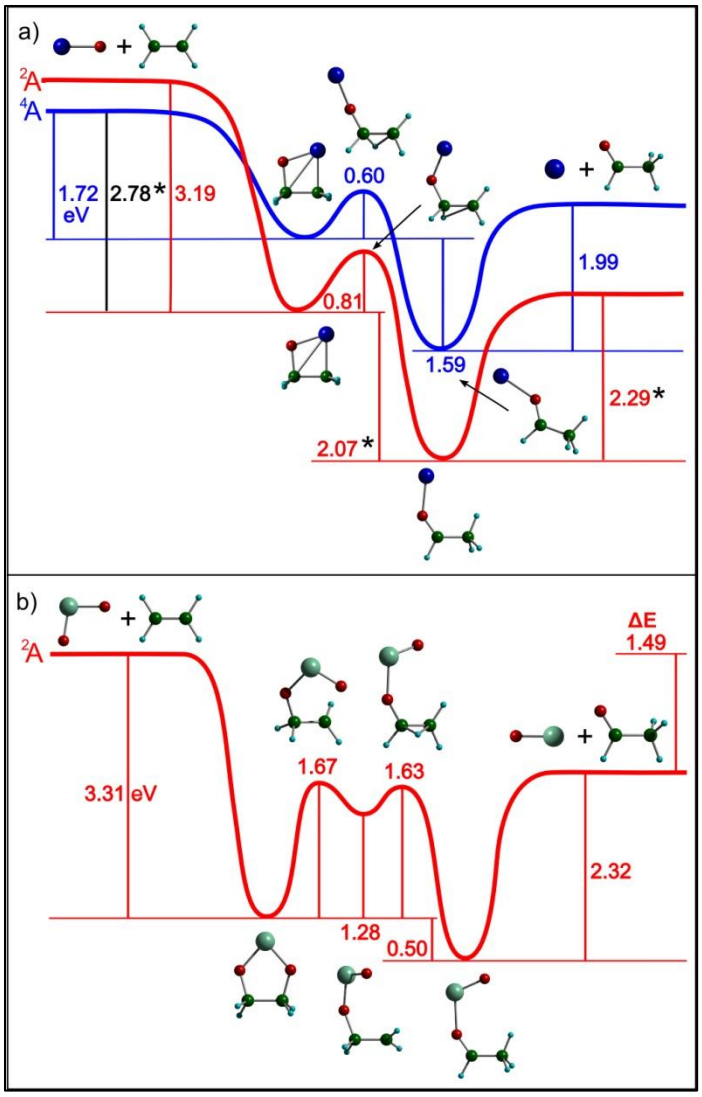

Figure 5-2. Calculated reaction profiles for the formation of acetaldehyde through oxidation of C_2H_4 by a) NiO^+ and b) TiO_2^+. The doublet and quartet state profiles are presented for interaction of NiO^+ with C_2H_4. Reaction in both states is exothermic by 2.97 eV and 1.32 eV, respectively. The energy differences labelled by * allows for the determination of the most favourable reaction energy by undergoing a spin-crossover which is exothermic by 2.56 eV. The exothermic energy difference ΔE for TiO_2^+ is shown in b). Reproduced from reference 18.

Energetic and mechanistic insight is gained through a theoretical investigation of the interaction of C_2H_4 with NiO^+ and TiO_2^+ performed by the Bonačić-Koutecký group at the Humboldt Universität zu Berlin. The ground state of the reactants, NiO^+ and C_2H_4, lie on the quartet state potential energy surface (Figure 5-2a). As the reaction proceeds to the initial encounter complex, a spin-crossing to the doublet state potential energy surface occurs. The remaining step in the mechanism requires a hydrogen transfer leading to the exothermic release (2.56 eV) of acetaldehyde (Figure 5-2a). The spin crossover increases the overall exothermicity of the oxidation reaction from 1.32 eV for the ground state quartet profile to 2.56 eV. In order to compare the individual reactivities of NiO^+ and TiO_2^+ towards C_2H_4 the reaction profile for TiO_2^+ is presented in Figure 5-2b. The mechanism proceeds through transitions for isomerization and hydrogen transfer toward release of products along the doublet state potential energy surface in contrast to the NiO^+ reaction profile that undergoes a spin-crossover. Acetaldehyde is calculated to be the most exothermic oxidation product (1.49 eV) upon interaction of C_2H_4 with TiO_2^+. The creation of ethylene oxide is identified for reaction with both ions but the process is less exothermic than the reaction forming acetaldehyde (Figure 5.3). Significantly, our investigations has determined that the most favorable product for interaction of C_2H_4 with both NiO^+ and TiO_2^+ is acetaldehyde and a spin-crossover in the NiO^+ pathway increases the exothermicity of reaction.

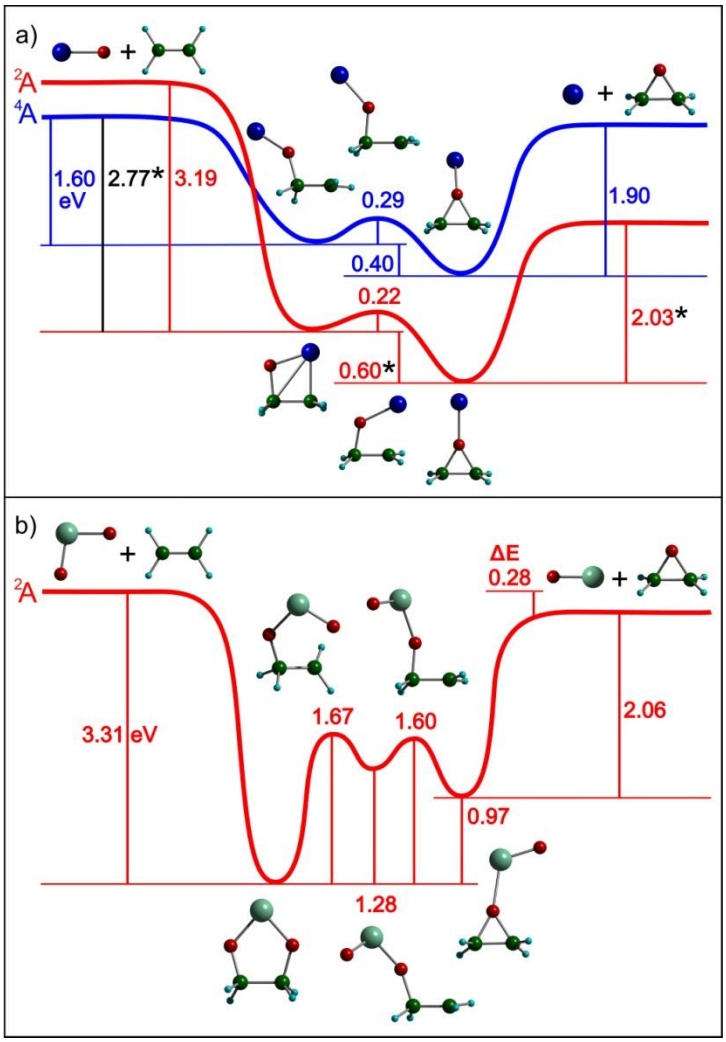

Figure 5-3. Calculated reaction profiles for oxidation of C_2H_4 to ethylene oxide by a) NiO^+ and b) TiO_2^+. The doublet and quartet state profiles are presented for interaction of NiO^+ with C_2H_4. Reaction in both states is exothermic by 1.76 eV and 0.10 eV, respectively. The energy differences labelled by * allow for the determination of the most favourable reaction energy by undergoing a spin-crossover which is exothermic by 1.34 eV. The exothermic energy difference ΔE for TiO_2^+ is shown in b). Reproduced from reference 18.

The profound observation of similar reactivity between the isovalent species NiO^+ and TiO_2^+ motivated an investigation of PdO^+ and isovalent ZrO_2^+. The interaction of the ions PdO^+ and ZrO_2^+ with the molecules C_2H_4, C_2H_2, and CO is studied and the results are presented as branching ratios in Figure 5-4. A major reaction channel due to oxygen transfer to C_2H_4 is observed for both ions. Comparison of the branching ratios at the equivalent pressure of 3 mTorr

displays oxygen loss products accounting for 14% of the total ions detected during interaction with PdO^+ while the oxygen loss product in the ZrO_2^+ branching ratio comprises 9% of the ions detected. Additional products identified during the reaction with PdO^+ are $PdC_2H_4^+$, due to a replacement reaction, and minor amounts of ionized hydrocarbons (Figure 5-4a). While ZrO_2^+ reacts primarily through oxidation of C_2H_4 a minor product for an association reaction, $ZrO_2C_2H_4^+$, is observed as well (Figure 5-4b). Although differences are observed in the branching ratios, the primary oxygen transfer product is observed for the interaction of PdO^+ and ZrO_2^+ with C_2H_4.

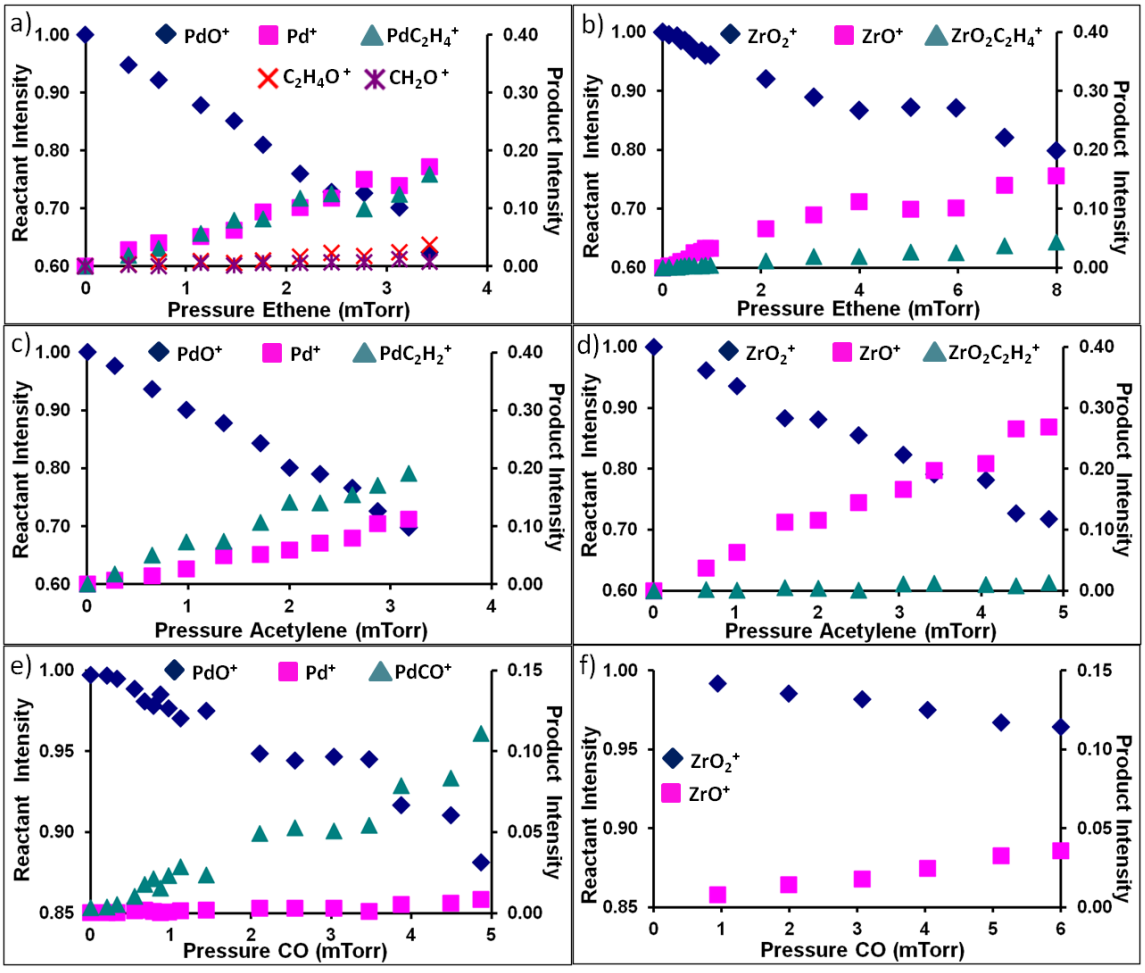

Figure 5-4. Branching ratios presented in normalized ion intensities for the reaction of a) PdO^+ and b) ZrO_2^+ with C_2H_4, c) PdO^+ and d) ZrO_2^+ with C_2H_2, and e) PdO^+ and f) ZrO_2^+ with CO.

The interaction of PdO^+ and ZrO_2^+ with C_2H_2 and CO provides further evidence of the similar reactive nature between the isovalent ions. Upon interaction with roughly 3 mTorr C_2H_2, a major reaction channel for oxygen transfer of 10% and 17% is identified for PdO^+ and ZrO_2^+, respectively (Figures 5-4c and d). Additional processes occurring during interaction with C_2H_2 are replacement of oxygen in PdO^+ forming $PdC_2H_2^+$ and a minor association to ZrO_2^+ creating $ZrO_2C_2H_2^+$. Upon introduction of CO, both ions are rather inactive for oxygen transfer in comparison to the reaction with the investigated hydrocarbons (Figures 5-4e and f).

The reaction rate constants have been calculated for oxygen transfer between the ions and reactants to provide a further comparison between PdO^+ and ZrO_2^+. The rate constants are calculated utilizing the method described in Chapter 2.4 that assumes pseudo first order kinetics. The slope taken from the plot of $\ln I_r/I_0$ vs. R is equivalent to –kt. The rate constants for oxygen transfer between the ions PdO^+ and ZrO_2^+ and the reactants C_2H_4, C_2H_2, and CO are presented in Table 5-2.

Table 5-2 Reaction Rate Constants for PdO^+ and ZrO_2^+

Reactant	*PdO^+*	*ZrO_2^+*
C_2H_4	4.08×10^{-12} cm^3 s^{-1}	2.65×10^{-12} cm^3 s^{-1}
C_2H_2	2.84×10^{-12} cm^3 s^{-1}	4.97×10^{-12} cm^3 s^{-1}
CO	1.00×10^{-13} cm^3 s^{-1}	4.95×10^{-13} cm^3 s^{-1}

The rate constants for oxygen transfer to C_2H_4 and C_2H_2 from PdO^+ and ZrO_2^+ are very similar as they are all on the order of 10^{-12} cm^3 s^{-1}. PdO^+ has a slightly higher rate constant for oxygen transfer to C_2H_4 while ZrO_2^+ has a higher value for transfer to C_2H_2 as can be seen in Table 5-2. Additionally, both ions are significantly less active for oxygen transfer to CO as their rate constants are an order of magnitude less.

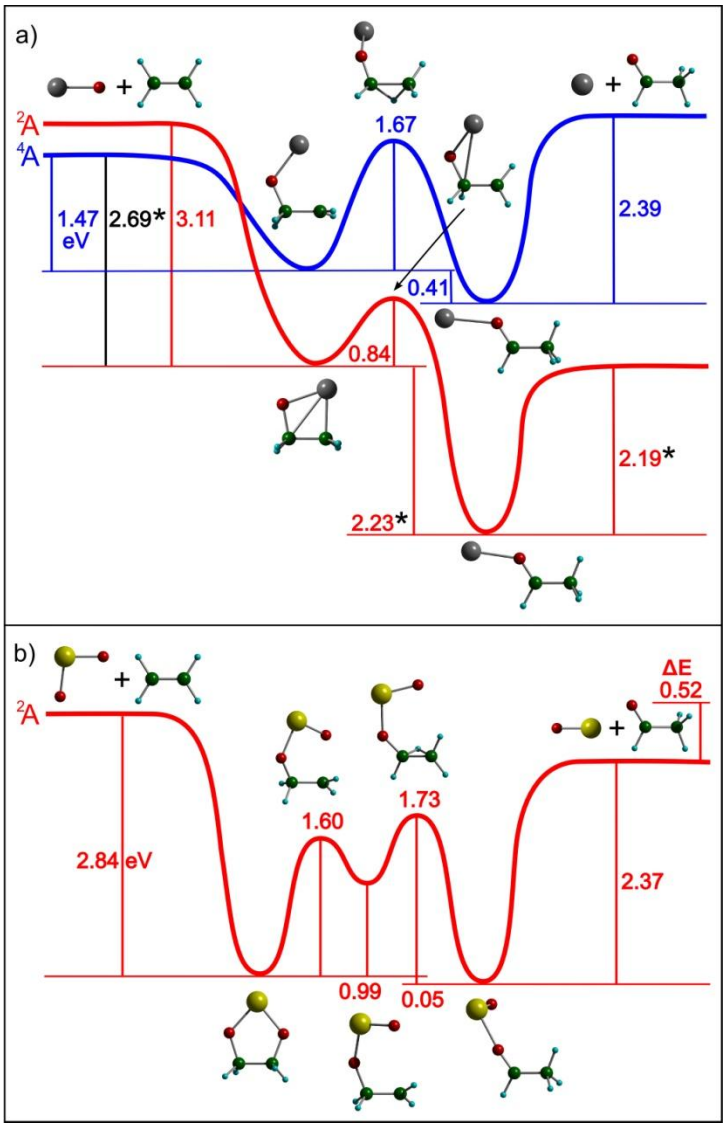

Figure 5-5. Calculated reaction profiles for the formation of acetaldehyde through oxidation of C_2H_4 by a) PdO^+ and b) ZrO_2^+. The doublet and quartet state profiles are presented for interaction of PdO^+ with C_2H_4. Reaction is exothermic by 3.15 eV in the doublet state and endothermic by 0.51 eV in the quartet state. The energy differences labelled by * allows for the determination of the most favourable reaction energy by undergoing a spin-crossover which is exothermic by 2.73 eV. The exothermic energy difference ΔE for ZrO_2^+ is shown in b). Reproduced from reference 18.

The reaction profiles for interaction of C_2H_4 with PdO^+ and isovalent ZrO_2^+ are depicted in Figure 5-5. In a similar manner to NiO^+, the PdO^+ profile for oxidation of C_2H_4 begins in the quartet spin state (Figure 5-5a). A spin-crossover to the doublet state potential energy surface

results in an encounter complex that is lower in energy than the corresponding quartet state. Within the doublet state, the required hydrogen transfer is an easily surmountable transition while the transfer presents a barrier along the quartet potential energy surface. Additionally, the release of acetaldehyde in the doublet state is exothermic while the process in the quartet spin state is endothermic. Overall, the formation of acetaldehyde upon interaction of C_2H_4 and PdO^+ is 2.73 eV exothermic and requires a spin-crossover to the doublet state to proceed (Figure 5-5a). Creation of ethylene oxide is 1.51 eV exothermic and also requires a spin-crossover (Figure 5-6). The reaction between ZrO_2^+ and C_2H_4 (Figure 5-5b) creates acetaldehyde in a process that is 0.52 eV exothermic. It is seen that transitions for isomerization and hydrogen transfer are encountered

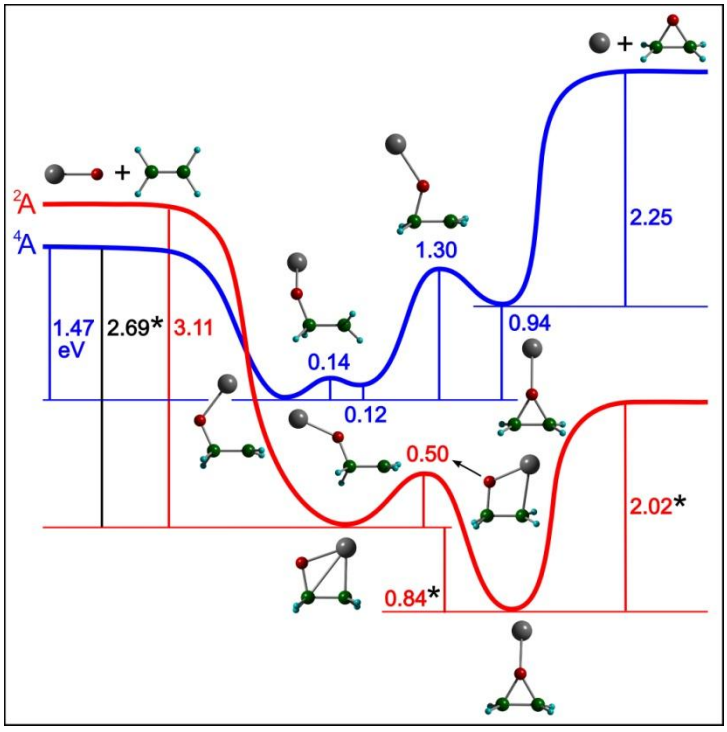

Figure 5-6. Calculated reaction profile for oxidation of C_2H_4 to ethylene oxide by PdO^+. Profiles for doublet and quartet states are shown. The reaction is exothermic by 1.93 eV in the doublet state and endothermic by 1.72 eV in the quartet state. The energy differences labelled by * allows for the determination of the most favourable reaction energy by undergoing a spin-crossover that is exothermic by 1.51 eV. Reproduced from reference 18.

in the reaction profile that are easily overcome. The reaction lies solely in the doublet spin state and is selective for the formation of acetaldehyde as the creation of ethylene oxide is 0.69 eV endothermic. The theoretical investigation probing the interaction of C_2H_4 with PdO^+ and ZrO_2^+ has shown an exothermic pathway for creation of acetaldehyde in both cases.

5.5 Conclusion

It is shown that the general concept of isovalent mimics can be extended to more complex systems in the frameworks of reactive characteristics. The findings from the joint theoretical and experimental investigation reveal similar reaction behavior for the isovalent pairs NiO^+/TiO_2^+ and PdO^+/ZrO_2^+ with C_2H_4, C_2H_2, and CO. Experimentally, a primary oxidation channel is observed for interaction of C_2H_4 and C_2H_2 with both pairs and similar reaction rate constants are calculated. It has been determined through theory that creation of acetaldehyde is the most energetically favorable product for interaction of C_2H_4 with both pairs of isovalent ions. As the early transition metal oxides are congeners, they follow similar reaction pathways along the doublet potential energy surface for the creation of acetaldehyde. The group 10 metal oxide congeners begin in the quartet state and undergo a spin-crossover to the doublet state that increases the exothermicity of the process and provides a pathway with surmountable transitions for the creation of acetaldehyde. Additionally, limited oxidation is observed upon interaction with CO, providing further similarities in reactive nature between the isovalent pairs. The presented evidence supports the future application of titanium oxide and zirconium oxide as replacements for nickel oxide and palladium oxide in catalytic materials through directed design concerning stoichiometry, charge state, size, and structure of the active species.

As catalytic technology expands, the use of large quantities of precious metals will become prohibitively expensive; thus replacements need to be found. Our investigations of molecular-

level phenomenon have discovered similar electronic structure and reactivity between isovalent systems. The addition of oxygen or carbon, as dopants, changes the electron distribution of transition metal containing species to present characteristics of isovalent group 10 metal species. As we extend this concept to systems of larger and varied composition, great benefit will be attained through the realization of catalysts designed utilizing superatomic building blocks.

5.5 References

1. Levy, R. B.; Boudart, M. *Science* **1973**, *181*, 547.
2. Leclercq, L.; Imura, K.;Yoshida, S.; Barbee, T.; Boudart, M. *Preparation of Catalysis II* (Eds. Delmon, B.;Grange, P.; Jacobs, P. A.;Poncelet, G.), Elsevier, Amsterdam, **1978**, p. 627.
3. Weigert, E. C.; Stottlemyer, A. L.; Zellner, M. B.; Chen, J. G. *J. Phys. Chem. C* **2007**, *111*, 14617.
4. Peppernick, S. J.; Gunaratne, K. D. D.; Castleman, A. W., Jr., *Proc. Natl. Acad. Sci. U.S.A.* **2010**, *107*, 975.
5. Peppernick, S. J.; Gunaratne, K. D. D.; Castleman, A. W., Jr., *Chem. Phys. Lett.* **2010**, *489*, 1.
6. Tyo, E. C.; Castleman, A. W., Jr.; Reber, A. C.; Khanna, S. N. *J. Phys. Chem. C* **2011**, *115*, 16797.
7. Castleman, A. W. Jr., *J. Phys. Chem. Lett.* **2011**, *2*, 1062.
8. Tyo, E. C.; Nößler, M.; Mitrić, R.; Bonačić-Koutecký, V.; Castleman, A. W., Jr., *Phys. Chem. Chem. Phys.* **2011**, *13*, 4243.

9. Johnson, G. E.; Mitrić, R.; Tyo, E. C.;Bonačić-Koutecký, V.; Castleman, A. W., Jr., *J. Am. Chem. Soc.* **2008**, *130*, 13912.

10. Becke, A. D. *Phys. Rev. A* **1988**, *38*, 3098.

11. Becke, A. D. *J. Chem. Phys.* **1993**, *98*, 5648.

12. Lee, C.; Yang, W.;Parr, R. G. *Phys. Rev. B* **1998**, *37*, 785.

13. Bell, R. C.; Zemski, K. A.; Justes, D. R.; Castleman, A . W., Jr., *J. Chem. Phys.* **2001**, *114*, 798-811.

14. Moore, N. A.; Mitrić, R.; Justes, D. R.; Bonačić-Koutecký, V.; Castleman, A. W., Jr. *J. Phys. Chem. B* **2006**, *110*, 3015.

15. Weigend, F.; Ahlrichs, R. *Phys. Chem. Chem. Phys.* **2005**, *7*, 3297.

16. Andrea, D.; Haeussermann, U.; Dolg, M.; Stoll, H.; Preuss, H. *Theor. Chim. Acta* **1990**, *77*, 123.

17. Božović, A.; Feil, S.; Koyanagi, G. K.; Viggiano, A. A.; Zhang, X.; Schlangen, M.; Schwarz, H.;Bohme, D. K. *Chem. Eur. J.* **2010**, *16*, 11605.

18. Tyo, E. C.; Nößler, M.; Rabe, S.; Harmon, C. L.; Mitrić, R.; Bonačić-Koutecký, V.; Castleman, A. W., Jr. *Phys Chem. Chem. Phys* (accepted 2011).

Chapter 6

Conclusions and Future Outlook

6.1 Conclusions and Future Outlook

The use of mass spectrometry to model catalytic active sites and investigate reaction mechanisms has gained popularity due to the ability to study species with well defined composition, stoichiometry, charge and oxidation state, size, and geometry.[1-3] The reduced size of clusters makes them amenable to detailed theoretical investigations that determine mechanistic pathways involved in various reactions.[1-4] Such detail is lacking for many catalytic processes and will provide for the development of more effective catalytic materials in the future.

Ionic metal oxide clusters provide a method of investigating isolated activated oxygen species and determine their reactivity with a variety of molecules. Previous investigations in the Castleman group identified vanadium oxide clusters ($V_2O_5^+$ and $V_4O_{10}^+$) to be highly active for oxidation of ethene to acetaldehyde.[5,6] Theoretical investigations determined these species contain an active site with a spin unpaired electron localized about a peripheral oxygen, know as a radical oxygen center. Investigations of zirconium oxide cationic and anionic clusters also identified species that contain radical oxygen centers.[7,8] The clusters containing radical oxygen are the cationic species $Zr_xO_{2x}^+$ (x = 2-4) that readily oxidize CO, ethene, and acetylene and the anionic species $Zr_xO_{2x+1}^-$ (x = 2-4) that oxidize CO but are unreactive towards ethene and acetylene. As several species have been identified to contain radical oxygen centers, I performed an investigation of $Ti_xO_{2x}^+$ clusters[9] to determine if they have similar structures and reactive properties to the congener $Zr_xO_{2x}^+$ species. $Ti_2O_4^+$ has a nearly identical structure to $Zr_2O_4^+$ with a radical oxygen center that is active for oxidation of CO, acetylene, ethene, and propene. The reaction rate constants for oxygen transfer from $Ti_2O_4^+$ to CO, ethene, and acetylene are in the

high 10^{-12} cm^3 s^{-1} that is greater than transfer from $Zr_2O_4^+$ to each reactant. As comparison has been made between the titanium and zirconium oxide cationic clusters, future investigations should be performed on titanium oxide anionic clusters to determine if the congener also has a greater reaction rate than $Zr_2O_5^-$. As new catalysts are being developed with supports tailored to donate or withdraw electron density to catalyst nanoparticles,[10,11] investigations of clusters are beneficial as they provide a method to study isolated charged model catalytic sites.

Having performed investigations on one form of activated oxygen, my focus turned towards the reactive properties of superoxide that has been identified on many surfaces.[12,13] Through theoretical investigations, the clusters of stoichiometry $Zr_xO_{2x+1}^+$ (x = 1-3) were determined to contain an O_2^- unit in which a spin unpaired electron is localized about a peripherally bound O_2.[14] Oxygen transfer from $Zr_2O_5^+$ to acetylene, propene, and butadiene was observed through experimental investigation.[14] Of great interest was the observation of multiple oxygen transfers to acetylene when in the presence of excess acetylene. As $Zr_2O_5^+$ transfers one oxygen to acetylene the resulting $Zr_2O_4^+$ contains a radical oxygen center that reacts to oxidize another acetylene. Quantitative analysis between $Zr_2O_4^+$ and $Zr_2O_5^+$ has determined the rate constant for oxygen transfer to acetylene to be twice as great for $Zr_2O_4^+$. Additional comparison of the reactive nature shows distinctive differences between the two forms of activated oxygen as the superoxide containing $Zr_2O_5^+$ is unreactive towards CO and ethene that $Zr_2O_4^+$ is highly active towards. Furthermore, $Zr_2O_5^+$ will transfer oxygen to propene and butadiene while evidence points towards $Zr_2O_4^+$ being unreactive with these species. Such investigations of isolated gas-phase clusters are providing a wealth of knowledge as to the reactive nature of various catalytic active sites. One recommendation from this investigation is that superoxide units should be utilized as the active species for oxidation of acetylene as the superoxide unit will oxidize acetylene revealing a radical oxygen unit that is also active for oxidation of acetylene. Further

investigations of superoxide containing clusters should be performed to determine how elemental composition and charge state influence reactive nature as well as rate.

As many studies have investigated the reactive nature of metal oxide clusters, significant benefit will be gained through further studies in areas including hydrogen abstraction and mixed metal species. Hydrogen abstraction has long been an important industrial process yet further interest has grown for research in hydrocarbon transformations as natural gas increases in utility. Investigations have observed cationic radical oxygen containing species to abstract hydrogen from various hydrocarbons.[15,16] It is of interest to compare the ability of anionic species to participate in similar reactions as well as investigate the ability for hydrogen abstraction to occur at superoxide sites. Furthermore, catalyst/support interactions have been determined to be of greater importance than initially thought. Clusters of mixed composition are currently a hot topic as they provide new species having distinctive electronic properties and electron distribution beyond those possible in species containing one metal.[16,17] New active sites may be identified with greater activity and selectivity for the future incorporation in catalytic materials.

With growing application of catalytic technology in industrial processes, many attempts have been made to develop alternative catalysts based on less costly materials for those currently employing precious metals. Bulk phase catalytic investigations have found metal oxide and carbide surfaces to present similar reactive nature as many late transition metals including platinum and palladium.[18-20] Photoelectron spectroscopy (PES) investigations identified common electronic transitions between several isovalent pairs including Pt^-/WC^-, Pd^-/ZrO^-, and Ni^-/TiO^-.[21,22] These PES studies link the similarities observed in surface catalyst with molecular level properties through the superatomic mimic concept in which commonality is observed between isovalent species. As an initial reactivity investigation, the isovalent species Pd^+ and ZrO^+ were interacted with ethane and propane at 20 eV in the lab frame.[23] Similar reactivity patterns were observed for both ions with the scission of a C—C bond being the primary mechanism as well as

significant amounts of hydrogen abstraction during interaction with ethane and propane. Theoretical investigations determined that the addition of an oxygen atom to Zr^+ moderates the reactivity with ethane and propane leading to a potential energy surface similar to Pd^+. This investigation provides the first evidence that species of isovalence react in a similar manner when under parallel conditions. Further investigations of ions having diverse composition and increased size will aid in forming a more detailed definition of superatomic mimics with respect to common reactivity.

To expand the concept of superatomic mimics, experiments were performed to determine the reactivity of larger isovalent ions. The pair PdO^+ and ZrO_2^+ was chosen as species of interest as they build upon the previously discussed investigation of Pd^+ and ZrO^+ by the addition of an oxygen to each ion. Another pair of isovalent ions studied was NiO^+ and TiO_2^+. The pairs of ions were interacted with CO, ethene, and acetylene at thermal energy; dominant oxygen transfer pathways were revealed with ethene and acetylene while limited oxidation of CO was observed. The rate constants calculated for oxygen transfer are very similar within each pair. Theoretical investigation of the reactions identified a spin crossover from quartet to doublet state in the most energetically favorable reaction profiles of PdO^+ and NiO^+. Two state reactivity is necessary to overcome energetic barriers and increase the exothermicity of the process for the group 10 ions while the reaction profiles lie on the doublet potential energy surface for ZrO_2^+ and TiO_2^+. Study of the isovalent pairs PdO^+/ZrO_2^+ and NiO^+/TiO_2^+ have provided additional evidence towards the superatomic mimics concept. Future work should continue to investigate isovalent species of larger size and varied composition to determine if the superatomic mimics concept can be extended. In addition, studies of nanocatalysts should be performed to advance the concept toward application in catalytic processes.

A further example of the superatomic mimics concept can be seen through a brief literature review. I have presented NiO^+ and TiO_2^+ as isovalent species with similar reactivity

towards various molecules, the next logical step would be to investigate the pair $Ni_2O_2^+$ and $Ti_2O_4^+$ that have the same stoichiometry as the smaller ions. Chapter 2 reports the structure and reactivity of $Ti_2O_4^+$; in particular, $Ti_2O_4^+$ is active for the transfer of oxygen to CO.[9] $Ni_2O_2^+$ may have a peroxide structure containing an attached O_2 unit or may form a dioxide species with dissociated oxygen. The stable structure created by the LaVa source has the peroxide unit as determined by CID, interaction with both N_2 and CO results in the dissociation of O_2. A gas-phase investigation utilizing a Fourier-transform ion-cyclotron-resonance mass spectrometer was successful in creating the dioxide isomer of $Ni_2O_2^+$.[24] In this study, the interaction of $Ni_2O_2^+$ with CO resulted in an oxygen transfer. Results from these studies support the superatomic mimics concept yet add complexity as it is apparent that the structure of the isovalent species have influence towards the reactive behavior and must be accounted for in the theory.

Gas-phase mass spectrometry investigations of ionic clusters are a method for modeling catalytic active sites to determine mechanistic insight of catalytic processes. Investigations have been performed to determine the reactivity of isolated radical oxygen and superoxide units. Additionally, major experimental support for the superatomic mimic concept has been reported through the investigation of isovalent ions. As the next generation of catalytic materials are developed, such insights will be beneficial to increase selectivity and activity of catalytic processes.

6.2 References

1. Bohme, D. K.; Schwarz, H. *Angew. Chem. Int. Ed.* **2005**, *44*, 2336.
2. Lang, S. M.; Bernhardt, T. M.; Barnett, R. N.; Yoon, B.; Langman, U. *J. Am. Chem. Soc.* **2009**, *131*, 8939.

3. Johnson, G. E.; Mitrić, R.; Bonačić-Koutecký, V.; Castleman, A. W., Jr. *Chem. Phys. Lett.* **2009**, *475*, 1.

4. Feyel, S.; Döbler, J.; Höckendorf, R.; Beyer, M. K.; Sauer, J.; Schwarz, H. *Angew. Chem. Int. Ed.* **2008**, *47*, 1946.

5. Justes, D. R.; Mitrić, R. Moore, N. A.; Bonačić-Koutecký, V.; Castleman, A. W., Jr. *J. Am. Chem. Soc.* **2003**, *125*, 6289.

6. Moore, N. A.; Mitrić, R.; Justes, D. R.; Bonačić-Koutecký, V.; Castleman, A. W., Jr. *J. Phys. Chem. B* **2006**, *110*, 3015.

7. Johnson, G. E.; Mitrić, R.; Nößler, M.; Tyo, E. C.; Bonačić-Koutecký, V.; Castleman, A. W., Jr. *J. Am. Chem. Soc.* **2009**, *131*, 5460.

8. Johnson, G. E.; Mitrić, R.; Tyo, E. C.; Bonačić-Koutecký, V.; Castleman, A. W., Jr. *J. Am. Chem. Soc.* **2008**, *130*, 13912.

9. Tyo, E. C.; Nößler, M.; Mitrić, R.; Bonačić-Koutecký, V.; Castleman, A. W., Jr. *Phys. Chem. Chem. Phys.* **2011**, *13*, 4243.

10. Sterrer, M.; Risse, T.; Pozzoni, U. M.; Giordano, L.; Heyde, M.; Rust, H.-P.; Pacchioni, G.; Freund, H.-J. *Phys. Rev. Lett.* **2007**, *98*, 096107.

11. Giordano, L.; Pacchioni, G.; Goniakowski, J.; Nilius, N.; Rienks, E. D. L.; Freund, H.-J. *Phys. Rev. Lett.* **2008**, *101*, 026102.

12. Bedilo, A. F.; Poltnikov, M. A.; Mezentseva, N. V.; Volodin, A. M.; Zhidomirov, G. M.; Rybkin,I. M.; Klabunde, K. J. *Phys. Chem. Chem. Phys.* **2005**, *7*, 3059.

13. Zhao, Q.; Wang, X.; Cai, T. *Appl. Surf. Sci.* **2004**, *225*, 7.

14. Tyo, E. C.; Nößler, M.; Harmon, C. L.; Mitrić, R.; Bonačić-Koutecký, V.; Castleman, A. W., Jr. *J. Phys. Chem. C* **2011**, *115*, 21559.

15. Feyel, S.; Döbler, J.; Schröder, D.; Sauer, J.; Schwarz, H. *Angew. Chem. Int. Ed.* **2006**, *45*, 4681.

16. Dietl, N. Höchendorf, R. F.; Schlangen, M.; Lerch, M.; Beyer, M. K.; Schwarz, H. *Angew. Chem. Int. Ed.* **2011**, *50*, 1430.

17. Nößler, M.; Mitrić, R.; Bonačić-Koutecký, V.; Johnson, G. E.; Tyo, E. C.; Castleman, A. W., Jr. *Angew. Chem. Int. Ed.* **2010**, *49*, 407.

18. Leclercq, L.; Imura, K.; Yoshida, S.; Barbee, T.; Boudart, M. "Preparation of Catalysis II" (B. Delmon, P. Grange, P. A. Jacobs, and G. Poncelet, Eds.), p. 627. Elsevier, Amsterdam, 1978.

19. Levy, R. B.; Boudart, M. *Science* **1973**, *181*, 547.

20. Weigert, E. C.; Stottlemyer, A. L.; Zellner, M. B.; Chen, J. G. *J. Phys. Chem. C* **2007**, *111*, 14617.

21. Peppernick, S. J.; Gunaratne, K. D. D.; Castleman, A. W., Jr. *PNAS* **2010**, *107*, 975.

22. Peppernick, S. J.; Gunaratne, K. D. D.; Castleman, A. W., Jr. *Chem. Phys. Lett.* **2010**, *489*, 1.

23. Tyo, E. C.; Castleman, A. W., Jr.; Reber, A. C.; Khanna, S. N. *J. Phys. Chem. C.* **2011**, *115*, 16797.

24. Koszinowski, K.; Schlangen, M.; Schröder, D.; Schwarz, H. *Eur. J. Inorg. Chem.* **2005**, 2464.

Appendix

Instrumental Upgrades

Improvements to the guided-ion-beam mass spectrometer have been made to increase the resolution, ion throughput, and data analysis system. The original system consisted of two 9.5 mm quadrupole mass filters powered by 150 Quadrupole Controllers operating at 880 KHz. Mass command was controlled by two separate Mass Programmers model 091-3. All equipment was purchased from Extrel CMS. The first quadrupole has been replaced by a 19 mm Tri-filter Quadrupole Mass Filter powered by a newly purchased 150 Quadrupole Controller operating at 880 KHz. According to Extrel CMS. documentation, the resolution of a 19 mm Tri-filter operating at 880 KHz is 1800 M/ΔM FWHM compared to a 9.5 mm Tri-filter operating at 880 KHz with resolution of 1200 M/ΔM FWHM.

As the original quadrupole was not a Tri-filter model, it did not contain pre and post filters. The pre and post filters greatly increase transmission of ions through the RF and DC fringing fields produced at the end of the quadrupole. Beyond the addition of a quadrupole having pre and post filters, the transmission is increased by changing to a 19 mm Quadrupole from a 9.5 mm. According to Extrel CMS. documentation, operating at 880 KHz a 9.5 mm Tri-filter has a relative transmission of 20% while a 19 mm Tri-filter has a relative transmission of 50%. Greater quantities of reactant ion will be introduced to the reaction cell through the installation of a 19 mm Tri-filter Quadrupole Mass Filter.

The model 091-3 Mass Programmers have been replaced by a model 5221 QMS Controller that is commanded by the Merlin Automation Data System Software. The new command and data acquisition system is capable of controlling both quadrupole mass filters and

the ion lenses within the instrument. The Merlin system provides a host of data manipulation capabilities for analysis of results. Control of the system will become much simpler through these improvements. Mass command and resolution is expected to improve through the application of the new QMS Controller and Merlin system as the previous Mass Programmers had been repaired numerous times with accuracy decreasing over the many years of use.

The aforementioned improvements will facilitate in performing numerous investigations that were previously unfeasible. Metals having numerous isotopes can be studied through the introduction of one isotope to the reaction cell. In previous studies, with lower resolution, a large mass range of ions would pass into the reaction cell. A complicated mass spectrum would be detected having many unreacted isotopes mixed with reaction products to be deciphered. Proposed studies to be performed will include the interaction of $Pd_2O_4^+$ and $Pd_2O_5^+$ with CO and ethene.

Studies of mixed metal oxide ions have been a topic of interest. This system presents a similar difficulty to the study of metals with multiple isotopes as both systems create a complex mass spectrum. The increased mass resolution will aid in selection of a reactant ion of interest while excluding any ions of nearly degenerate mass. Finally, the increase in ion transmission will have a large impact on the investigation of ions created in low quantity as well as detection of minor products.

VITA

Eric C. Tyo

EDUCATION

- **The Pennsylvania State University**, University Park, PA Ph.D., Physical Chemistry, Graduation 2012
- **Clarkson University**, Potsdam, NY Bachelor of Science, Chemistry, Graduation 2006

PROFESIONAL EXPERIENCE

- Graduate Research Assistant, The Pennsylvania State University, 2006-2012
- Environmental Laboratory Technician, ALCOA Inc. May 2005 - January 2006

AWARDS

- Central Europe Summer Research Institute Fellowship, Prague, CZ, May - June 2008
- Weyenberg Fellowship - Department of Chemistry, The Pennsylvania State University, 2010 - 2011
- Alexander von Humboldt Foundation Visiting Junior Scientist, Berlin, Germany, Summer 2010

PRESENTATIONS

- Gordon Conference: Clusters, Nanocrystals & Nanostructures, 2007
- 3rd Prize Physical Sciences & Mathematics Category, Penn State Graduate Exhibition 2011

PROFESSIONAL AFFILIATIONS

- American Chemical Society, 2008 - Present
- American Association for the Advancement of Science, 2008 – Present

SELECT PUBLICATIONS

- Tyo, E. C.; Nőβler, M.; Mitrić, R.; Bonačić-Koutecký, V.; Castleman, A. W., Jr.; "Reactivity of Stoichiometric Titanium Oxide Cations" *Phys. Chem. Chem. Phys.* **2011**, *13*, 4243.
- Tyo, E. C.; Castleman, A. W., Jr.; Reber, A. C.; Khanna, S. N. "Analogous Reactivity of Pd^+ and ZrO^+: Comparing the Reactivity with Small Hydrocarbons" *J. Phys. Chem. C*. **2011**, *115*, 16797.
- Tyo, E. C.; Harmon, C. L.; Nőβler, M.; Mitrić, R.; Bonačić-Koutecký, V.; Castleman, A. W., Jr. "Reactivity of Superoxide Containing Zirconium Oxide Cations" *J. Phys. Chem. C* **2011**, *115*, 21559.
- Tyo, E. C.; Nößler, M.; Rabe, S.; Harmon, C. L.; Mitrić, R.; Bonačić-Koutecký, V.; Castleman, A. W., Jr. *Phys Chem. Chem. Phys* (accepted 2011).